Department
of
APPLIED MATHEMATICS

NONLINEAR PROPAGATION AND INTERACTION OF COLLINEAR SOUND BEAMS

by

Erlend H. Vefring

Report No.86 October 1989

UNIVERSITY OF BERGEN
Bergen, Norway

Department of Mathematics
University of Bergen
5007 Bergen

ISSN 0084-778x

NONLINEAR PROPAGATION AND INTERACTION OF COLLINEAR SOUND BEAMS

by

Erlend H. Vefring

Report No.86 October 1989

ABSTRACT

Nonlinear propagation and interaction of collinear sound beams are investigated within the scheme of the Khokhlov-Zabolotskaya-Kutznetsov (KZK) equation. The solution of the KZK equation is written in form of a Fourier series, and equations are obtained for the Fourier coefficients. The infinite Fourier series has to be truncated, and an algorithm is presented which selects harmonic components retained. A test problem, which is a simplification of solving the KZK equation, is analysed and the analysis leads to an efficient method for solving the KZK equation numerically. The propagation of both focused and unfocused sound beams are considered. Propagation curves and beampatterns for various components of the acoustic field (harmonics and combination frequencies) are presented. The analysis extends to ranges beyond the shock formation distance. Various source levels, absorption lengths, downshift ratios and focusing gains are considered. The results are compared with that obtained for sources operating at moderate intensity (quasilinear theory).

REPORTS PUBLISHED BY THE DEPARTMENT OF APPLIED MATHEMATICS UNIVERSITY OF BERGEN BERGEN, NORWAY

No. 1. A. Kildal and S. Tjøtta.
On acoustic streaming in magneto-hydrodynamics, February 1964.

No. 2. G. Berge.
On the stability of a magnetized plasma with a continuous density force field, June 1964.

No. 3. J. Falnes.
Coaxial waveguide consisting of a circular metal tube surrounding a coaxial unidirectionally conducting sheet, August 1965.

No. 4. K.B. Dysthe.
On nonlinear interaction between two beams of plane electromagnetic waves in an anisotropic medium, December 1964.

No. 5. K.J. Overholt.
Extended Aitken acceleration, March 1965.

No. 6. G. Berge.
On the stability of a rotating plasma from the two fluid equations including finite radius of gyration effects, May 1965.

No. 7. A. Svardal.
On acoustical streaming between two coaxial cylinders, May 1965.

No. 8. K.B. Dysthe.
On convective and absolute instability, November 1965.

No. 9. L. Engevik.
On linear and non-linear hydro-magnetic vortex motion generated by the interaction of a gravity wave with a solid boundary, April 1966.

No. 10. S. Tjøtta.
Some non-linear effects in sound fields, July 1966.

No. 11. L. Engevik.
On a stability problem in hydrodynamics. Part I, November 1966.

No. 12. L. Engevik.
On the stability of plane inviscid Couette flow, November 1966.

No. 13. L. Engevik.
On a stability problem in hydrodynamics. Part II, January 1967.

Report NTNF, L. Storesletten.
On non-linear magneto-hydro-dynamic wave motion in dissipative media, September 1967.

No. 14. K.B. Dysthe.
Self-trapping and self-focusing of electromagnetic waves in a plasma, May 1968.

Report no. 15 not written.

No. 16. K.B. Dysthe.
Force on a small inclusion in a standing acoustic wave, July 1968.

No. 17. A. Svardal and S. Tjøtta.
Oscillatory viscous flows in the vicinity of a cylinder, June 1969.

No. 18. A.H. Øien and J. Naze Tjøtta.
Kinetic theory of a weakly coupled and weakly inhomogeneous gas, June 1969.

No. 19. M.S. Espedal.
Hydrodynamic equations for a F.L.R. plasma, August 1969.

No. 20. J. Naze Tjøtta and A.H. Øien.
Kinetic theory of a weakly coupled and weakly inhomogeneous plasma in a magnetic field, August 1969.

No. 21. K.S. Eckhoff.
On stability.
Part I: General theory, November 1969.

No. 22. K.S. Eckhoff.
On stability.
Part II: Linear problems, December 1969.

No. 23. K.S. Eckhoff.
On stability.
Part III: The energy principle in MHD, December 1969.

No. 24. K.B. Dysthe.
On the stability of a cylindrical surface-film, December 1969.

No. 25. M.S. Espedal.
The effects of ion-ion collision on a ion-acoustic plasma pulse, April 1970.

No. 26. A.H. Øien.
Derivation of kinetic equations of a plasma using a multiple time and space scale method, September 1970.

No. 27. K.S. Eckhoff.
On stability.
Part IV: Nonlinear partial differential equations, October 1970.

No. 28. O. Faltinsen and S. Tjøtta.
Interaction between sound waves propagating in the same direction, April 1971.

No. 29. T. Leversen and J. Naze Tjøtta.
Solution of a stationary Fokker-Plank equation, June 1971.

No. 30. E. Mæland.
Application of the Galerkin's method on the problem of cellular convection induced by surface tension gradients, November 1971.

No. 31. S. Nissen-Meyer.
A note on the problem of reversibility of mathematical models. (Preliminary issue.), December 1971.

No. 32. L. Hinderaker.
On the foundations of the method of matched asymptotic approximations to two meeting orthogonal boundary-layers, December 1971.

No. 33. A. Bertelsen, A. Svardal and S. Tjøtta
Non-linear streaming effects associated with oscillating cylinders, December 1971.

No. 34. S. Nissen-Meyer
Some theorems on the problem of reversibilty of mathematical models.
(This report is a revised issue of report no. 31.), April 1972.

No. 35. I. Eidhammer
A minimum resource sorting method, June 1972.

No. 36. T.O. Espelid
On the behaviour of the secant method near a multiple root, September 1971.

No. 37. H.B. Drange
The linearized Boltzmann collision operator for cut-off potentials, December 1972.

No. 38. J. Naze Tjøtta and S. Tjøtta
Sur le transport de masse produit par des oscillations en milieu compressible, dissipatif et inhomogene, December 1972.

No. 39. M. Aksland
On the twodimentional birth and death process with mutation, January 1973

No. 40. A. H. Øien
Kinetic theory for evolution of a plasma in external electro-magnetic fields toward a state characterized by balance of forces transverse to the magnetic field, April 1973.

No. 41. H.B. Drange.
On the Boltzmann equation with external forces. April 1973.

No. 42. J. Naze Tjøtta and S. Tjøtta
On the mass transport induced by time-dependent oscillations of finite amplitude in a nonhomogeneous fluid.
I General results for a perfect gas, May 1973.

No. 43. L. Engevik
Pertubation about neutral solutions occuring in shear flows in stratified, incompressible and viscid fluids, June 1973.

No. 44. J. Naze Tjøtta and S. Tjøtta
On the mass transport induced by time-dependent oscillations of finite amplitude in a nonhomogeneous fluid.
II General results for a liquid. August 1973.

No. 45. G.Dahl and S. Storøy
Enumeration of vertices in the linear programming problem, October 1973.

No. 46. M. S. Espedal.
The effects of trapped and untrapped particles on an electrostatic wave packet. December 1973.

No. 47 M. S. Espedal.
A procedure to solve the Fokker-Planck - Poisson equations consistently, April 1974

No. 48. E. Mjølhus.
Application of the reductive perturbation method to long hydromagnetic waves parallel to the magnetic field in a cold plasma, May 1974.

No. 49. K. S. Eckhoff.
The propagation of discontinuities for linear hyperbolic partial differential equations, August 1974.

No. 50. T. O. Espelid.
An algorithm for internal merging of two subsets with small extra storage requirements, September 1974.

No. 51. E. Mæland.
Mass transport induced by wave motion in a rotating fluid, October 1974.

No. 52. I.S. Helland.
A random exchange model with constant decrements, December 1974.

No. 53. A. H. Øien.
On the evolution of a two component, two temperature, fully ionized plasma in electromagnetic fields, January 1975.

No. 54. K.S. Eckhoff.
Stability problems for linear hyperbolic systems, May 1975.

No. 55. K. S. Eckhoff.
On stability in ideal compressible hydrodynamics, May 1975.

No. 56. L. Storesletten.
A note on the stability of horizontal shear flow of an inviscid compressible fluid, July 1975.

No. 57. K. S. Eckhoff and L. Storesletten.
On the stability of shear flow in a rotating compressible and inviscid fluid, July 1975.

No. 58. E.N. Håland and G. Berge.
Dynamic stabilization of the m = 1 instability in a diffuse linear pinch, July 1975.

No. 59. E. Mæland.
Mass transport induced by wave motion in a stratified and rotating fluid, August 1975.

No. 60. T. O. Espelid.
On replacement-selection and Dinsmore's improvement, August 1975.

No. 61. L. Storesletten.
A note on the stability of steady inviscid helical gas flows, January 1976.

No. 62. E. Mæland.
A time-dependent model of coastal currents and upwelling, June 1976.

No. 63. A. H. Øien.
Corrections to classical kinetic and transport theory for a two-temperature, fully ionized plasma in electromagnetic fields, June 1977.

No. 64. S. D. Flåm.
Convergence in law of a series of φ-mixing random variables implies convergence in probability, August 1977.

No. 65. A. H. Øien.
Kinetic equation for an electron gas (non-neutral) plasma in strong fields and inhomogenities, June 1978.

No. 66. H. Hobæk and S. Tjøtta.
Theory of parametric acoustic arrays, July 1978.

No. 67. T.O. Espelid.
On floating-point summation, December 1978.

No. 68. E.N. Håland.
Stability of an inverted pendulum with hard spring and oscillating support, December 1978.

No. 69. S. Storøy.
An efficient least distance algorithm based on a general quadratic programming method, November 1979.

No. 70. L. E. Engevik.
Amplitude evolution equation for linearly unstable modes in stratified shear flows, November 1979.

No. 71. F. Oliveira-Pinto.
Argument reduction for elementary mathematical functions : An overview, July 1980.

No. 72. A. H. Øien.
A quasi moment description of the evolution of an electron gas towards a state dominated by a reduced transport equation, September 1980.

J. Berntsen.
User-documentation. Program HALF. A subroutine for numerical evaluation of three-dimensional complex integrals, spring 1983.

No. 73. S.I. Aanonsen.
Numerical computation of the nearfield of a finite amplitude sound beam, September 1983.

No. 74. L.K. Sandal.
Influence of equilibrium flows on viscous tearing modes, December 1983.

No. 75. Ø. Pettersen.
The nearfield of a high frequency amplitude shaded baffled piston. An analytical/numerical investigation, July 1981.

No. 76. Ø. Pettersen.
Numerical solution of the Buckley-Leverett equation with a general fractional flow function, November 1984.

No. 77. T. Mannseth.
Sound propagation in the Pekeris waveguide with application to directional sources.
November 1984.

No. 78. T. Barkve.
A study of the Verigin problem with application to analysis of water injection tests.
March 1985.

No. 79. S.I. Aanonsen.
Nonlinear Effects During Transient Fluid Flow in Reservois as Encountered in Well-Test Analysis.
March 1985.

No 80. T. Mannseth.
Sound propagation in the Pekeris model of acoustic shallow water: Validity of the Ray, and discrete normal mode solutions in the vicinity of mode Cutoff's.
January 1986.

No 81. J. Berntsen and E. Vefring.
Numerical computation of a finite amplitude sound beam.
November 1986.

No 82. J. Berntsen.
On the use of the Richtmyer procedure to compute a finite amplitude sound beam from a piston source.
April 1987.

No. 83 T. Barkve.
Solution of a non-strictly system modelling non-isothermal two-phase flow in a porous medium.
April 1987.

No. 84 K.S. Eckhoff.
Linear waves and stability in ideal magnethohydrodynamics.
May 1987.

No. 85 H. K. Dahle
Adaptive Characteristic Operator Splitting Techniques for Convection-Dominated Diffusion Problems in One and Two Space Dimensions.

December 1988.

No. 85. Helge K. Dahle.
Adaptive Characteristic Operator Splitting Techniques for Convection-Dominated Diffusion Problems in one and two Space Dimensions.

No. 86. Erlend H. Vefring.
Nonlinear Propagation and Interaction of Collinear Sound Beams.
October 1989.

No. 87. G. Berge & J. P. Freidberg.
Stellarator-Tokamak Configurations.
January 1990.

Contents

Acknowledgments

This report is a main part of my work for the Dr. Scient. degree in applied mathematics. The research has been supported by the Norwegian Research Council for Science and Humanities (NAVF) and VISTA, a research cooperation between the Norwegian Academy of Science and Letters and Den norske stats oljeselskap a.s. (STATOIL). A major part of the computing resources for this work were provided by The University of Texas System Center for High Performance Computing.

I wish to thank Professor Jacqueline Naze Tjøtta and Professor Sigve Tjøtta for all kinds of help and advice during this work, and Dr. Scient. Jarle Berntsen for his valuable help on the numerical part. I also want to express my gratitude to the members of the acoustic group at the University at Bergen for making this group a very pleasent place to work. During the sabbatical year 1987-88 of Professor Naze Tjøtta and Professor Tjøtta, which they spent at Applied Research Laboratories, The University of Texas at Austin, I had the opportunity to stay at the Department of Mechanical Engineering at the same University. Professor Mark F. Hamilton and his colleagues in the Nonlinear Acoustics Division made my stay very fruitful and pleasant. I and my family were shown great hospitality by everybody, and by Professor Mark Hamilton and his wife Karla Hamilton especially.

Finally, I wish to thank Rigmor for her support and patience.

List of symbols

A	=	see Eq. 3.11
A_1, B_1	=	see Eqs. 3.16 and 3.17
a	=	source radius
a_1	=	source radius of highest primary
a_2	=	source radius of lowest primary
$c_{b,n}, d_{b,n}$	=	Fourier coefficients in expansion of T_b
$c_{bb,n}, d_{bb,n}$	=	Fourier coefficients in expansion of T_{bb}
$c_{bp,n}, d_{bp,n}$	=	Fourier coefficients in expansion of T_{bp}
$c_{f,n}, d_{f,n}$	=	Fourier coefficients in expansion of T_f
$c_{ff,n}, d_{ff,n}$	=	Fourier coefficients in expansion of T_{ff}
$c_{fp,n}, d_{fp,n}$	=	Fourier coefficients in expansion of T_{fp}
c_n, d_n	=	Fourier coefficients in expansion of $\overline{p}$
$c_{s,n}, d_{s,n}$	=	Fourier coefficients in expansion of T_s
c_0	=	ambient sound speed
D	=	sound diffusivity
d	=	focal distance
d_m	=	$(d_1 + d_2)/2$
d_1	=	focal distance for highest primary
d_2	=	focal distance for lowest primary
f	=	basic frequency
f_m	=	$(f_1 + f_2)/2$
f_1	=	highest primary frequency
f_2	=	lowest primary frequency
f_-	=	$f_1 - f_2$, difference frequency
f_+	=	$f_1 + f_2$, sum frequency
G	=	r_0/d, focusing gain for basic frequency
G_1	=	r_1/d_1, focusing gain for highest primary
G_2	=	r_2/d_2, focusing gain for lowest primary
G_m	=	r_m/d_m, focusing gain for mean primary frequency
h	=	stepsize in ξ - direction
I	=	identity matrix
j	=	$\sqrt{-1}$
k	=	ω/c_0, wave number
	=	stepsize in σ - direction
k_m	=	$(k_1 + k_2)/2$
k_1	=	$2\pi f_1/c_0$, highest primary wave number
k_2	=	$2\pi f_2/c_0$, lowest primary wave number

L	=	linear differential operator
l_D	=	$1/(\beta\epsilon k)$, shock formation distance for a plane wave with wavenumber k
l_{Dm}	=	$1/(\beta\epsilon k_m)$, shock formation distance for a plane wave with wavenumber k_m
N_1	=	f_1/f, highest primary frequencys multiplicity of the basic frequency
N_2	=	f_2/f, lowest primary frequencys multiplicity of the basic frequency
N_+	=	$N_1 + N_2$
N_-	=	$N_1 - N_2$
n_m	=	$(N_1 + N_2)/2$
P_0	=	on-source pressure amplitude
p	=	acoustic pressure
$\overline{p}$	=	p/P_0
$\mathcal{P}_{av}$	=	$\rho_0 c_0 V_0^2 a^2 \overline{\mathcal{P}}_{av}$
$\overline{\mathcal{P}}_{av}$	=	See Eq. 2.6
q_n	=	coefficient in complex Fourier series expansion of $\overline{p}$
r_0	=	$ka^2/2$ = Rayleigh distance for basic frequency
r_1	=	$k_1 a^2/2$= Rayleigh distance for highest primary
r_2	=	$k_2 a^2/2$= Rayleigh distance for lowest primary
r_m	=	$k_m a^2/2$= Rayleigh distance for mean primary frequency
T_b	=	$(\sigma_b + 1)\overline{p}$
T_{bb}	=	$(\sigma_{bb} + 1)\overline{p}$
T_{bp}	=	$(\sigma_{bp} + 1)\overline{p}$
T_f	=	$(\sigma_f + 1)\overline{p}$
T_{ff}	=	$(\sigma_{ff} + 1)\overline{p}$
T_{fp}	=	$(\sigma_b + 1)\overline{p}$
T_s	=	$\sigma_s \overline{p}$
T	=	characteristic time, $T = \omega^{-1}$ for periodic excitation
	=	block tridiagonal matrix, see Eq. 3.18
t	=	time
U	=	unit step function

$\underline{u}_b = \underline{\xi}/(\sigma_b + 1)$
$\underline{u}_{bb} = \underline{\xi}/(\sigma_{bb} + 1)$
$\underline{u}_{bp} = \underline{\xi}/(\sigma_{bp} + 1)$
$\underline{u}_f = \underline{\xi}/(\sigma_f \pm \delta)$
$\underline{u}_{ff} = \underline{\xi}/(\sigma_{ff} \pm \delta)$
$\underline{u}_{fp} = \underline{\xi}/(\sigma_{fp} \pm \delta)$
$\underline{u}_s = \underline{\xi}/\sigma_s$
$u_b = |\underline{u}_b|$
$u_{bb} = |\underline{u}_{bb}|$
$u_{bp} = |\underline{u}_{bp}|$
$u_f = |\underline{u}_f|$
$u_{ff} = |\underline{u}_{ff}|$
$u_{fp} = |\underline{u}_{fp}|$
$u_s = |\underline{u}_s|$
V_0 = peak fluid velocity component in z - direction
v_z = fluid velocity component in z - direction
$\underline{x} = (x_1, x_2)$
$x = |\underline{x}|$
z = coordinate along acoustic axis

α = $D\omega^2/2c_0^3$, linear absorption coefficient for basic frequency

α_m = $D\omega_m^2/2c_0^3$, linear absorption coefficient for
= the mean primary frequency

α_- = $D\omega_-^2/2c_0^3$, linear absorption coefficient
= for the difference frequency

β = coefficient of nonlinearity

$\nabla_\perp^2$ = $\partial^2/\partial\xi^2 + (1/\xi)\partial/\partial\xi$

δ = small positive parameter which governs the rate at which the geometry converges towards focus

ϵ = V_0/c_0, Mach number

$\underline{\xi}$ = $(\xi_1, \xi_2) = (x_1/a, x_2/a)$

ξ = $|\underline{\xi}|$

ρ_0 = ambient density

σ = z/r_0

σ_{bb} = z/r_m

σ_{bp} = z/r_1

σ_f = $(z-d)/d$

σ_{ff} = $(z-d_m)/d_m$

σ_{fp} = $(z-d)/d$

σ_s = z/r_m

τ = $t/T - z/c_0T$, $\tau = \omega(t - z/c_0)$ for perodic excitation

τ_{bb} = $\tau - \xi^2 f/f_m(\sigma_{bb}+1)$

τ_{bp} = $\tau - \xi^2 f/f_1(\sigma_{bp}+1)$

τ_f = $\tau - \xi^2 r_0/d(\sigma_f \pm \delta)$

τ_{ff} = $\tau - \xi^2 r_0/d_m(\sigma_{ff} \pm \delta)$

τ_{fp} = $\tau - \xi^2 r_0/d(\sigma_{fp} \pm \delta)$

τ_s = $\tau - \xi^2 f/f_m\sigma_s$

Ω = see Eq. 3.10

ω = $2\pi f$

ω_m = $2\pi f_m$

ω_1 = $2\pi f_1$

ω_2 = $2\pi f_2$

Chapter 1

Introduction

Acoustics is mainly concerned with small amplitude disturbances for which linear theory is sufficient. There are several important instances, however, when the nonlinear terms in the fluid-dynamic equations cannot be neglected. Perhaps the most famous nonlinear phenomenon in acoustics is the steepening and development of shock in a plane travelling wave.

Nonlinear acoustics has several applications. Supersonic aircrafts generate shock waves which propagate to long ranges. The parametric array [1] is capable of producing a low frequency beam of high directivity from a source with relatively small dimensions. A parametric receiving array has also been constructed and is used to determine the parameters of a signal. It is based on the nonlinear interaction between the signal and a strong acoustic pump wave of higher frequency. Acoustic microscopes operating at nonlinear power levels achieve resolution beyond the linear diffraction limit [2]. Lithotripters [3] which transmit focused sound at very high amplitudes are used to disintegrate kidneystones.

In order to study practical applications of nonlinear effects in beams it is often necessary to consider the combined effects of nonlinearity, diffraction and absorption. The propagation of a narrow beam is effectively described by the so-called

Khokhlov-Zabolotskaya-Kutznetsov (KZK) equation [4,5]. This equation has to be solved numerically since no general analytic solution is known.

Chapter 2 presents the KZK equation and gives a brief description of how it can be derived. The solution of the KZK equation is written in form of a Fourier series, and equations are obtained for the Fourier coefficients [6]. Some properties of the power of a sound beam and its harmonic components are given.

Chapter 3 deals with the numerical solution of the KZK equation. Since the Fourier series expansion of the solution of the KZK equation contains infinitely many components, it has to be truncated. An algorithm is presented which selects harmonic components retained in the Fourier series. Section 3.2.2, "Analysis of two numerical techniques on a test problem" is based on a technical report [7] written with Jarle Berntsen as coauthor. A test problem, which is a simplification of the KZK equation, is introduced. Two finite difference methods are applied to the test problem and analyzed. The analysis leads to a more efficient way to solve the KZK equation than the method developed and used previously by Aanonsen et al.[6,8]. Further, in Sec. 3.2.2 additional improvements of the numerical method are discussed. By introducing different regions of integration for different harmonic components the computation time is reduced approximately by a factor of four. A stabilization procedure is given in order to prevent a possible instability caused by the truncation of the infinite Fourier series expansion.

In Chapter 4 the KZK equation is used to study different applications of nonlinear acoustics. Section 4.1 is devoted to parametric transmitting arrays. The numerical results are compared to low amplitude theoretical results and experimental measurements reported in the literature, in order to test the computer code. Effects of varying the different characteristic parameters are shown, and comparison is made with low

amplitude theory in order to see the effect of nonlinearity. Results are presented both in frequency and time domain. The possibility of matching the solution of the KZK equation with that of the spherical Burgers' equation in the farfield is also analyzed.

Section 4.2 considers focused sound beams and their interaction. A coordinate transform[9,10,11,12] is introduced which follows the geometry of the focused sound beam and enhances the computational efficiency. Nonlinear effects in focused soundbeams are shown and energy exchange between harmonic wave components are studied. The difference frequency wave component generated by interaction between two focused sound beams is computed and compared to results from the literature. Also, the sum frequency wave generated by interaction between two focused sound beams is studied. The effect of varying the characteristic parameters is shown, and comparison are made with low amplitude theory. Interaction between focused sound beams with different focal distances are also considered. Finally, applications are made to the parametric receiving array. Donskoi et al.[13] have suggested that the pump transducer should be focused in order to generate difference and sum frequency waves more efficiently. We have compared the results obtained using unfocused pumps to results obtained using pumps with different focal distances.

Chapter 2

Governing equation

2.1. The KZK equation

The Khokhlov-Zabolotskaya-Kutznetsov (KZK) wave equation which accounts for the combined effects of absorption, diffraction and nonlinearity can be written in the following nondimensional form

$$\frac{\partial^2 \overline{p}}{\partial \sigma \partial \tau} = \alpha r_0 \frac{\partial^3 \overline{p}}{\partial \tau^3} + \frac{1}{4} \nabla_\perp^2 \overline{p} + \frac{r_0}{2 l_D} \frac{\partial^2 (\overline{p})^2}{\partial \tau^2}, \tag{2.1}$$

where $\sigma = z/r_0$ is a dimensionless range in terms of the axial coordinate z and the Rayleigh distance $r_0 = ka^2/2$, $k = \omega/c_0$ is the wave number, $\omega/2\pi$ is the source frequency, c_0 is the sound speed and a is the source radius. Further, $\tau = \omega(t - z/c_0)$ is a dimensionless retarded time, $\overline{p} = p/P_o$ is a dimensionless pressure in terms of the acoustic pressure p and the on-source pressure amplitude P_o, $\alpha = D\omega^2/2c_0^3$ is the termoviscous attenuation coefficient, where D is the sound diffusivity. $l_D = 1/(\beta \epsilon k)$ is the plane wave shock formation distance, where β is the coefficient of nonlinearity and $\epsilon = V_0/c_0$ is the Mach number, where V_0 is the on-source fluid velocity component in the z-direction. The two dimensional Laplace operator $\nabla_\perp^2$ is applied with respect to the dimensionless vector $\underline{\xi} = \underline{x}/a$, where $\underline{x} = (x_1, x_2)$ is the transverse coordinate vector. For an axisymmetric sound field we may write $\nabla_\perp^2 = \partial^2/\partial\xi^2 + (1/\xi)\partial/\partial\xi$,

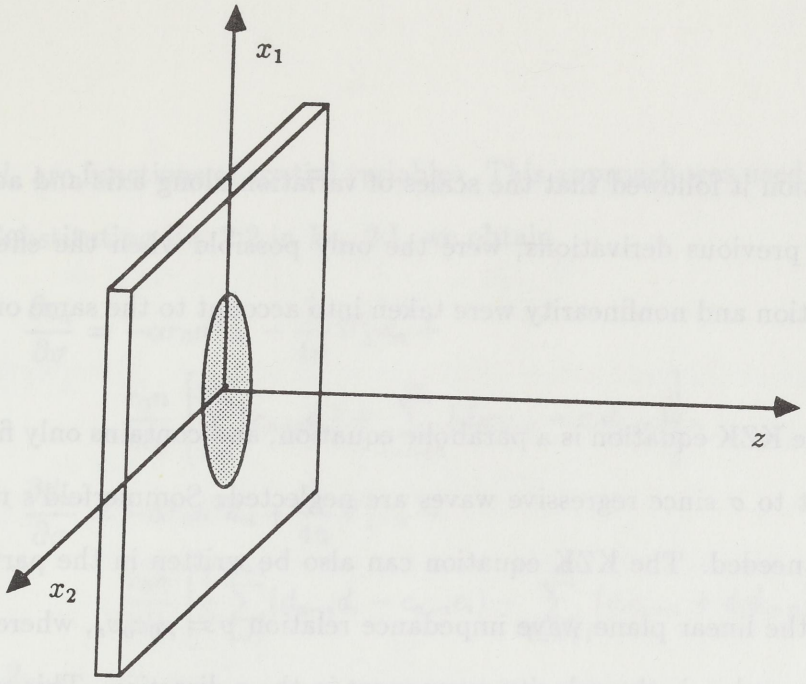

FIG. 2.1. The geometry and dimensional spatial variables of the problem

where $\xi = |\underline{\xi}|$. In Fig. 2.1 the dimensional coordinate system for the problem is shown. The first term on the right hand side of Eq. 2.1 represents absorption, the second diffraction and the third nonlinearity. In the derivation of the KZK equation it is assumed that the soundbeam is well collimated (i.e.$ka \gg 1$).

In the case of abscence of absorption the equation was derived by Zabolotskaya and Khokhlov[4]. They derived the equation from the equations of hydrodynamics on the assumption that the shape of the wave varied slowly both along the beam and transversely to it. These variations were ascribed different scales. Kutznetsov[5] included absorption and thereby added one term to the equation derived by Zabolotskaya and Khokhlov. He linearized terms in the hydrodynamical equations due to absorption, and ascribed the same scales of variations of the shape of the wave both along axis and transversely to it as did Zabolotskaya and Khokhlov.

Naze Tjøtta and Tjøtta[14] derived the KZK equation in a different way. They used the method of multiple scales and required that the effects of absorption, diffraction and nonlinearity all were accounted for to the same order of magnitude. From their

derivation it followed that the scales of variation along axis and across axis assumed in the previous derivations, were the only possible when the effects of absorption, diffraction and nonlinearity were taken into account to the same order of approximation.

The KZK equation is a parabolic equation, and contains only first derivative with respect to σ since regressive waves are neglected. Sommerfeld's radiation condition is not needed. The KZK equation can also be written in the particle velocity [14] by using the linear plane wave impedance relation $p = \rho_0 c_0 v_z$, where ρ_0 is the ambient density and v_z is the velocity component in the z-direction. This substitution is valid because $ka \gg 1$ and local effects are not accounted for in the KZK equation. Local effects are effects which are significant only on the order of one wavelength. It is consistent [6], within the approximations used when deriving the KZK equation, to linearize the boundary condition.

There are two nondimensional parameters in Eq. 2.1

$$\alpha r_0 = \text{Rayleigh distance relative to absorption length.}$$

$$r_0/l_D = \text{Rayleigh distance relative to shock formation distance.}$$

The parameter αr_0 increases with increasing importance of absorption, and the parameter r_0/l_D increases with increasing importance of nonlinear effects.

2.2. Fourier decomposition and power considerations

If we assume that the boundary condition is periodic with period $2\pi\omega^{-1}$, we can seek a solution of Eq. 2.1 in the form of a Fourier series

$$\overline{p} = \sum_{n=1}^{\infty} (c_n \cos n\tau + d_n \sin n\tau) = \sum_{n=1}^{\infty} \overline{p}_n, \tag{2.2}$$

where c_n and d_n are functions of spatial variables. This approach was used by Aanonsen et al.[6,8]. Substituting Eq. 2.2 in Eq. 2.1, we obtain

$$\begin{aligned}
\frac{\partial c_n}{\partial \sigma} &= -\alpha r_0 n^2 c_n - \frac{1}{4n}\nabla_\perp^2 d_n + \\
&\quad \frac{r_0 n}{2 l_D}\left[\sum_{i=1}^{n-1}(c_{n-i}d_i) + \sum_{i=n+1}^{\infty}(d_i c_{i-n} - c_i d_{i-n})\right], \\
\frac{\partial d_n}{\partial \sigma} &= -\alpha r_0 n^2 d_n + \frac{1}{4n}\nabla_\perp^2 c_n + \\
&\quad \frac{r_0 n}{2 l_D}\left[\frac{1}{2}\sum_{i=1}^{n-1}(d_{n-i}d_i - c_{n-i}c_i) - \sum_{i=n+1}^{\infty}(c_i c_{i-n} + d_i d_{i-n})\right], \\
n &= 1, 2, ...
\end{aligned} \tag{2.3}$$

The spectral form of Eqs. 2.3 permits generalization to fluids with arbitrary absorption and dispersion. Such effects can be taken into account by replacing the first term on the right hand side of Eqs. 2.3 by a more general expression of the form $\alpha(n)c_n + \beta(n)d_n$, where $\alpha(n)$ and $\beta(n)$ are given functions of n. See Ref. 15 for a discussion in the case of plane waves.

We specify a boundary condition in the plane $\sigma = 0$

$$\overline{p} = g(\underline{\xi}, \tau). \tag{2.4}$$

This leads to the following boundary conditions for c_n and d_n

$$\begin{aligned}
c_n(\underline{\xi}, \tau) &= \frac{1}{\pi}\int_{-\pi}^{\pi} g \cos n\tau \, d\tau, \\
d_n(\underline{\xi}, \tau) &= \frac{1}{\pi}\int_{-\pi}^{\pi} g \sin n\tau \, d\tau.
\end{aligned} \tag{2.5}$$

The Eqs. 2.3 together with the boundary conditions, Eqs. 2.5, form a complete mathematical model.

The overall power of a wave is found by integrating the intensity across the entire field. Within the parabolic approximation the linear plane wave impedance relation

is valid [14], and the nondimensional power of a wave is given by

$$\overline{\mathcal{P}}_{av}(\sigma) = \frac{1}{2\pi}\int_0^{2\pi}\int_0^{\infty} \overline{p}^2(\xi,\sigma,\tau)\xi \, d\xi \, d\tau. \tag{2.6}$$

The nondimensional power of an individual harmonic component is given by

$$\overline{\mathcal{P}}_{av,n}(\sigma) = \frac{1}{2\pi}\int_0^{2\pi}\int_0^{\infty} \overline{p}_n^2(\xi,\sigma,\tau)\xi \, d\xi \, d\tau. \tag{2.7}$$

In the case of no absorption the total power is constant [16] :

$$\overline{\mathcal{P}}_{av}(\sigma) = const. \tag{2.8}$$

Substituting Eq. 2.2 in Eq. 2.8 we obtain

$$\overline{\mathcal{P}}_{av}(\sigma) = \sum_{n=1}^{\infty} \overline{\mathcal{P}}_{av,n}(\sigma) = const. \tag{2.9}$$

The total power of a wave is equal to the sum of the power of all the individual harmonic components, which is again constant. The power of individual harmonic components is generally not constant in the nondissipative case, because of energy transfer between different components. For linear nondissipative propagation the power is constant also for individual harmonic components.

Chapter 3

Numerical work

3.1. Selection of harmonic components in computations

In the following we will study the interaction between two monofrequency sound beams, called primaries, of different frequencies. Let us denote the highest primary frequency by f_1 and the lowest primary frequency by f_2. For the resulting signal to be periodic the frequencies f_1 and f_2 must be commensurable. This means that there exist integers N_1 and N_2 and a basic frequency f such that

$$f_i = N_i f, \tag{3.1}$$

for i=1,2. Let furthermore f denote the largest frequency which satisfies Eq. 3.1. The requirement of commensurability is purely theoretical since no frequency can be measured exactly.

When the boundary condition is periodic, we can seek a Fourier series solution as shown in the previous section, and we obtain an infinite set of coupled partial differential equations for the different harmonic components. To perform the computations we have to select a finite number of harmonic components. In the case of a single frequency on the source the selection procedure is easy. Computations are done with all the harmonic components up to a specific number.

The KZK equation can be written in the following form

$$L\overline{p} = \epsilon \frac{\partial^2(\overline{p}^2)}{\partial \tau^2}, \tag{3.2}$$

where L is a linear differential operator and ϵ is the Mach number. The boundary condition in the case of two frequencies on the source can be written

$$\overline{p}(\underline{\xi}, \sigma = 0) = g_1 e^{jN_1\tau} + h_1 e^{-jN_1\tau} + g_2 e^{jN_2\tau} + h_2 e^{-jN_2\tau}, \tag{3.3}$$

where g_1, h_1, g_2 and h_2 are functions of $\underline{\xi}$. To solve Eq. 3.2 together with the boundary condition, Eq. 3.3, we seek a solution in the form

$$\overline{p} = \sum_{k=0}^{\infty} \left[\epsilon^k \sum_{i=1}^{M_k} (c_{ki} e^{jN_{ki}\tau} + d_{ki} e^{-jN_{ki}\tau}) \right], \tag{3.4}$$

where c_{ki} and d_{ki} are functions of spatial variables. We want to determine M_k, (k=0,1,...) and N_{ki}, (k=0,1,...; i=1,...M_k). The boundary condition implies $M_0 = 2$,$N_{01} = N_1$ and $N_{02} = N_2$. We substitute Eq. 3.4 in Eq. 3.2 and require that the equation is satisfied to every order in the parameter ϵ. This gives us a recursive procedure to calculate N_{ki}, (k=0,1,...; i=1,...,M_k) . First we use N_{0i}, (i=0,1,...,M_0) to determine N_{1i}, (i=0,1,...M_1), and then we use N_{0i}, (i=0,1,...,M_0) and N_{1i}, (i=0,1,...,M_1) to determine N_{2i}, (i=0,1,...,M_2). We want to have an algorithm for finding all N_{ki}, (k=0,1,...; i=0,1,...,M_k). For each order in ϵ we have the following equation

$$\epsilon^k : L \left[\sum_{i=1}^{M_k} (c_{ki} e^{jN_{ki}\tau} + d_{ki} e^{-jN_{ki}\tau}) \right] = \sum_{i=1}^{I_k} (q_{ki} e^{jK_{ki}\tau} + r_{ki} e^{-jK_{ki}\tau}), \tag{3.5}$$

where q_{ki} and r_{ki} are functions of spatial variables. The operator L has the property

$$L(qe^{jC\tau}) = q' e^{jC\tau}, \tag{3.6}$$

where q and q' are functions of spatial variables and C is a constant. With this property we construct the complete solution of Eq. 3.5 by superposition, and we have

$I_k = M_k$. Furthermore we can choose $N_{ki} = K_{ki}$, and K_{ki}, (k=0,1,...; i=0,1,...,M_k) are calculated from N_{li}, (l=0,1,...,k-1), (i=0,1,...,M_l). The recursive procedure to determine M_k, (k=0,1,...) and N_{ki}, (k=0,1,...; i=0,1,...,M_k), gives

$$\begin{aligned}
&\epsilon^0 : M_0 = 2, N_{01} = N_1, N_{02} = N_2, \\
&\epsilon^1 : M_1 = 4, N_{11} = 2N_1, N_{12} = N_1 + N_2, N_{13} = 2N_2, N_{14} = N_1 - N_2, \\
&\epsilon^2 : M_2 = 6, N_{21} = 3N_1, N_{22} = 2N_1 + N_2, N_{23} = N_1 + 2N_2, \\
&\quad N_{24} = 3N_2, N_{25} = 2N_1 - N_2, N_{26} = 2N_2 - N_1.
\end{aligned} \tag{3.7}$$

We note that all harmonic components of order ϵ^n can be written $|xN_1 + yN_2|$, where $|x| + |y| = n + 1$ and x, y are members of Z. This gives us the desired algorithm for associating an order to each harmonic.

The Fourier series representation of the solution of the KZK equation contains infinitely many harmonic components. If we retain only harmonic components up to a certain order, then the Fourier series is truncated consistently. Let M denote the total number of harmonic components retained in the Fourier series and K the highest order of all harmonics retained. When the Fourier series is truncated consistently, we have two upper limits for M

$$\begin{aligned}
M &\leq (K+1)(K+2), \\
M &\leq (K+1)N_1.
\end{aligned} \tag{3.8}$$

The first upper limit is the typical number of harmonic components retained in the Fourier series in the case of $N_1, N_2 \gg K$, and the lower limit is the typical number of harmonic components retained if $N_1 \leq K$

3.2. Numerical method

3.2.1. Previous work

After the KZK equation was derived a large number of articles appeared in the Soviet literature devoted to results from numerical solutions of the equation. In these articles the numerical method used was not described in detail. Zhileikin[16] later described and analyzed the method used. The acoustic pressure was expanded in a Fourier series, and equations were obtained for the Fourier coefficients. The infinite system of equations were truncated and solved by a finite difference method. They used a conservative finite difference scheme, the Crank-Nicholson method. The resulting difference equations were solved by the method of difference matrix pivotal condensation.

Aanonsen et al. [6,8] also solved the KZK equation by a finite difference method. Their work was independent of the work in the Soviet Union. They did not apply the same method as Zhileikin et al., but used a fully implicit method instead. The resulting algebraic equations were solved by iterations, thus putting severe restrictions on the choice of step sizes in order to ensure the convergence in the iteration process. Furthermore, the computations were restricted to the nearfield, because of the enormous computation times required at larger ranges. Aanonsen et al.[6,8] studied the sound field from uniform sources as opposed to the study of Gaussian, polynomial and exponential shaped sources carried out in the Soviet Union. Aanonsen et al.[9] and Hamilton et al.[10] continued the work of Aanonsen et al. in Refs. 6,8 and introduced a coordinate transform which facilitated computations beyond the nearfield. In the same article a seven point difference formula was used to approximate the Laplace operator in order to speed up the computations.

3.2.2. Improvement of numerical method

Analysis of two numerical techniques on a test problem

This subsection is based on a report written with Jarle Berntsen as coauthor, Ref. 7.

As we have mentioned earlier, different methods have been used to solve Eq. 2.3. To simplify the analysis of the different numerical methods, we consider the case of no absorption and no nonlinearity. In Ref. 18 and Ref. 19 the solution of the system of partial differential equations

$$\begin{aligned} \frac{\partial v}{\partial \sigma} &= -\frac{\partial^2 w}{\partial \xi^2}, \\ \frac{\partial w}{\partial \sigma} &= \frac{\partial^2 v}{\partial \xi^2}, \end{aligned} \tag{3.9}$$

subject to initial conditions $v(\sigma = 0, \xi) = v_0(\xi)$, $w(\sigma = 0, \xi) = w_0(\xi)$, and boundary conditions $v(\sigma, \xi = 0) = f_0(\sigma)$, $v(\sigma, \xi = 1) = f_1(\sigma)$, $w(\sigma, \xi = 0) = g_0(\sigma)$, $w(\sigma, \xi = 1) = g_1(\sigma)$, is studied. A numerical method for the solution of Eqs. 2.3 must be able to solve Eqs. 3.9 since these equations are a special case. We will describe a solution technique due to Richtmeyer[19].

We introduce some notation used by Fairweather and Gourlay[20]:

$$\Omega = \begin{bmatrix} v \\ w \end{bmatrix}, \tag{3.10}$$

$$A = \begin{bmatrix} 0 & -1 \\ 1 & 0 \end{bmatrix}. \tag{3.11}$$

Equation 3.9 may then be written

$$\frac{\partial \Omega}{\partial \sigma} = A \frac{\partial^2 \Omega}{\partial^2 \xi}. \tag{3.12}$$

A rectangular network of points with mesh sizes k and h in the σ and ξ directions respectively, where Nh=1, is superimposed on the region $\sigma \geq 0$, $0 \leq \xi \leq 1$. The

values of the functions $v(\sigma,\xi)$, $w(\sigma,\xi)$ and $\Omega(\sigma,\xi)$ at the mesh points $\xi = ih$, $\sigma = nk, (n = 0,1,...; i = 0,1,...,N)$ are given by $v_{n,i}$, $w_{n,i}$ and $\Omega_{n,i}$ respectively.

When we apply Crank-Nicholson's method [21] to Eq. 3.12, we obtain the algorithm used by Richtmeyer in the form

$$(I - \frac{1}{2}rA\delta_\xi^2)\Omega_{n+1,i} = (I + \frac{1}{2}rA\delta_\xi^2)\Omega_{n,i}, \tag{3.13}$$

where $r = k/h^2$ and $i = 1,...,N-1$. I is the 2×2 unit matrix, and δ_ξ^2 is the central difference operator in the ξ-direction.

For each σ step we have to solve a system of $(N-1)$ linear equations for the $(N-1)$ unknowns

$$\Omega_{n,i} = \begin{pmatrix} v_{n,i} \\ w_{n,i} \end{pmatrix}, \tag{3.14}$$

which can be written in the form

$$A_1 W_{n+1} = B_1 W_n + c, \tag{3.15}$$

where $W_m = [\Omega_{m,1},...,\Omega_{m,N-1}]^T$, $m = n, n+1$, and c is a constant arising from the boundary conditions. A_1 and B_1 are given by

$$A_1 = I + \frac{1}{2}rT, \tag{3.16}$$

$$B_1 = I - \frac{1}{2}rT, \tag{3.17}$$

where I is the identity matrix, and T is a block tridiagonal matrix given by

$$T = \begin{pmatrix} 2A & -A & & & \\ -A & 2A & -A & & \\ & \ddots & \ddots & \ddots & \\ & & -A & 2A & -A \\ & & & -A & 2A \end{pmatrix}. \tag{3.18}$$

The block tridiagonal system Eq. 3.15 may be solved by the well known algorithm described in Ref.19 where also the stability properties of the algorithm are proved to be very satisfactory.

If we integrate the nonlinear terms in Eqs. 2.3 by an explicit difference formula, the described method for solving Eqs. 3.9 may also be applied to Eqs. 2.3 . If we compare this method with the method described and used by Aanonsen et al.[6,8], we find that the two methods differ in two ways:

1. Richtmeyer's method uses an implicit second order approximation in the σ-direction, whereas the method of Aanonsen et al.[6,8] uses a fully implicit first order approximation.

2. The numbering of the linear equations is different. If we use the notation of Eqs. 3.10 and 3.11, we transform the wide band matrix into a narrow band matrix which can be solved by a direct method. In Ref. 6,8 an iterative solution is used for solving the linear system of equations appearing in each step in the σ-direction. In order to make the iterations converge, we have to impose constraints on the stepsize in the σ-direction ($r \leq 1/2$). When we apply Richtmeyer's method, we have no such constraints on the stepsize, and moreover, the solution of Eq. 3.15 is very stable. Tests show that we obtain W_{N+1} to almost full machine precision.

We have tried to use Richtmeyer's method to solve Eqs. 2.3. In Ref. 20 Eqs. 3.9 is used as a test problem together with the initial and boundary conditions:

$$\Omega(\sigma = 0, \xi) = \begin{pmatrix} 0 \\ \xi - \xi^2 \end{pmatrix},$$

$$\Omega(\sigma, \xi = 1) = \Omega(\sigma, \xi = 1) = \begin{pmatrix} 0 \\ 0 \end{pmatrix}. \qquad (3.19)$$

Where $\sigma \geq 0$ and $0 \leq \xi \leq 1$. This problem has a simple analytical solution, see Ref.20. The numerical solution compared very well to the analytical solution. For

a uniform piston, the initial conditions are discontinuous and the solution is highly oscillatory. If we replace Eqs. 3.19 with

$$\Omega(\sigma = 0, \xi) = \begin{pmatrix} 0 \\ 0 \end{pmatrix}, \tag{3.20}$$

when $0 \leq \xi \leq 0.1$ and $0.9 \leq \xi \leq 1.0$ and with

$$\Omega(\sigma = 0, \xi) = \begin{pmatrix} 1 \\ 1 \end{pmatrix}, \tag{3.21}$$

when $0.1 \leq \xi \leq 0.9$ and with

$$\Omega(\sigma, \xi = 0) = \Omega(\sigma, \xi = 1) = \begin{pmatrix} 0 \\ 0 \end{pmatrix}, \tag{3.22}$$

when $\sigma \geq 0$, and solve this problem using Richtmeyer's method, artificial numerical oscillations appear in the solution. We replaced the second order method with the fully implicit method and solved the same problem with the result that the oscillations disappeared. In Fig. 3.1 we have plotted the numerical approximations to $v(\sigma = 0.2, \xi)$ given by the two methods, with h=0.05 and k=0.00125. The plots for $w(\sigma = 0.2, \xi)$ are similar. The explanation of this phenomenon must lie in the stability properties of the two methods. In Ref. 19 Richtmeyer applies von Neumann's technique for studying stability properties of his second order method. He defines

$$\omega = 4r[\sin(\beta h/2)]^2. \tag{3.23}$$

The amplification matrix is then given by

$$H_1 = \frac{1}{1 + \omega^2/4} \begin{pmatrix} 1 - \omega^2/4 & \omega \\ -\omega & 1 - \omega^2/4 \end{pmatrix}. \tag{3.24}$$

The eigenvalues of H_1 lie on the unit circle, and the numerical solution is always stable.

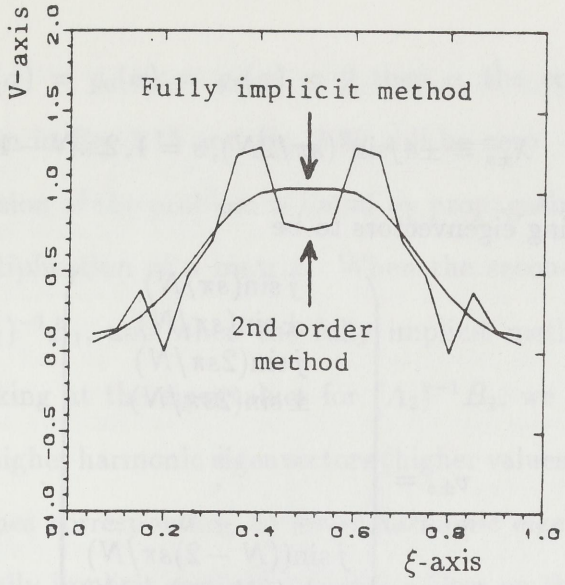

FIG. 3.1. Numerical approximations to $v(\sigma = 0.2, \xi)$ versus ξ.

We have used the same technique to study the stability properties of the fully implicit method applied to Eqs. 3.9, and the amplification matrix is

$$H_2 = \frac{1}{1+\omega^2} \begin{pmatrix} 1 & \omega \\ -\omega & 1 \end{pmatrix}. \tag{3.25}$$

The eigenvalues of this matrix are

$$\lambda_{1,2} = \frac{1 \pm j\omega}{1+\omega^2}, \tag{3.26}$$

and consequently, for βh close to odd multiplies of π, we should have a dramatic (and unphysical) numerical damping when we apply the fully implicit method.

When we apply the fully implicit method to Eqs. 3.9 with the initial and boundary conditions given by Eqs. 3.20, 3.21, and 3.22, the damping effect is almost negligible compared to what could be expected from Eq. 3.26. We have therefore applied the matrix method, see Ref. 21, in order to study in more detail the stability properties of the two methods. The eigenvectors of the matrices A_1 and B_1 are the same as the eigenvectors of the matrix T. Using the theory in Ref. 21 we find the eigenvalues of

T to be

$$\lambda_{\pm s} = \pm 4j\sin^2(s\pi/2N), s = 1, 2...N-1, \tag{3.27}$$

and the corresponding eigenvectors to be

$$v_{\pm s} = \begin{pmatrix} j\sin(s\pi/N) \\ \pm\sin(s\pi/N) \\ j\sin(2s\pi/N) \\ \pm\sin(2s\pi/N) \\ \cdot \\ \cdot \\ \cdot \\ j\sin((N-2)s\pi/N) \\ \pm\sin((N-2)s\pi/N) \\ j\sin((N-1)s\pi/N) \\ \pm\sin((N-1)s\pi/N) \end{pmatrix}. \tag{3.28}$$

We observe that the eigenvectors appear like components of a discrete Fourier series. The eigenvalues of $(A_1)^{-1}B_1$ will then be

$$\lambda_{\pm s} = \frac{1 \mp 2rj\sin^2(s\pi/2N)}{1 \pm 2rj\sin^2(s\pi/2N)}, \tag{3.29}$$

which lie on the unit circle.

When we apply the fully implicit method to Eqs. 3.9, the corresponding system of linear equations may be written

$$A_2 W_{n+1} = B_2 W_n + c, \tag{3.30}$$

where $A_2 = I + rT$ and $B_2 = I$. The eigenvectors of $(A_2)^{-1}B_2$ are given by Eq. 3.28, and the corresponding eigenvalues are

$$\lambda_{\pm s} = \frac{1 \mp 4rj\sin^2(s\pi/2N)}{1 + 16r^2\sin^4(s\pi/2N)}, \tag{3.31}$$

which all lie inside the unit circle. This means that we get the damping predicted from Eq. 3.26, but the damping will depend on s. We shall take a closer look at what this means.

If $f_0(\sigma) = f_1(\sigma) = g_0(\sigma) = g_1(\sigma) = 0$ then c, the constant arising from the boundary condition in Eq. 3.15 and Eq. 3.30 will be zero. In this case the solution of the discrete version of the problem is found by propagating the vector Ω from the boundary by multiplication of a matrix. When the second order method is used, this matrix is $(A_1)^{-1}B_1$, and when the fully implicit method is used, this matrix is $(A_2)^{-1}B_2$. Looking at the eigenvalues for $(A_2)^{-1}B_2$, we see that the eigenvalues corresponding to higher harmonic eigenvectors (higher values of s) is lower in modulus than the eigenvalues corresponding to lower harmonic eigenvectors. This property implies that the fully implicit method acts like a filter on the solution i.e., the rapid oscillations are damped. For the second order method there is no damping of any component and therefore no filtering.

We can express the initial value of Ω as a linear combination of the eigenvectors Eq. 3.28. If the boundary condition is slowly varying then Ω is represented well by the lower harmonic eigenvectors (small values of s) which means that there are no problems associated with ripples. When a discontinuous boundary condition is used, all of the harmonic eigenvectors are present. Attempting to represent a rapid varying function by a Fourier series with too few terms gives rise to Gibbs oscillations. The ripples are representing higher harmonic eigenvectors, and this explains why the fully implicit method works better than the second order method on problems with discontinuous boundary conditions. The ripples are filtered out because of the artificial damping inherent in the fully implicit method.

Another aspect of the analysis is that when using the fully implicit method, care must be taken when choosing step sizes in order to avoid unacceptable numerical damping.

Finite difference approximation across the beam

In both Ref. 16 and Ref. 8 the Laplace operator was approximated by a three point formula. Later in Refs. 9,10 the three point formula was replaced by a seven point formula. It was argued that using a seven point method instead of a three point method made the computations more efficient. In their case where an iterative technique was used, the increase from a three point formula to a seven point formula was inexpensive in terms of computation time.

In Ref. 17 three subroutines were given which attempted to solve a generalized KZK equation. The subroutines differed in the way the Laplacian was approximated. The Laplace operator was approximated by the usual three point formula, a five point formula and a seven point formula. An analysis of the algorithms involved showed that the time required increased rapidly with number of points used to approximate the Laplacian. To compare the different subroutines, they were applied to a test problem. The conclusion of the limited experiments was that the three point method was the one to prefer, at least when a small number of harmonics were retained in the calculations.

Numerical tests were also performed in Ref. 7, in order to study the damping effect of the fully implicit method for various step sizes along and across axis of propagation. The tests showed that the step size along axis could be increased by a factor of 10 compared to the method of Refs.6,8.

Adjustments to make the second order method applicable

In Ref. 22 Berntsen used the insight gained in Ref. 7 to make the Crank-Nicholson procedure applicable for discontinuous boundary conditions. He argued in the following way: The first order implicit method gives accurate results for small step sizes,

and it acts like a filter on the solution. Berntsen's idea was to use a filter similar to the effect of taking some steps with the fully implicit method on the boundary condition and then use the second order method. He used the Fast Fourier Transform to filter the boundary condition. Berntsen[23] later suggested a better way to make the second order method applicable. The original boundary conditions were used, and for the first few steps the fully implicit method was applied. After these initial fully implicit steps, the second order method is used all the way, except for an implicit step at regular intervals to ensure that no ripples occur. The advantage is that the FFT routine is not needed, and that the creation of ripples is constantly checked.

Different integration widths for different harmonic components

In the program described in Ref. 8 which solves the KZK equation, the same integration region was used for all harmonic components. The fact that higher harmonic components are much more directive than lower harmonic components, and consequently do not require as wide integration regions as lower harmonic components, was not utilized to make the computations more efficient. The code was modified to use dynamic variables which allows the user to specify different integration widths for different harmonic components. When several harmonic components are included, this technique reduce the computation time by a factor of four.

Stabilization procedure

Truncating the infinite number of harmonic components in the Fourier series expansion of the solution of the KZK equation can cause problems. Trivett and Van Buren[24] who studied plane, cylindrical and spherical waves, found that a simple truncation of the Fourier series was insufficient when attempts were made to examine the

propagation of sound beams beyond the shock formation distance. The flow of energy from lower to higher harmonic components terminates with the last harmonic component retained in the series. The calculated value of the last harmonic component may become abnormally large relative to the lowest harmonic components. Trivett and Van Buren circumvented this problem by requiring that the amplitude of a higher harmonic component never exceeded the amplitude of a lower harmonic component. In Ref. 8 Aanonsen compared results of computations made with and without this requirement. He considered the case of plane wave propagation. His conclusion was that the simple truncation of the series did not lead to any significant error in the lowest harmonic components as long as the value of Γ is not too large. If Γ took a larger value, greater than 100-150, an instability could occur if the integration exceeded the shock formation distance. Aanonsen did not apply any amplitude modification is his programs for computing the field of a sound beam.

We want to avoid the risk of instability when computing the field of sound beams. The nonlinear effects are strongest along the axis of propagation, so that is where we suspect an eventual instability to occur. Because of the rapid oscillations in the nearfield, we cannot impose an amplitude requirement there. The requirement should be imposed from a point in the transition region (the region between the nearfield and the farfield) and beyond. We have implemented this modification, and tests shows that this requirement prevents instability.

We are also interested in computing the soundfield from a bifrequency source. How do we generalize the amplitude requirement in this case? Instead of comparing amplitudes of individual harmonic components, we can compare the energy of families of harmonic components. We could define the n'th order family as all the harmonic components of n'th order, where the ordering of the harmonic components

is as described in Sec. 3.1, and require that the energy in a higher order family is lower than the energy in a lower order family. This requirement imposes for instance the difference frequency component to have less energy than the primary components, which is an unproper requirement for long range propagation in media with high absorption. If we redefine the families to include only the harmonic components which are higher in frequency than those in the previous family, we have a better requirement. This requirement was first used to study plane parametric radiation. Without this requirement the amplitude of the difference frequency wave was overestimated, and the modification was indeed needed to avoid a numerical instability beyond the shock formation distance.

For the case of parametrically generated beams, we have to impose the requirement beyond some point in the transition zone of both primaries.

Chapter 4

Applications

4.1. Interaction between two beams

4.1.1. Introduction

One of the best known applications of nonlinear acoustics is the parametric array, which was first suggested by Westervelt[1]. The principle is that two high frequency sound beams, called primaries, interact nonlinearly to produce a sound beam of frequency equal to the difference between the primary frequencies. The parametric array creates a difference frequency wave with high directivity, and practically no sidelobes. Because the difference frequency is much lower than the primary frequencies, the difference frequency wave is much less affected by absorption than the primaries, and can therefore be the only survivor at several absorption lengths from the source. Another advantage is that large relative changes in the difference frequency can be achieved by small relative changes in the primary frequencies. The low efficiency of the parametric array is the weak part of it. When the parametric array is operated at high amplitude, the effect of nonlinear damping must be taken into account. For the case of low amplitudes, a quasilinear analysis can be applied. Quasilinear analysis means that the linear solutions for the primary sound fields are

inserted into the nonlinear sourceterms of the governing equations. The equations for the difference frequency, sum frequency and second harmonic sound fields then becomes linear, which simplifies the analysis considerably.

Westervelt's analysis [1] was quasilinear, and he assumed that the interaction was absorption limited to the nearfield. He furthermore assumed that the primary components could be modeled by perfectly plane collimated beams in the nearfield and ignored the finite width of the beam. Westervelt also assumed that the observation of the difference frequency wave took place outside the interaction region. Naze Tjøtta and Tjøtta[25] later modified Westervelt's model to account for finite width of the beam and included phase variations across the beams. This lead to an aperture factor correction. Westervelt's theoretical findings were later verified experimentally by Bellin and Beyer[26].

Studies of the parametric array, both experimental and theoretical, were initiated in several countries following the article by Westervelt.

Lauvstad, Naze and Tjøtta[27] studied the nonlinear interaction of two spherically spreading waves. Berktay[28,29] modified Westervelt's model to cases where the primary waves were spreading cylindrically or spherically. Applications of acoustic nonlinearities to sonar systems were discussed and evaluated.

Muir and Willette[30] obtained numerical solutions of Westervelt's inhomogeneous wave equation to descriebe the difference frequency wave and the sum frequency wave in the farfield of a circular uniform source. Experimental results supported the numerical solutions.

The nearfield of the parametric array was considered by Hobæk[31] and by Hobæk and Vestrheim[32,33]. A model of plane collimated primary waves was applied. The effect of nonlinear damping of the primary waves was included in the model. Exper-

iments compared favourably with their model.

Bartram[34] introduced a model for nonlinear damped parametric arrays. His model is closely related to Westervelts. The modification he made was to replace the simple linear damping by the damping for a shocked sound wave. Merklinger[35] studied finite amplitude effects in plane waves. He found that the nonlinear damping could be described by a simple taper function. Later Merklinger et al.[36] used the same approach to study finite amplitude losses in spherical waves. Mellen and Moffett[37] also developed a model for the difference frequency wave generated by a parametric source. The primary waves were assumed to be radiated by a piston source, but modeled as plane waves out to the Rayleigh distance and spherically spreading beyond that range. Taper functions were used to account for nonlinear damping. The theoretical results were found to be in fair agreement with experimental results. In Ref. 38 Mellen and Moffett devoted their attention to the nearfield of parametric sources. Their previously developed model was compared with experimental data from several sources.

Recently a textbook devoted to parametric arrays written by Novikov et al.[39] was translated to English. The textbook includes results from theoretical and experimental investigations of the parametric array, and a description of parametric apparatus. A series of papers have used the KZK equation as a basis. In Ref. 40 Novikov et al. studied the parametric array in the quasilinear approximation and neglected diffraction of the primary waves. Later in Ref. 41 the constraint of nondiffracting primary waves was removed, but the primary waves were assumed to have a Gaussian distribution at the source. An integral solution was found which compared well to experimental results.

A textbook written by Bakhvalov et al.[42] has also recently been translated to En-

glish. This textbook reviews results from numerical solution of the KZK equation. The monochromatic case was studied by Bakhvalov et al. in Refs. 43,44,45,46,47. All articles were concerned with Gaussian or polynomial boundary conditions except for Ref. 47 which was concerned with an exponential boundary condition. The computations were restricted to the nearfield. Waveforms and amplitude distributions for different harmonic components along and across axis, zones of existence of shock waves, distribution of initial phases and intensity were calculated. In Ref. 48,49 the same methods were used to analyze the parametric array. Again only Gaussian and polynomial boundary conditions were used. The difference frequency wave was computed for various levels of nonlinearity, absorption and downshift ratio, f_m/f_-, ($f_m = (f_1 + f_2)/2$ and $f_- = f_1 - f_2$). Amplitude modulated signals were studied in Ref. 48, while bifrequency signals were studied in Ref. 49. In Ref. 49 results are only shown for ranges less than a couple of Rayleigh distances.

Several articles on nonlinear acoustics have been written by Naze Tjøtta and Tjøtta and coworkers the last decade. In Ref. 50 the linear nearfield of a uniform source was investigated. The validity of the parabolic equation was studied, and some properties of the solution were derived. Naze Tjøtta and Tjøtta [14] derived the KZK equation in a new way, and applications were made to parametric arrays. A series of papers [51,52,53,54] were devoted to the nearfield of a large acoustic transducer. Linear radiation, second harmonic generation and parametric generation were considered. Quasilinear parabolic models were developed and compared to experimental results. Asymptotic formulas were also derived. A computer program was developed to solve the nonlinear KZK equation[8], and used to study the nearfield of a monocromatic finite amplitude sound beam [6].

The computations were later extended to the farfield [9,10]. A transformation was

introduced which made the analysis of the farfield possible. The numerical results were successfully compared to experimental results. The transition from the nearfield solution to the spherical solution was studied.

Baker et al.[55] measured the nearfield pressure of a monofrequency circular piston operating at high amplitude. The measurements were compared to numerical results obtained from the computer program introduced in Refs. 6,8. Comparison were made for the fundamental, second and third harmonic components, and good agreement was shown.

Kamakura et al.[56] also measured the nearfield pressure of a circular piston operating at high amplitude. Both monofrequency and bifrequency excitation were used. The measurements compared well to results from computations using the computer program of Refs.6,8. A disadvantage of applying Aanonsen's program[8] directly to the bifrequency case is that a large number of harmonic components have to be retained when high downshift ratios are considered. This is caused by the fact that all the successive harmonic components up to a certain limit are retained. If the method of Refs. 6,8 was modified to include our selection procedure (See Sec. 3.1), and different integration regions for different harmonic components were used, the computation time would still be about a factor of $10 f_m/f_-$ times the computation time of our method.

In order to study the interaction between two soundbeams we will use a transform similar to the one used by Aanonsen et al. [9] and Hamilton et al. [10]:

$$\begin{aligned} \sigma_{bb} &= z/r_m\,, \\ \tau_{bb} &= \tau - \xi^2/[n_m(\sigma_{bb}+1)]\,, \\ \underline{u}_{bb} &= \underline{\xi}/(\sigma_{bb}+1)\,, \\ T_{bb} &= (\sigma_{bb}+1)\overline{p}\,, \end{aligned} \tag{4.1}$$

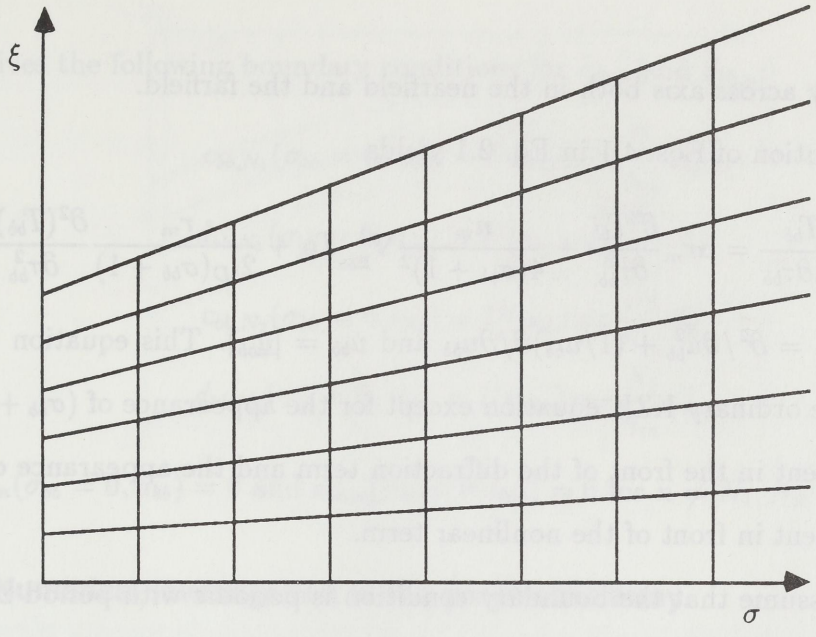

FIG. 4.1. The numerical integration region for the transformed equation shown in the cartesian coordinate system

where $r_m = k_m a^2/2$ is the Rayleigh distance for the mean primary frequency, $k_m = (k_1 + k_2)/2$, $k_1 = 2\pi f_1/c_0$, $k_2 = 2\pi f_2/c_0$ and $n_m = (N_1 + N_2)/2$. The retarded time τ_{bb} is close to the retarded time for a plane wave in the nearfield and close to the retarded time for a spherical spreading wave in the farfield. By introducing T_{bb} the effect of spherical spreading is factored out. The same transform can be used for focusing with converging geometry before focus and diverging geometry after focus. We will consider focusing in Sec. 4.2.2.

The new variables are more appropriate than the old ones for two reasons. First, the region of integration is changed from a rectangular one to a region which extends in ξ - direction as σ increases, see Fig. 4.1. This change of integration region has for effect to remove the problems of reflections from the artifical boundary which is introduced in order to terminate the discretization in the ξ - direction. Second, the introduction of the new retarded time makes the transformed pressure T_{bb} change

more slowly across axis both in the nearfield and the farfield.

Substitution of Eqs. 4.1 in Eq. 2.1 yields

$$\frac{\partial^2 T_{bb}}{\partial\sigma_{bb}\partial\tau_{bb}} = \alpha r_m \frac{\partial^3 T_{bb}}{\partial\tau_{bb}^3} + \frac{n_m}{4(\sigma_{bb}+1)^2}\nabla^2_{\underline{u}_{bb}} T_{bb} + \frac{r_m}{2l_D(\sigma_{bb}+1)}\frac{\partial^2 (T_{bb})^2}{\partial\tau_{bb}^2} \tag{4.2}$$

where $\nabla^2_{\underline{u}_{bb}} = \partial^2/\partial u_{bb}^2 + (1/u_{bb})\partial/\partial u_{bb}$ and $u_{bb} = |\underline{u}_{bb}|$. This equation has the same form as the ordinary KZK equation except for the appearance of $(\sigma_{bb}+1)$ and n_m in the coefficient in the front of the diffraction term and the appearance of $(\sigma_{bb}+1)$ in the coefficient in front of the nonlinear term.

If we assume that the boundary condition is periodic with period $2\pi\omega^{-1}$, we can seek a solution of Eq. 4.2 in the form of a Fourier series

$$T_{bb} = \sum_{n=1}^{\infty}(c_{bb,n}\cos n\tau_{bb} + d_{bb,n}\sin n\tau_{bb}), \tag{4.3}$$

where $c_{bb,n}$ and $d_{bb,n}$ are functions of spatial variables. Substituting Eq. 4.3 in Eq. 4.2, we obtain

$$\begin{aligned}
&\frac{\partial c_{bb,n}}{\partial\sigma_{bb}} = -\alpha r_m n^2 c_{bb,n} - \frac{n_m}{4n(\sigma_{bb}+1)^2}\nabla^2_{\underline{u}_{bb}} d_{bb,n} + \\
&\quad \frac{r_m n}{2l_D(\sigma_{bb}+1)}\left[\sum_{i=1}^{n-1}(c_{bb,n-i}d_{bb,i}) + \sum_{i=n+1}^{\infty}(d_{bb,i}c_{bb,i-n} - c_{bb,i}d_{bb,i-n})\right], \\
&\frac{\partial d_{bb,n}}{\partial\sigma_{bb}} = -\alpha r_m n^2 d_{bb,n} + \frac{n_m}{4n(\sigma_{bb}+1)^2}\nabla^2_{\underline{u}_{bb}} c_{bb,n} + \\
&\quad \frac{r_m n}{2l_D(\sigma_{bb}+1)}\left[\frac{1}{2}\sum_{i=1}^{n-1}(d_{bb,n-i}d_{bb,i} - c_{bb,n-i}c_{bb,i}) - \sum_{i=n+1}^{\infty}(c_{bb,i}c_{bb,i-n} + d_{bb,i}d_{bb,i-n})\right], \\
&n = 1, 2, \ldots.
\end{aligned} \tag{4.4}$$

For an axisymmetric source that oscillates bisinusoidally with uniform amplitude distribution, the boundary condition is

$$\overline{p}(\sigma = 0, \underline{\xi}, \tau) = U(|\underline{\xi}|)\sin N_1\tau + U(|\underline{\xi}|)\sin N_2\tau, \tag{4.5}$$

which gives the following boundary conditions for $c_{bb,n}$ and $d_{bb,n}$:

$$c_{bb,N_1}(\sigma_{bb} = 0, u_{bb}) = U(u_{bb}) \sin \frac{N_1}{n_m} u_{bb}^2 \tag{4.6}$$

$$d_{bb,N_1}(\sigma_{bb} = 0, u_{bb}) = U(u_{bb}) \cos \frac{N_1}{n_m} u_{bb}^2 \tag{4.7}$$

$$c_{bb,N_2}(\sigma_{bb} = 0, u_{bb}) = U(u_{bb}) \sin \frac{N_2}{n_m} u_{bb}^2 \tag{4.8}$$

$$d_{bb,N_2}(\sigma_{bb} = 0, u_{bb}) = U(u_{bb}) \cos \frac{N_2}{n_m} u_{bb}^2 \tag{4.9}$$

with $c_{bb,n}(\sigma_{bb} = 0, u_{bb}) = 0$ and $d_{bb,n}(\sigma_{bb} = 0, u_{bb}) = 0$ for $n \neq N_1, N_2$

4.1.2. Numerical investigation of the parametric array

We have three nondimensional parameters to consider when we study the parametric array. These parameters are

$\alpha_m r_m$ = Rayleigh distance relative to absorption length,

r_m / l_{Dm} = Rayleigh distance relative to shock formation distance,

f_m / f_- = Ratio between mean primary frequency and difference frequency .

The parameters $\alpha_m r_m$ and r_m / l_{Dm} refer to the mean primary frequency f_m. Since nondimensional variables are used, one may consider that the radius a and the mean primary frequency f_m are given, so that the Rayleigh distance r_m for the mean primary frequency is fixed but not specified. Varying the absorption coefficient and the on-source peak amplitude then corresponds to varying $\alpha_m r_m$ and r_m / l_{Dm}, respectively. Varying the primary frequencies with the constraint of keeping their mean value fixed corresponds to varying the ratio f_m / f_-.

Garrett et al.[52] and Berntsen et al.[54] obtained an integral representation for the difference frequency wave within the quasilinear approximation. The integral was evaluated by numerical methods. In Fig. 4.2 comparisons have been made between

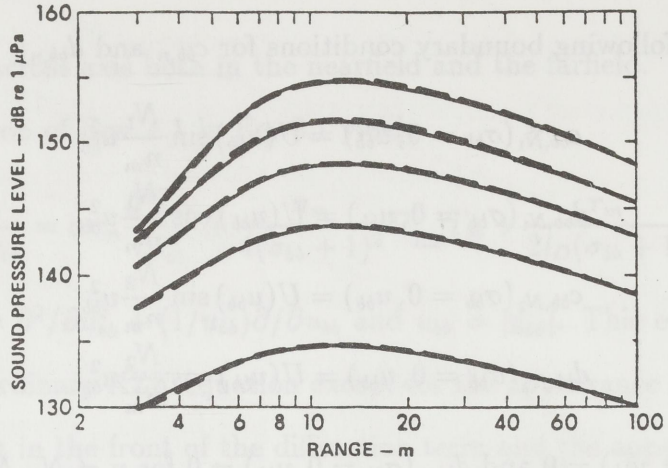

FIG. 4.2. On-axis pressure amplitude of the difference frequency wave versus range for various values of the difference frequency. From Fig. 3 of Ref. 52(———), and computed using Eq. 4.4(— —).

results for the difference frequency waves shown in Fig. 3 of Ref. 52 and results for the difference frequency waves computed using Eqs. 4.4. The parameters used are c_0 = 1494.7 m/s and a = 0.87 m, for difference frequencies 1, 2 and 3kHz and a_1 = 0.87 m, a_2 = 0.83 m for 4 and 5 kHz, where a_1 is the source radius for the primary with frequency f_1 and a_2 is the source radius for the primary with frequency f_2. Table I in Ref. 52 shows the primary frequencies corresponding to the various difference frequencies. We observe that the results for the difference frequency wave computed using Eqs. 4.4 compares well to the results obtained in Ref. 52.

Moffett and Mellen[37] have measured the difference frequency wave for source levels sufficiently high to make nonlinear damping important. The amplitude of the difference frequency wave was measured at a fixed distance of 84.5 m from the source for various downshift ratios and various source levels. The mean primary frequency was 245 kHz, the radius of the source was 12.7 cm, the downshift ratios were 4.9, 9.8, 19.6 and 49.0, c_0 = 1500 m/s, r_m = 8.276 m, $\alpha_m r_m$ = 0.076 and β = 3.5. The source

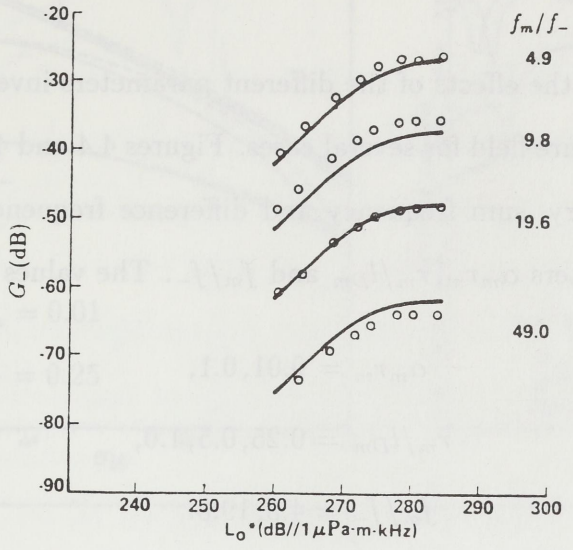

FIG. 4.3. On-axis parametric gains G_- at $\sigma = 10.21$ as a function of primary source level for different downshift ratios, measured by Moffett and Mellen (o o), and computed using Eqs. 4.4(———).

level was varied so that $0.09 \leq r_m/l_{Dm} \leq 1.5$. The results are shown in Fig. 4.3. The on axis pressure amplitude of the difference frequency wave is given in terms of parametric gain G_- defined by

$$G_- = 20 \log_{10} \left(\overline{p}_-(\sigma_{bb}, 0) \right) \sigma_{bb}, \tag{4.10}$$

where $\overline{p}_- = p_-/P_0$ and p_- is the difference frequency component of the acoustic pressure. The primary source level is given in terms of L_0^* defined by

$$L_0^*(dB/1\mu Pa - m - kHz) = 20 \log_{10}(P_0 r_m/\sqrt{2}) + 20 \log_{10} f_m(kHz). \tag{4.11}$$

For $f_m/f_- = 19.6$ there is very good agreement between measurements and computations. The computed curve is below the measurements for $f_m/f_- = 4.9, 9.8$ and above the measurements for $f_m/f_- = 49$. The systematic measurement errors were estimated to be less than ± 2 dB. Moffett and Mellen compared their experimental results to theory they developed. We will later in this section return to their theory and how it compared to the experimental results.

In order to study the effects of the different parameters involved, we have calculated the sound pressure field for several cases. Figures 4.4 and 4.5 show propagation curves for the primary, sum frequency and difference frequency waves for various values of the parameters $\alpha_m r_m, r_m/l_{Dm}$ and f_m/f_-. The values used are

$$\alpha_m r_m = 0.01, 0.1, \tag{4.12}$$

$$r_m/l_{Dm} = 0.25, 0.5, 1.0, \tag{4.13}$$

$$f_m/f_- = 4.5, 19.5. \tag{4.14}$$

The results of the computations have been compared with linear theory for the primary waves, and quasilinear theory for the sum and difference frequency waves. For low amplitudes [51,52,53,54] results obtained using linear and quasilinear theory compare very well with experiments. The solid lines represent fully nonlinear theory, and dashed lines represent linear theory for the primariy waves and quasilinear theory for the sum and difference frequency waves. The discrepancy between the fully nonlinear and the linear/quasilinear theory is caused by nonlinear damping. A general trend is that the linear/quasilinear theory compares better with fully nonlinear theory for higher absorption. Computations have also been made for $\alpha_m r_m = 1.0$. In this case the agreement between fully nonlinear theory and linear/quasilinear theory is perfect for $r_m/l_{Dm} = 0.25, 0.5$ and nearly perfect for $r_m/l_{Dm} = 1.0$. When the absorption is high, the amplitudes decay quickly and the nonlinear effects become less important. The nonlinear damping occurs because higher harmonic components are generated. Absorption affects the higher harmonic components more than the lower harmonic components, because of frequency dependence of the absorption. This also suggests that fully nonlinear theory compares better with linear/quasilinear theory for higher absorption. As expected, fully nonlinear theory compares better with

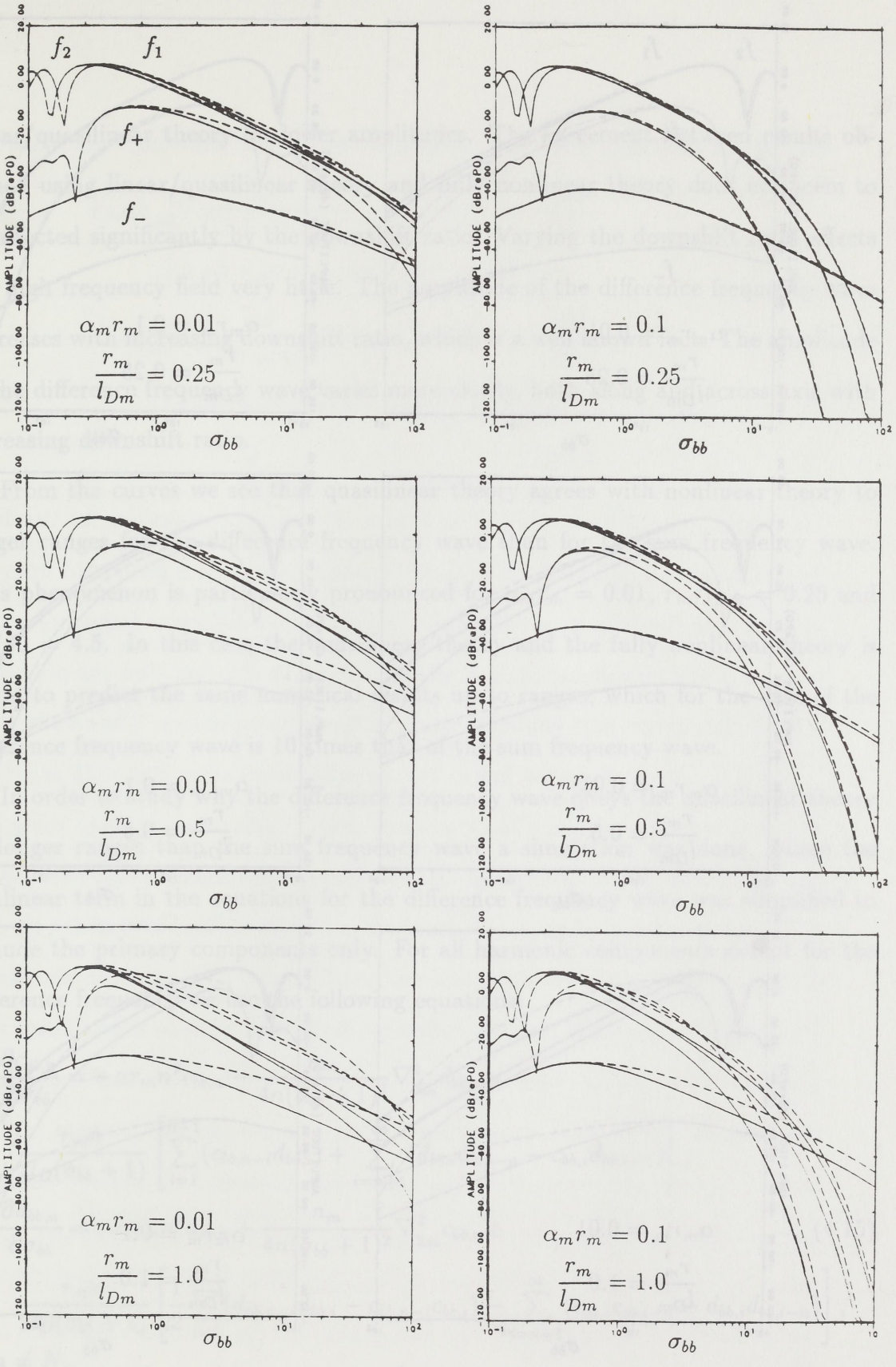

FIG. 4.4. On-axis amplitude of the primary, sum frequency and difference frequency waves, with $f_m/f_- = 4.5$. Fully nonlinear theory (———), and linear/quasilinear theory (— — —).

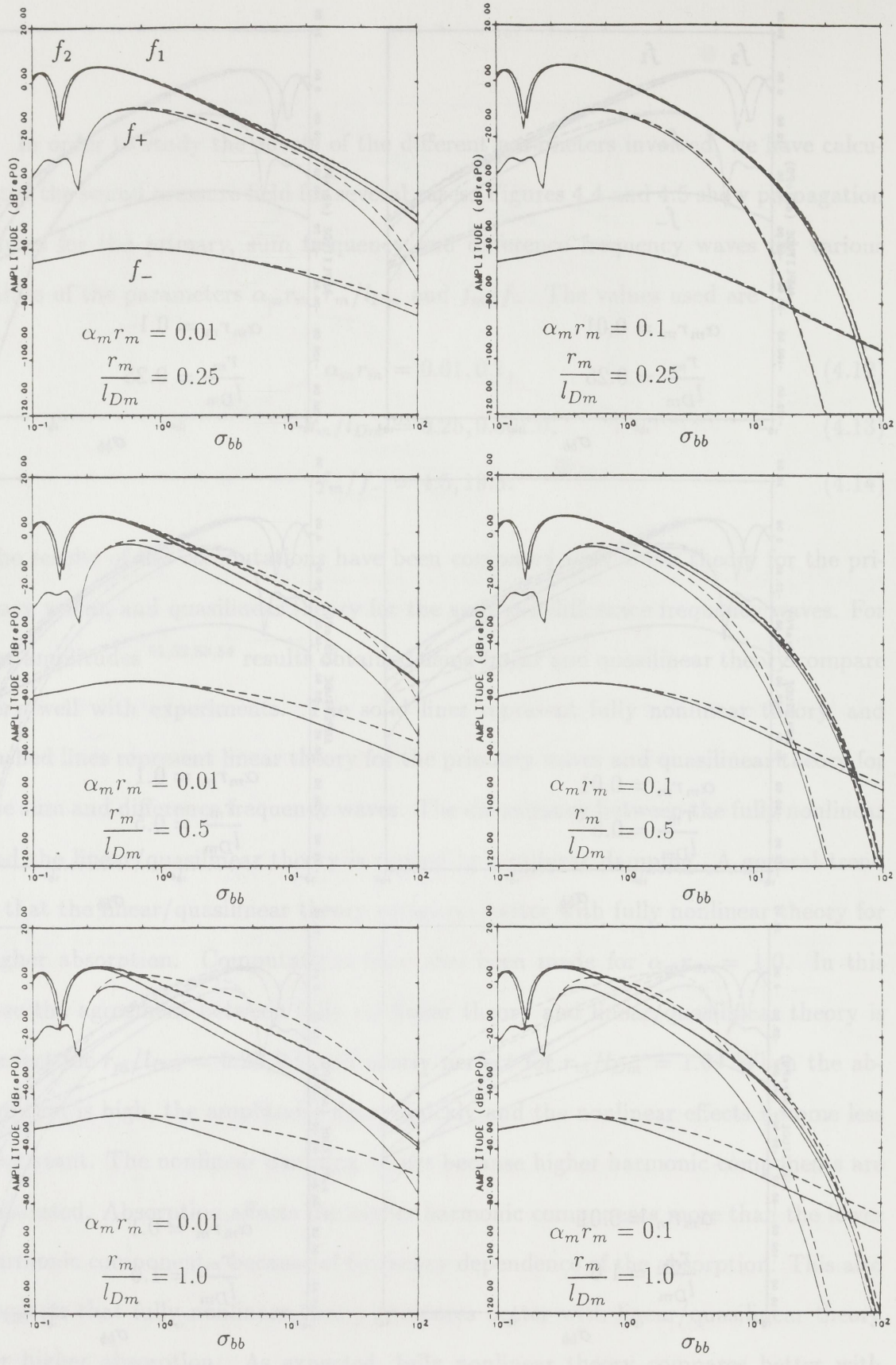

FIG. 4.5. On-axis amplitude of the primary, sum frequency and difference frequency waves, with $f_m/f_- = 19.5$. Fully nonlinear theory (———), and linear/quasilinear theory (— —).

linear/quasilinear theory for lower amplitudes. The agreement between results obtained using linear/quasilinear theory and fully nonlinear theory does not seem to be affected significantly by the downshift ratio. Varying the downshift ratio affects the high frequency field very little. The amplitude of the difference frequency wave decreases with increasing downshift ratio, which is a well known fact. The amplitude of the difference frequency wave varies more slowly, both along and across axis with increasing downshift ratio.

From the curves we see that quasilinear theory agrees with nonlinear theory to longer ranges for the difference frequency wave than for the sum frequency wave. This phenomenon is particularly pronounced for $\alpha_m r_m = 0.01$, $r_m/l_{Dm} = 0.25$ and $f_m/f_- = 4.5$. In this case the quasilinear theory and the fully nonlinear theory is found to predict the same numerical results up to ranges, which for the case of the difference frequency wave is 10 times that of the sum frequency wave.

In order to study why the difference frequency wave obeys the quasilinear theory to longer ranges than the sum frequency wave a simulation was done, where the nonlinear term in the equations for the difference frequency wave was simplified to include the primary components only. For all harmonic components except for the difference frequency we use the following equations:

$$\begin{aligned}
&\frac{\partial c_{bb,n}}{\partial \sigma_{bb}} = -\alpha r_m n^2 c_{bb,n} - \frac{n_m}{4n(\sigma_{bb}+1)^2}\nabla^2_{\underline{u}_{bb}} d_{bb,n} + \\
&\frac{r_m n}{2l_D(\sigma_{bb}+1)}\left[\sum_{i=1}^{n-1}(c_{bb,n-i}d_{bb,i}) + \sum_{i=n+1}^{\infty}(d_{bb,i}c_{bb,i-n} - c_{bb,i}d_{bb,i-n})\right], \\
&\frac{\partial d_{bb,n}}{\partial \sigma_{bb}} = -\alpha r_m n^2 d_{bb,n} + \frac{n_m}{4n(\sigma_{bb}+1)^2}\nabla^2_{\underline{u}_{bb}} c_{bb,n} + \\
&\frac{r_m n}{2l_D(\sigma_{bb}+1)}\left[\frac{1}{2}\sum_{i=1}^{n-1}(d_{bb,n-i}d_{bb,i} - c_{bb,n-i}c_{bb,i}) - \sum_{i=n+1}^{\infty}(c_{bb,i}c_{bb,i-n} + d_{bb,i}d_{bb,i-n})\right], \\
&n \neq N_-
\end{aligned} \tag{4.15}$$

and for the difference frequency component we use the following equations:

$$\begin{aligned}
&\frac{\partial c_{bb,n}}{\partial \sigma_{bb}} = -\alpha r_m n^2 c_{bb,n} - \frac{n_m}{4n(\sigma_{bb}+1)^2}\nabla^2_{\underline{u}_{bb}} d_{bb,n} + \\
&\frac{r_m n}{2l_D(\sigma_{bb}+1)}\left[d_{bb,N_1} c_{bb,N_2} - c_{bb,N_1} d_{bb,N_2}\right], \\
&\frac{\partial d_{bb,n}}{\partial \sigma_{bb}} = -\alpha r_m n^2 d_{bb,n} + \frac{n_m}{4n(\sigma_{bb}+1)^2}\nabla^2_{\underline{u}_{bb}} c_{bb,n} - \\
&\frac{r_m n}{2l_D(\sigma_{bb}+1)}\left[c_{bb,N_1} c_{bb,N_2} + d_{bb,N_1} d_{bb,N_2}\right], \\
&n = N_-
\end{aligned} \tag{4.16}$$

The implication of the simplified nonlinear terms in the equations for the difference frequency wave is that the difference frequency wave only is generated from interaction between the primary waves. The equation for the difference frequency wave is the same as in the quasilinear approximation, except for the fact that the primary waves are calculated with fully nonlinear theory and not linear theory. The results are shown in Fig. 4.6. The dash-dotted line is the result obtained using Eqs. 4.15 and 4.16. The solid line is fully nonlinear theory without any simplification obtained using Eqs. 4.4, and the dashed line is quasilinear theory. The computations clearly show that if the difference frequency wave is calculated on the basis of Eqs. 4.15 and 4.16, then the difference frequency wave departs from quasilinear theory at much shorter ranges. We are left to conclude that the difference frequency wave to a significant degree is generated from higher order interactions, for instance between the second harmonic and sum frequency wave components. This means that the decrease in difference frequency wave generation from the interaction between the primary waves, due to the fact that the primary waves are nonlinearly damped, to some extent is compensated by the generation of difference frequency wave from the interaction between higher harmonic components. This also shows that earlier results based on nonlinear tapering of the primary waves lead to wrong results.

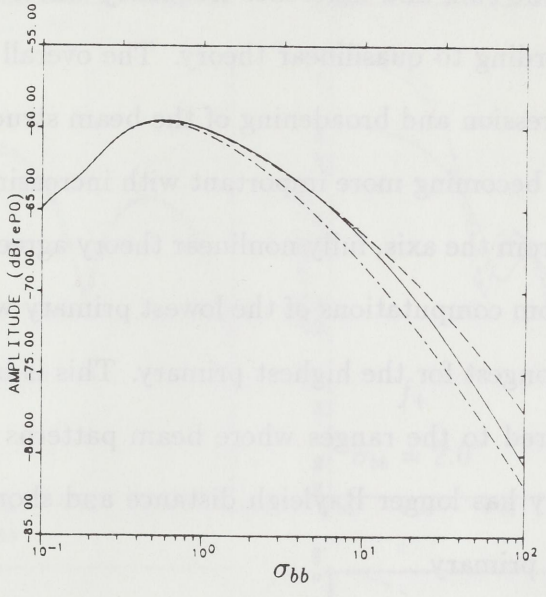

FIG. 4.6. On-axis amplitude of the difference frequency wave, with $\alpha_m r_m = 0.001$, $r_m/l_{Dm} = 0.25$ and $f_m/f_- = 19.5$. Fully nonlinear theory (———), quasilinear theory (— —), and computed using Eqs. 4.15and 4.16(— - —).

In Figs. 4.7 and 4.8 beampatterns are shown for the primary, sum frequency and difference frequency waves. The simulations have been done with $\alpha_m r_m = 0.01$, $r_m/l_{Dm} = 0.5, 1.0$ and $f_m/f_- = 4.5$. Results from computations are compared with linear theory for the primary waves and quasilinear theory for the sum and difference frequency waves. In order to illustrate the nonlinear effects the amplitudes of the primary (f_1) have been normalized to on-axis value according to linear theory and amplitudes of the sum and difference frequency waves have been normalized to on-axis value according to quasilinear theory. The overall effect of nonlinearity is seen to be the suppression and broadening of the beam structure near the axis, the effect of nonlinearity becoming more important with increasing range and source strength. Further away from the axis, fully nonlinear theory agrees with quasilinear/linear theory. Results from computations of the lowest primary wave shows that the nonlinear damping is strongest for the highest primary. This is because the absorption length is large compared to the ranges where beam patterns are calculated, and that the highest primary has longer Rayleigh distance and shorter shock formation distance than the lower primary.

We see that the beam structure for the primary and sum frequency waves is shifted outwards. This is not an effect that is caused by the fact that a bifrequency source is used. We have observed the same effect in the monofrequency case. To our knowledge this effect has not been reported before. We are not able to find an explanation for this phenomenon. A careful analysis is difficult to perform because of the presence of strong diffraction and nonlinearity.

In the beam pattern for the sum frequency wave we observe extra sidelobes called fingers [54]. In the case of a monofrequency source it is known that the harmonic component number n has $n-1$ fingers between two consecutive sidelobes, and that

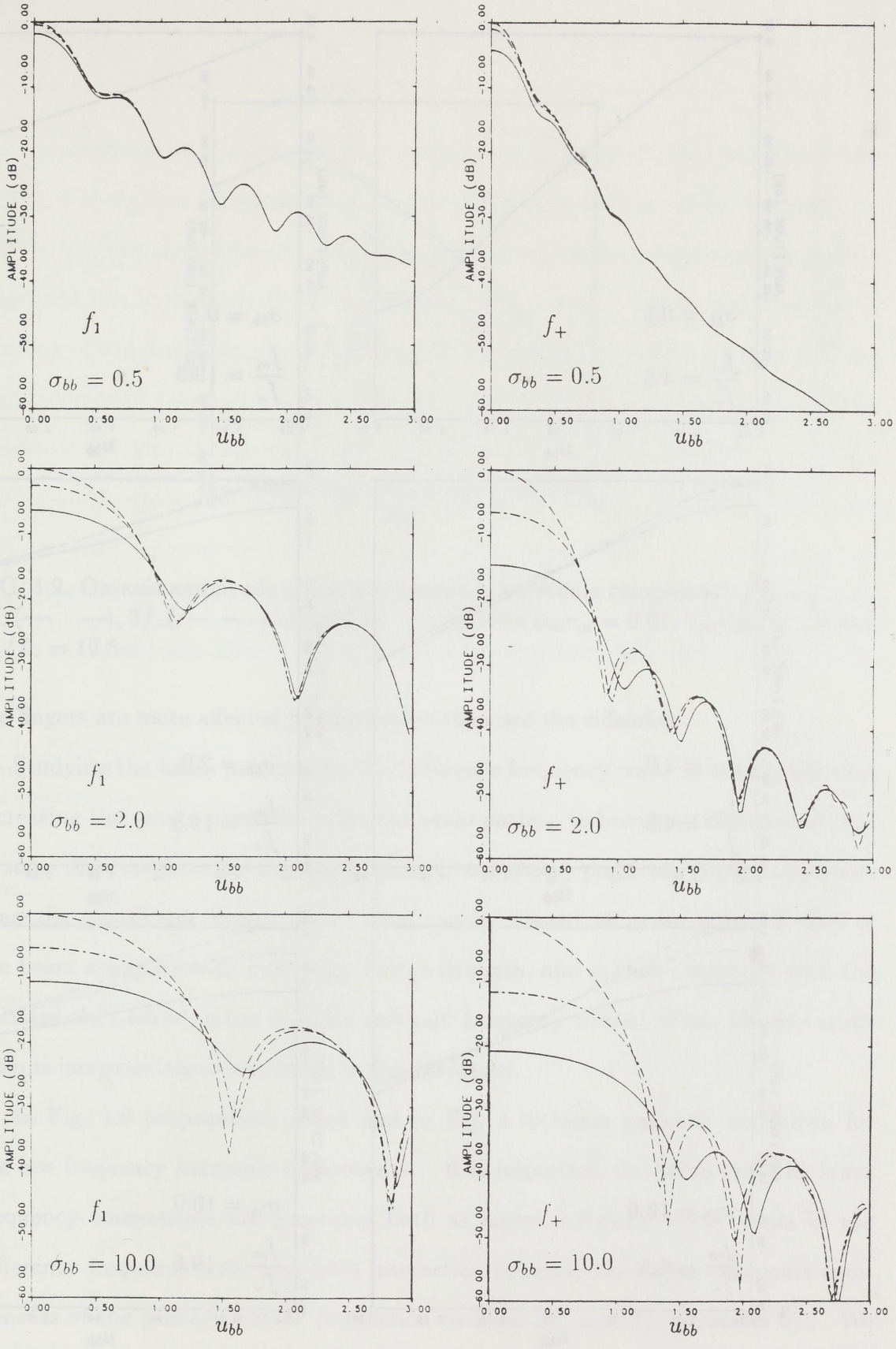

FIG. 4.7. Beam patterns of the primary (f_1) and sum frequency waves, with $\alpha_m r_m = 0.01$ and $f_m/f_- = 4.5$. Fully nonlinear theory and $r_m/l_{Dm} = 1.0$ (———), fully nonlinear theory and $r_m/l_{Dm} = 0.5$ (— - - —),and linear/quasilinear theory (— —). Amplitudes of the primary (f_1)have been normalized to on-axis value according to linear theory. Amplitudes of the sum frequency wave have been normalized to on-axis value according to quasilinear theory.

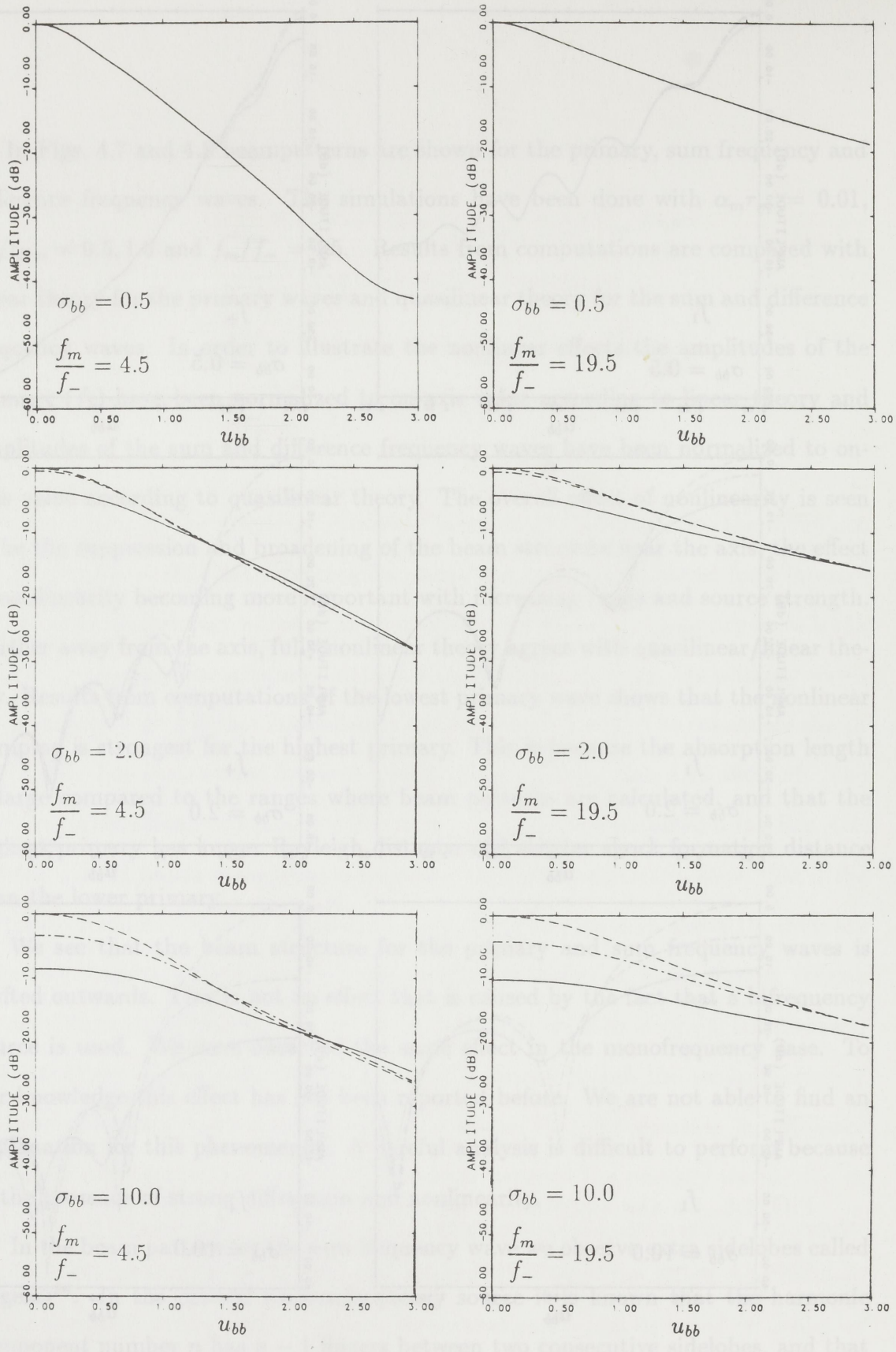

FIG. 4.8. Beam patterns of the difference frequency waves, with $\alpha_m r_m = 0.01$. Fully nonlinear theory and $r_m/l_{Dm} = 1.0$ (———), fully nonlinear theory and $r_m/l_{Dm} = 0.5$ (— - —), and quasilinear theory (— —). Amplitudes of the difference frequency wave have been normalized to on-axis value according to quasilinear theory.

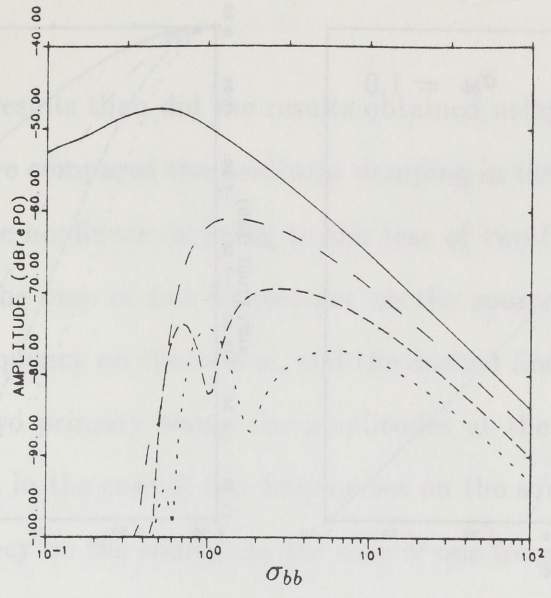

FIG. 4.9. On-axis amplitude of the low frequency harmonic components f_-(———), $2f_-$(— —), $3f_-$(— — —) and $4f_-$(- - - -), with $\alpha_m r_m = 0.01$, $r_m/l_{Dm} = 1.0$ and $f_m/f_- = 19.5$.

the fingers are more affected by absorption than are the sidelobes.

Studying the beam patterns for the difference frequency wave we clearly see that increasing the source strength causes the beam pattern to broaden. We also see that at some distance from the axis the fully nonlinear theory predicts a higher amplitude than the quasilinear theory does. This can be viewed of as an outward shift of the beam structure with increasing source strength, and is thus consistent with the outward shift found in the primary and sum frequency waves. When the downshift ratio is increased the beam width is also increased.

In Fig. 4.9 propagation curves and in Fig. 4.10 beam patterns are shown for the low frequency harmonic components. It is important to realize that the lower frequency components are generated both as higher harmonic components of the difference frequency wave and from interaction between the higher harmonic components of the primary waves. Interaction between $2f_1$ and $2f_2$ generates $2f_-$. We see that $2f_-, 3f_-$ and $4f_-$ are built up around the shock formation distance. At

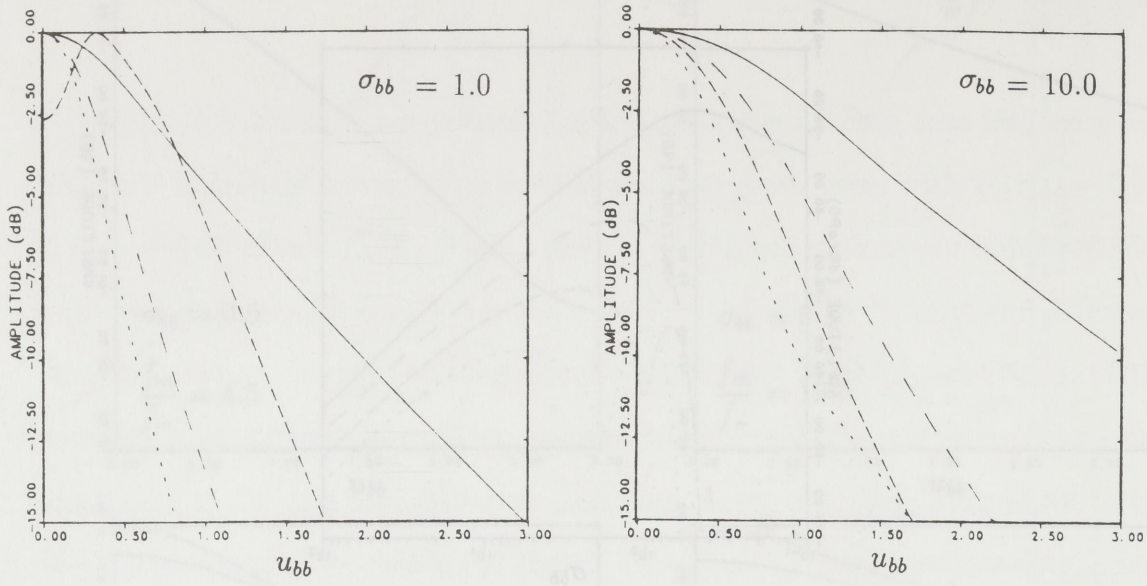

FIG. 4.10. Beampatterns of the low frequency harmonic components f_-(———), $2f_-$(— —), $3f_-$(— —) and $4f_-$(- - -), with $\alpha_m r_m = 0.01$, $r_m/l_{Dm} = 1.0$ and $f_m/f_- = 19.5$. The beampatterns are normalized to their maximas.

$\sigma_{bb} = 100$ the amplitude of the fourth harmonic low frequency component is about 10 dB below the difference frequency component. The third and fourth harmonic components experience a dip in the propagation curves. The dips on the axis corresponds to dips in beam patterns at the same ranges. From the beam patterns we observe that the higher low frequency harmonic components are much more directive than are the difference frequency wave.

Moffett and Mellen[37] did an theoretical and experimental investigation of the parametric arrays operating at high amplitudes. They compared their experimental results to results from a theoretical model they developed, where the difference frequency wave was calculated on the basis of tapered primary waves. Two different taper functions were used. The first taper function was derived by taking into account the nonlinear interaction between the primaries, while the second taper function was derived without taking into account this interaction. They found, quite surprisingly, that the theoretical results obtained using the second taper function fitted better to

the experimental results than did the results obtained using the first taper function. In Fig. 4.11 we have compared the nonlinear damping in the case of one frequency on the source with the nonlinear damping in the case of two frequencies on the source. The solid line is the case of two frequencies on the source, the dash-dotted line is the case of one frequency on the source, and the dashed line is linear theory. For the simulation with two primary waves the amplitudes at the source were equal. The nonlinear damping in the case of two frequencies on the source is higher than in the case of one frequency on the source. In the case of one frequency on the source, only one harmonic component is generated as a second-order effect. In the case of two frequencies, four harmonic components are generated as a second-order effect. This may explain why nonlinear damping is larger in the case of two frequencies on the source.

In Fig. 4.12 the time waveform at different points along the axis is studied. The parameters used are $\alpha_m r_m = 0.1$, $r_m/l_{Dm} = 1.0$ and $f_m/f_- = 4.5$. At $\sigma_{bb} = 0.5$ shocks have already formed. We see ripples in the waveform, due to the fact that we have a finite number of harmonic components in the computation. Increasing the number of harmonic components in the computation has the effect of smoothing the ripples. The symmetry of the waveform is destroyed by the prescence of diffraction. The shock close to 0 degrees is stronger than the two adjacent shocks and is therefore more affected by dissipation. Consequently the shock close to 0 degrees is damped more from $\sigma_{bb} = 0.5$ to $\sigma_{bb} = 1.0$ than the adjacent shocks. At $\sigma_{bb} = 1.0$ the shocks look very similar both in shape and magnitude. Compare this waveform with Fig. 3.5 of Ref. 39 where the envelope becomes square shaped after the shock formation distance. In Fig. 3.5 of Ref. 39 distortion of the waveform is shown for a plane wave. At $\sigma_{bb} = 10 = \alpha_m^{-1}$, the absorption length for a plane wave with frequency f_m, the

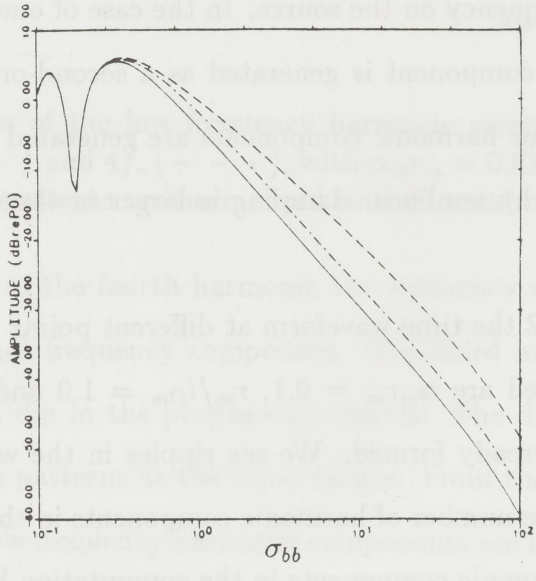

FIG. 4.11. On-axis amplitude of the primary wave (f_1), with $\alpha_m r_m = 0.01$, $r_m/l_{Dm} = 1.0$ and $f_m/f_- = 19.5$. Fully nonlinear theory with two frequencies on the source (———), linear theory with two frequencies on the source (— —), and fully nonlinear theory with one frequency at the source (— · —).

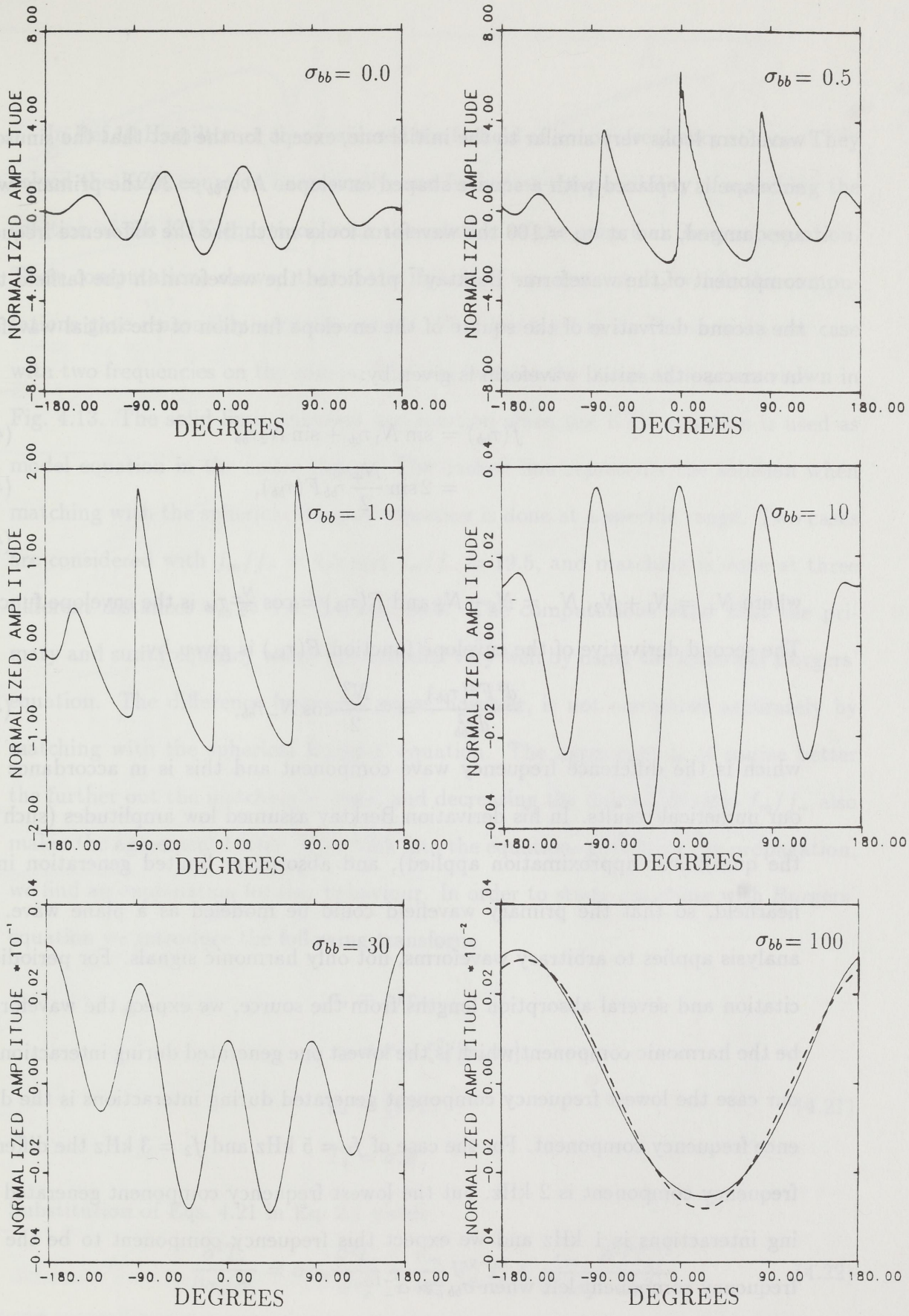

FIG. 4.12. Time waveforms normalized to P_0 for $\alpha_m r_m = 0.1$, $r_m/l_{Dm} = 1.0$ and $f_m/f_- = 4.5$. Difference frequency component of the waveform at $\sigma_{bb} = 100$ (— —). The abcissa indicates the relative phase, in retarded time frame $(t - z/c_0)$ within one cycle of waveform.

waveform looks very similar to the initial one, except for the fact that the sinusoidal envelope is replaced with a square shaped envelope. At $\sigma_{bb} = 30$ the primary waves are damped, and at $\sigma_{bb} = 100$ the waveform looks much like the difference frequency component of the waveform. Berktay[57] predicted the waveform in the farfield to be the second derivative of the square of the envelope function of the initial waveform. In our case the initial waveform is given by:

$$f(\tau_{bb}) = \sin N_1\tau_{bb} + \sin N_2\tau_{bb} \tag{4.17}$$

$$= 2\sin\frac{N_+}{2}\tau_{bb}F(\tau_{bb}), \tag{4.18}$$

$$\tag{4.19}$$

where $N_+ = N_1 + N_2$, $N_- = N_1 - N_2$ and $F(\tau_{bb}) = \cos\frac{N_-}{2}\tau_{bb}$ is the envelope function. The second derivative of the envelope function $F(\tau_{bb})$ is given by:

$$\frac{d^2F^2(\tau_{bb})}{d\tau_{bb}^2} = -\frac{N_-^2}{2}\cos N_-\tau_{bb}, \tag{4.20}$$

which is the difference frequency wave component and this is in accordance with our numerical results. In his derivation Berktay assumed low amplitudes (such that the quasilinear approximation applied), and absorption limited generation in the nearfield, so that the primary wavefield could be modeled as a plane wave. His analysis applies to arbitrary waveforms, not only harmonic signals. For periodic excitation and several absorption lengths from the source, we expect the waveform to be the harmonic component which is the lowest one generated during interactions. In our case the lowest frequency component generated during interactions is the difference frequency component. For the case of $f_1 = 5$ kHz and $f_2 = 3$ kHz the difference frequency component is 2 kHz, but the lowest frequency component generated during interactions is 1 kHz and we expect this frequency component to be the only frequency component left when $\sigma_{bb} \gg \alpha_-^{-1}$.

In Ref.10 Hamilton et al. considered the farfield of a monofrequency source. They solved the KZK equation numerically, and looked at the possibility of matching the solution of the KZK equatiuon with the solution of the spherical Burgers' equation. Their computations showed that if the matching was done at $\sigma_{bb} = 1.0$, the computations gave reasonably accurate results. We have tried to do the same in our case with two frequencies on the source. The results from the computations are shown in Fig. 4.13. The solid lines represent the solution when the KZK equation is used as model equation in the entire region. The dashed line represents the solution when matching with the spherical Burgers' equation is done at a specific range. Two cases are considered with $f_m/f_- = 4.5$ and $f_m/f_- = 19.5$, and matching is done at three different distances $\sigma_{bb} = 1.0$, 5.0 and 10.0. The computations show that the primary and sum frequency waves are modeled very well by using the spherical Burgers' equation. The difference frequency wave, however, is not computed accurately by matching with the spherical Burgers' equation. The agreement is of course better the further out the matching is done, and decreasing the downshift ratio f_m/f_- also makes the agreement better. If we look into the equations governing the propagation, we find an explanation for this behaviour. In order to study matching with Burgers' equation we introduce the following transform

$$\begin{aligned} \sigma_s &= z/r_m\,, \\ \tau_s &= \tau - \xi^2/[n_m\sigma_s]\,, \\ \underline{u}_s &= \underline{\xi}/\sigma_s\,, \\ T_s &= \sigma_s\overline{p}\,, \end{aligned} \tag{4.21}$$

Substitution of Eqs. 4.21 in Eq. 2.1 yields

$$\frac{\partial^2 T_s}{\partial\sigma_s\partial\tau_s} = \alpha r_m\frac{\partial^3 T_s}{\partial\tau_s^3} + \frac{n_m}{4\sigma_s^2}\nabla^2_{\underline{u}_s}T_s + \frac{r_m}{2l_D\sigma_s}\frac{\partial^2(T_s)^2}{\partial\tau_s^2} \tag{4.22}$$

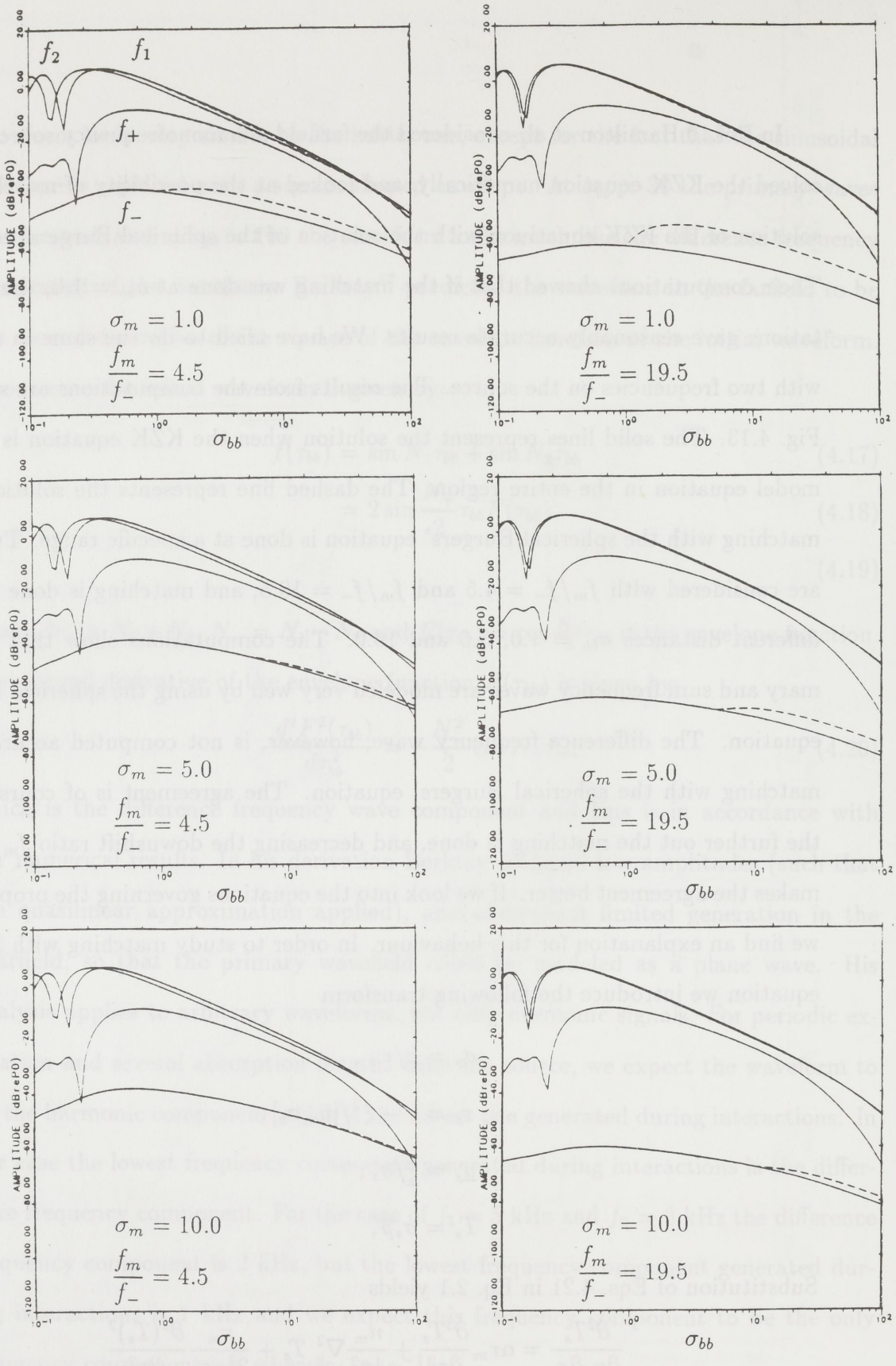

FIG. 4.13. On-axis amplitude of the primary, sum frequency and difference frequency waves, with $\alpha_m r_m = 0.01$, $r_m/l_{Dm} = 0.25$. Linear/quasilinear solution of the KZK equation in the entire region (———) and linear/quasilinear solution of spherical Burgers' equation from $\sigma_{bb} = \sigma_m$ (— —).

where $\nabla^2_{\underline{u}_s} = \partial^2/\partial u_s^2 + (1/u_s)\partial/\partial u_s$ and $u_s = |\underline{u}_s|$. If we assume that the boundary condition is periodic with period $2\pi\omega^{-1}$, we can seek a solution of Eq. 4.22 in the form of a Fourier series

$$T_s = \sum_{n=1}^{\infty}(c_{s,n}\cos n\tau_s + d_{s,n}\sin n\tau_s), \tag{4.23}$$

where $c_{s,n}$ and $d_{s,n}$ are functions of spatial variables. Substituting Eq. 4.23 into Eq. 4.22 we obtain

$$\begin{aligned}
&\frac{\partial c_{s,n}}{\partial \sigma_s} = -\alpha r_m n^2 c_{s,n} - \frac{n_m}{4n\sigma_s^2}\nabla^2_{\underline{u}_s} d_{s,n} + \\
&\frac{r_m n}{2l_D\sigma_s}\left[\sum_{i=1}^{n-1}(c_{s,n-i}d_{s,i}) + \sum_{i=n+1}^{\infty}(d_{s,i}c_{s,i-n} - c_{s,i}d_{s,i-n})\right], \\
&\frac{\partial d_{s,n}}{\partial \sigma_s} = -\alpha r_m n^2 d_{s,n} + \frac{n_m}{4n\sigma_s^2}\nabla^2_{\underline{u}_s} c_{s,n} + \\
&\frac{r_m n}{2l_D s\sigma_s}\left[\frac{1}{2}\sum_{i=1}^{n-1}(d_{s,n-i}d_{s,i} - c_{s,n-i}c_{s,i}) - \sum_{i=n+1}^{\infty}(c_{s,i}c_{s,i-n} + d_{s,i}d_{s,i-n})\right], \\
&n = 1, 2, ...
\end{aligned} \tag{4.24}$$

where $n_m = f_m/f$. The use of the spherical Burgers' equation is validated whenever the Laplace term is negligible. When σ_s increases, the factor in front of the Laplace operator decreases rapidly. We have to require

$$\frac{n_m}{n{\sigma_s}^2} \ll 1, \tag{4.25}$$

to neglect the Laplace term. For the primaries this requirement implies $\sigma_s^2 \gg 1$ since $n_m/N_1, n_m/N_2 \simeq 1$, but for the difference frequency wave it implies $\sigma_s^2 \gg n_m/N_-$, which is a more severe restriction. This means that we can use the spherical Burgers' equation for the description of the high frequency part of the field at shorter ranges, than we can do for the low frequency part of the field. The requirement also indicates that the ranges where we can start using the spherical Burgers' equation for the difference frequency wave increases with increasing value of f_m/f_-.

4.2. Focused beams and interaction between focused beams

4.2.1. Introduction

Much interest has been devoted to nonlinear effects in focused sound beams recently. This is in part due to the development of acoustic microscopes [2,58] and lithotripters [3], which both are capable of transmitting focused sound at very high amplitudes. The interaction between focused sound beams [59,68,69,71,72] has also been investigated.

In 1949 O'Neil[61] published a study of the sound field from a concave spherical radiator. He used the linear wave equation and an approximate Greens function. Explicit expressions were derived for the solution both along axis and in the focal plane.

Levin et al.[62] transformed the true boundary conditions on a spherical concave surface to a plane surface. They found an explicit analytical solution of the Helmholtz equation along the acoustic axis.

Naugol'nykh et al.[63] considered converging and diverging spherical waves of finite amplitude in a termoviscous medium. In an experimental investigation by Smith and Beyer[64] involving a spherical cap radiator, the experimental results compared roughly to the theory of Naugol'nykh et al.[63] in the prefocal region. Because of the strong diffraction effects near focus, the theory of Naugol'nykh et al. does not apply there.

Ostrovskii and Sutin[65] developed a model based on the assumption that the effects of nonlinearity and diffraction could be separated. Nonlinear spherical wave theory was used in the prefocal region, and linear diffraction theory was used near focus. The neglecting of diffraction in the prefocal region is specially doubtful for radiators with

sharp edges. Since the amplitudes are highest near focus the neglecting of nonlinear effects in this region is also doubtful. See Figs. 4.16 and 4.17 for numerical results obtained for the primary and second harmonic components radiated from a uniform focused source.

Several authors have studied the finite amplitude effects in focused sound fields by modeling the diffraction in the parabolic/Fresnel approximation. Hennion [59] used Fourier decomposition to obtain an integral representation for the difference frequency wave generated by a bifrequency focused source. In Refs.60,67,68,69,70 linear and quasilinear solutions of the KZK equation were shown to compare well to experimental results. The primary wave was studied in Ref. 67, the difference frequency wave in Refs. 68,69, and the second harmonic component in Refs. 60,70. The analysis can often be simplified by assuming Gaussian boundary conditions. Rugar[2] derived an explicit quasilinear solution for the second harmonic to explain his experimental results. Novikov et al.[39] used Gaussian boundary conditions and quasilinear analysis to study the effect of focusing the primary waves in the parametric array.

The farfield of the difference frequency wave, generated by a focused parametric array, was considered by Barannik et al.[71]. The width of the difference frequency beam was estimated, and it was found that large angle scattering is possible. Barannik and Kadnikov[72] studied the nonlinear interaction of convergent spherical waves. It was found that the beam pattern of the sum frequency wave cannot be wider than the beampattern of the primary waves, and that the beam pattern of the difference frequency wave becomes wider as the difference frequency is decreased.

For sufficiently high amplitudes the quasilinear approximation is not valid. The finite difference method developed by Bakhvalov et al.[42] to solve the KZK equation was also applied to focused sound beams [42,73]. In their investigation they only consid-

ered cases where the boundary conditions were Gaussian or fourth order polynomial. In addition only focusing gains less than 10 were studied. Hart and Hamilton[11,12] also solved the KZK equation numerically. They used the algorithm and program developed by Aanonsen et al.[6,8] modified to account for focusing geometry. Sound beams generated by sources with uniform amplitude distribution and focusing gains of order 50 were computed.

4.2.2. Nonlinear effects in focused sound beams

Our analysis of finite amplitude effects in focused sound beams is based on numerical solutions of the KZK equation. In order to enhance the efficiency of the numerical method a coordinate transform introduced in Refs. 9,10, but modified to account for focusing geometry is used

$$\begin{aligned} \sigma_f &= (z-d)/d, \\ \underline{u}_f &= \underline{\xi}/(\sigma_f \pm \delta), \\ \tau_f &= \tau - G\xi^2/(\sigma_f \pm \delta), \\ T &= (\sigma_f \pm \delta)\overline{p}. \end{aligned} \tag{4.26}$$

The minus sign is used before the focus and the plus sign is used after focus. If $\delta = 0$ the retarded time is close to retarded time of a spherical converging wave before focus, and close to retarded time for a spherical diverging wave after focus, and $|\underline{u}|$ represents an angle. These properties make this coordinate system well suited for calculating the focused sound field. The small positive quantity δ governs the rate at which the transformed geometry converges. Substitution of Eqs. 4.26 in Eq. 2.1 yields

$$\frac{\partial^2 T_f}{\partial \sigma_f \partial \tau_f} = \alpha d \frac{\partial^3 T_f}{\partial \tau_f^3} + \frac{1}{4G(\sigma_f \pm \delta)^2} \nabla^2_{\underline{u}_f} T_f + \frac{d}{2l_D(\sigma_f \pm \delta)} \frac{\partial^2 (T_f)^2}{\partial \tau_f^2} \tag{4.27}$$

where $\nabla^2_{\underline{u}_f} = \partial^2/\partial u_f^2 + (1/u_f)\partial/\partial u_f$ and $u_f = |\underline{u}_f|$. If we assume that the boundary condition is periodic with period $2\pi\omega^{-1}$, we can seek a solution of Eq. 4.27 in the form of a Fourier series

$$T_f = \sum_{n=1}^{\infty}(c_{f,n}\cos n\tau_f + d_{f,n}\sin n\tau_f), \tag{4.28}$$

where $c_{f,n}$ and $d_{f,n}$ are functions of spatial variables. Substituting Eq. 4.28 into Eq. 4.27 we obtain

$$\begin{aligned}
&\frac{\partial c_{f,n}}{\partial \sigma_f} = -\alpha d n^2 c_{f,n} - \frac{1}{4Gn(\sigma_f \pm \delta)^2}\nabla^2_{\underline{u}_f} d_{f,n} + \\
&\frac{dn}{2l_D(\sigma_f \pm \delta)}\left[\sum_{i=1}^{n-1}(c_{f,n-i}d_{f,i}) + \sum_{i=n+1}^{\infty}(d_{f,i}c_{f,i-n} - c_{f,i}d_{f,i-n})\right], \\
&\frac{\partial d_{f,n}}{\partial \sigma_f} = -\alpha d n^2 d_{f,n} + \frac{1}{4nG(\sigma_f \pm \delta)^2}\nabla^2_{\underline{u}_f} c_{f,n} + \\
&\frac{dn}{2l_D(\sigma_f \pm \delta)}\left[\frac{1}{2}\sum_{i=1}^{n-1}(d_{f,n-i}d_{f,i} - c_{f,n-i}c_{f,i}) - \sum_{i=n+1}^{\infty}(c_{f,i}c_{f,i-n} + d_{f,i}d_{f,i-n})\right], \\
&n = 1, 2, ...
\end{aligned} \tag{4.29}$$

For an axisymmetric focused source that oscillates sinusoidally with uniform amplitude distribution and focusing gain G, the boundary condition is

$$\overline{p}(\sigma = 0, \xi, \tau) = U(\xi)\sin(\tau + G\xi^2), \tag{4.30}$$

which gives the following boundary conditions for $c_{f,n}$ and $d_{f,n}$ when use is made of Eqs. 4.26 and 4.28:

$$c_{f,1}(\sigma_f = -1, u_f) = -(1+\delta)U\left(u_f(1+\delta)\right)\sin\left(G\delta(1+\delta)u_f^2\right) \tag{4.31}$$

$$d_{f,1}(\sigma_f = -1, u_f) = -(1+\delta)U\left(u_f(1+\delta)\right)\cos\left(G\delta(1+\delta)u_f^2\right) \tag{4.32}$$

with $c_{f,n}(\sigma_f = -1, u_{bb}) = 0$ and $d_{f,n}(\sigma_f = -1, u_f) = 0$ for $n \geq 1$. Hart and Hamilton used the program described in Ref.8 to solve Eq. 4.29. Results were presented

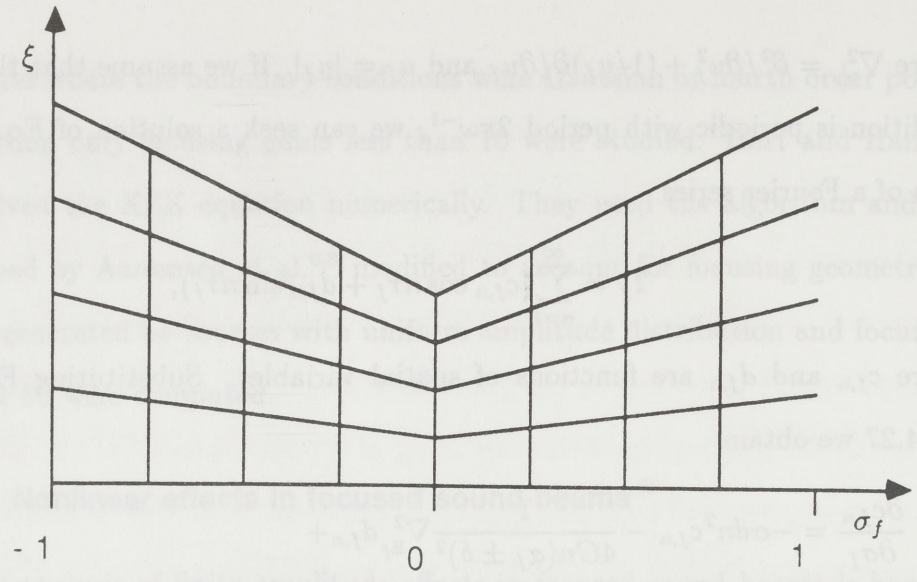

FIG. 4.14. Integration region for the transformed equation shown in cartesian coordinates

for sound beams influenced by the combined effects of nonlinearity, diffraction and absorption. The beam patterns in the focal region were found to be less sensitive to absorption and nonlinearity than were beam patterns in the farfield of unfocused sources.

We have solved Eq. 4.29 with the algorithm descriebed in Chapter 3, which is an order of magnitude faster than the algorithm of Aanonsen[8].

Shown in Fig. 4.15 is the normalized power of the second harmonic component of a focused sound beam with $G = 50$ and no absorption. The second harmonic component is computed quasilinearly. The power of the second harmonic component $\overline{\mathcal{P}}_{av,2}(\sigma)$ is defined by Eq. 2.7. Since the absorption is zero, any change in power with σ_f is caused by nonlinear effects. The power of the second harmonic component increases until it reaches a maximum slightly after focus. In contrast the amplitude of the second harmonic has a maximum before focus. Rugar[2] has studied the simpler case of a focused Gaussian beam. He also calculated the power of the second

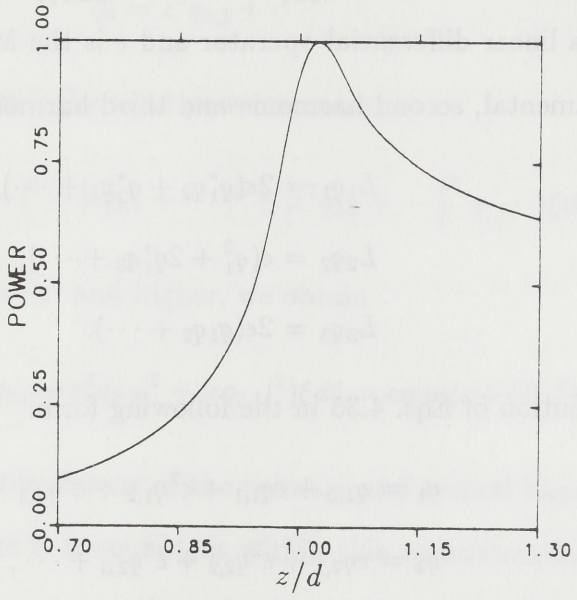

FIG. 4.15. Normalized power of second harmonic along axis, with $\alpha d = 0$, $G = 50$. Quasilinear theory.

harmonic component in the parabolic, quasilinear approximation and obtained the same qualitative result as we have.

If we seek a solution of the KZK equation in form of a complex Fourier series

$$\overline{p} = \sum_{n=1}^{\infty} (q_n e^{jn\tau} + q_n^* e^{-jn\tau}), \tag{4.33}$$

where q_n is a complex coefficient and q_n^* its complex conjugate, we obtain

$$L_n q_n = \epsilon \Big(\sum_{m=1}^{n-1} q_m q_{n-m} + 2 \sum_{m=n+1}^{N} q_m q_{m-n}^* \Big), \tag{4.34}$$

where L_n is a linear differential operator and ϵ is the Mach number. The equations for the fundamental, second harmonic and third harmonic components are given by

$$\begin{aligned} L_1 q_1 &= 2\epsilon(q_1^* q_2 + q_2^* q_3 + \cdots), \\ L_2 q_2 &= \epsilon(q_1^2 + 2q_1^* q_3 + \cdots), \\ L_3 q_3 &= 2\epsilon(q_1 q_2 + \cdots). \end{aligned} \tag{4.35}$$

We seek a solution of Eqs. 4.35 in the following form:

$$\begin{aligned} q_1 &= q_{1,0} + \epsilon q_{1,1} + \epsilon^2 q_{1,2} + \epsilon^3 q_{1,3} + \cdots, \\ q_2 &= \epsilon q_{2,1} + \epsilon^2 q_{2,2} + \epsilon^3 q_{2,3} + \cdots, \\ q_3 &= \epsilon^2 q_{3,2} + \epsilon^3 q_{3,3} + \cdots. \end{aligned} \tag{4.36}$$

Substituting Eqs. 4.36 in Eqs. 4.35 and identifying to any order of ϵ, we obtain

$$L_1 q_{1,0} = 0, \tag{4.37}$$

$$L_2 q_{2,1} = q_{1,0}^2, \tag{4.38}$$

$$L_3 q_{3,2} = 2q_{1,0} q_{2,0}, \tag{4.39}$$

$$L_1 q_{1,2} = 2q_{1,0}^* q_{2,1}, \tag{4.40}$$

$$L_2 q_{2,3} = q_{1,0}^* q_{3,2}, \tag{4.41}$$

where $q_{1,0}$ is the linear solution for the fundamental, $q_{2,1}$ is the quasilinear solution for the second harmonic, $q_{3,2}$ is the quasilinear solution of the third harmonic, $q_{1,2}$ is the first correction term to the primary and $q_{2,3}$ is the first correction term to the second harmonic. Since $q_{1,1} = 0$ and $q_{2,2} = 0$, we have

$$\begin{aligned} q_1 &= q_{1,0} + \epsilon^2 q_{1,2} + \cdots, \\ q_2 &= \epsilon q_{2,1} + \epsilon^3 q_{2,3} + \cdots, \\ q_3 &= \epsilon^3 q_{3,3} + \cdots. \end{aligned} \tag{4.43}$$

Since absorption is absent, the total power is constant :

$$\int_0^\infty (|q_{1,0} + \epsilon^2 q_{1,2} + \cdots|^2 + |\epsilon q_{2,1} + \cdots|^2 + \left|\epsilon^2 q_{3,2} + \cdots\right|^2 + \cdots)\xi d\xi = const. \tag{4.44}$$

Neglecting terms of order ϵ^4 and higher, we obtain

$$\int_0^\infty (|q_{1,0} + \epsilon^2 q_{1,2}|^2 + |\epsilon q_{2,1}|^2)\xi d\xi = const. + O(\epsilon^4). \tag{4.45}$$

To order ϵ^3 the sum of the powers of the primary and second harmonic components is constant. Furthermore it is consistent within this approximation to calculate the second harmonic component quasilinearly. Since the power of the second harmonic component increases until it reaches a maximum slightly after focus, energy is transfered from the fundamental component to the second harmonic component in this region. The power of the second harmonic component decreases after its maximum slightly after focus and energy is therefore pumped back to the fundamental component in this region.

In Figs. 4.16 and 4.17 we have compared the primay and second harmonic components computed using fully nonlinear theory with linear/quasilinear theory for the case $\alpha d = 1.0, d/l_D = 1.0$ and $G = 50$. Comparison between fully nonlinear

theory and linear/quasilinear theory illustrates the effect of nonlinearity, and the accuracy of linear/quasilinear theory. Hart and Hamilton[11,12] did not compare with linear/quasilinear theory. Figure 4.16 shows on-axis amplitude for the primary (f_1) and second harmonic ($2f_1$). The nonlinearity affects the second harmonic more than primary component. We see that an effect of nonlinearity, for both the primary and second harmonic components, is to move the maximum closer to the source. Hart[12] found that the peak values of the harmonic components move closer to the source as d/l_D increases. The nonlinear damping is increasing up to the focal region. It is remarkable that even if the shock formation distance equals the focal distance, the nonlinear damping of the primary wave is no more than 2.3 dB at focus.

We have studied the beam patterns in the vicinity of focus in Fig. 4.17. We have chosen $2G\xi$ as abcissas of the plots, since the linear solution of the amplitude distribution is $2J_1(2G\xi)/2G\xi$ [67]. The complex structure of the beam patterns in the vicinity of focus is similar to the beam patterns in Fig. 4.7 for an unfocused source. The extra sidelobes found in the beam patterns for the second harmonic component have been called fingers [54]. The discrepancy between fully nonlinear theory and linear/quasilinear theory is largest close to the axis.

We also observe that an effect of the nonlinearity is a shift of the beam structure outwards. This is specially pronounced in the second harmonic component. This is the same effect as found in Sec. 4.1.2 where unfocused sources were considered

4.2.3. Interaction between two focused sound beams

Interaction between two focused sound beams have been studied by Hennion[59], Lucas et al.[68], Naze Tjøtta and Tjøtta[69], Novikov et al.[39] and Barannik et al.[71,72]. In

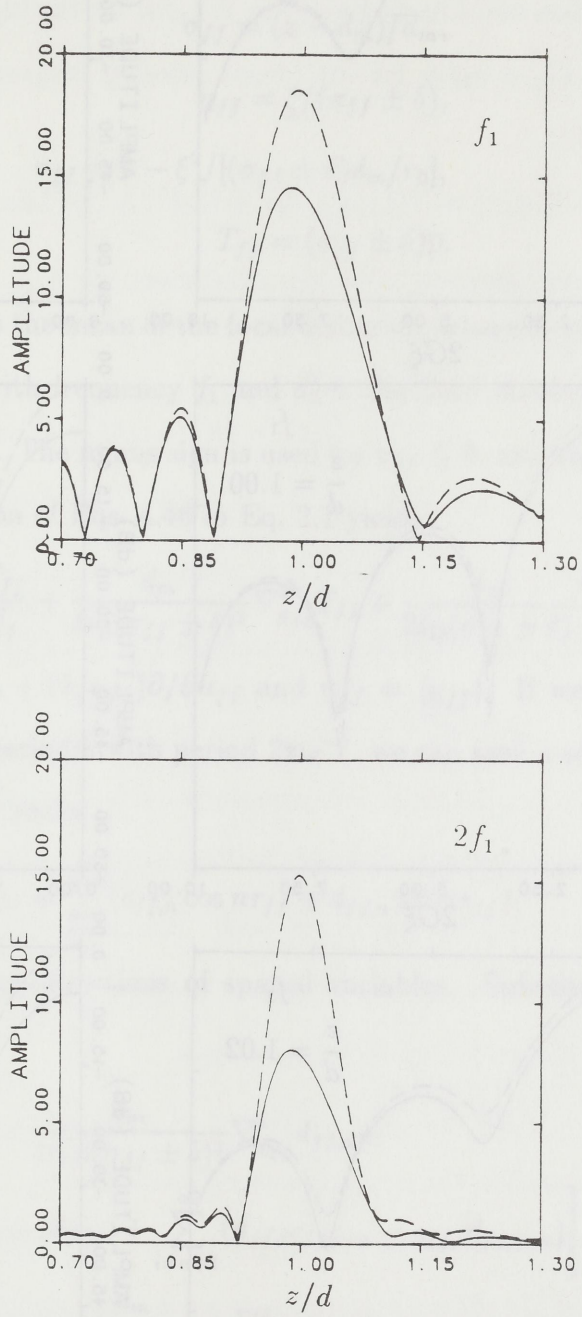

FIG. 4.16. On-axis amplitude normalized by P_0 for the primary and second harmonic components, $\alpha d = 1.0$. $d/l_D = 1.0$ and $G = 50$. Fully nonlinear theory (———) and linear/quasilinear theory (— —).

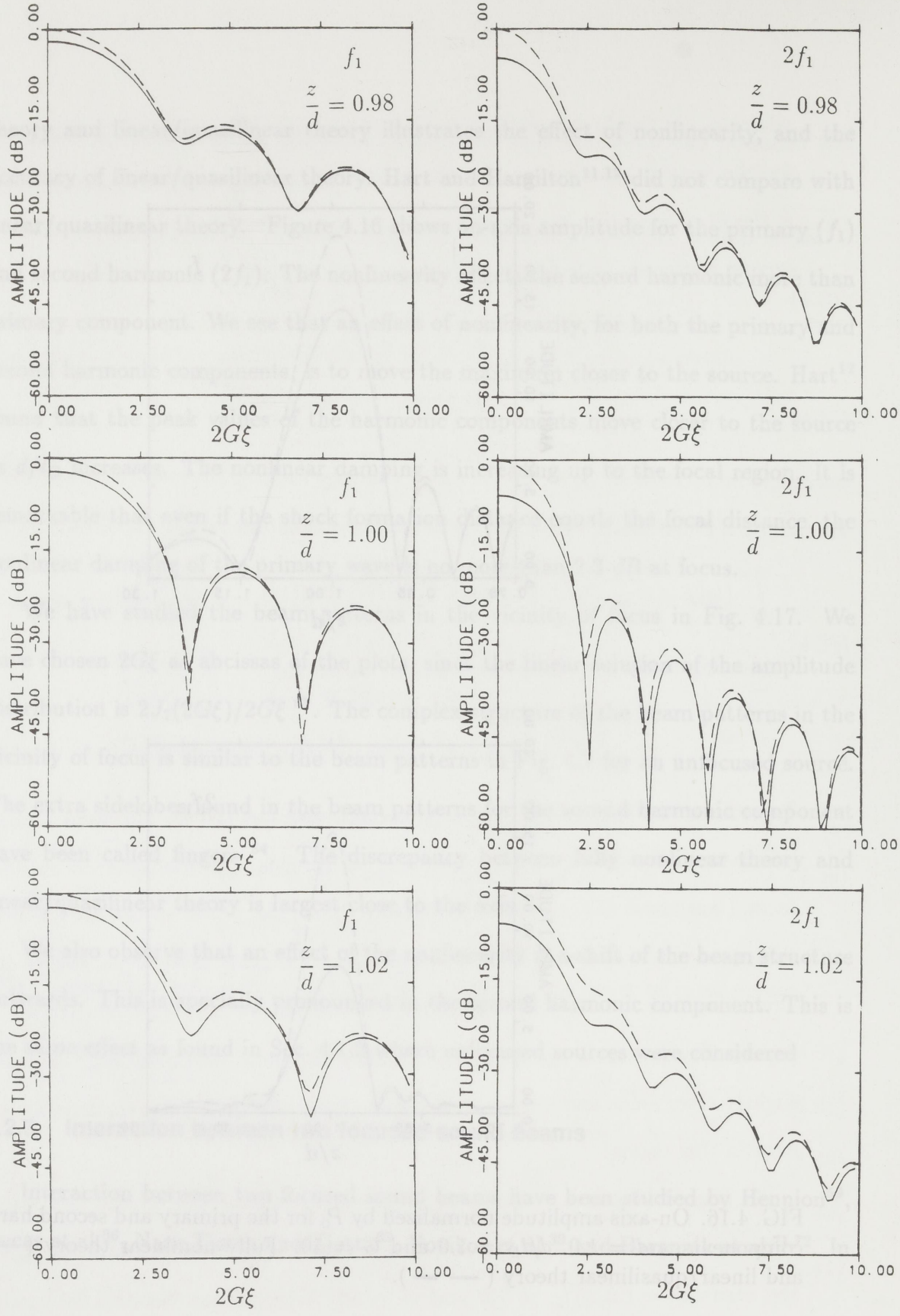

FIG. 4.17. Beampatterns for the primary and second harmonic in the focal region, with $\alpha d = 1.0$, $d/l_D = 1.0$ and $G = 50$. Fully nonlinear theory (——) and linear/quasilinear theory (— —).

order to study the interaction between focused sound beams we introduce a transform

$$\sigma_{ff} = (z - d_m)/d_m,$$

$$\underline{u}_{ff} = \underline{\xi}/(\sigma_{ff} \pm \delta),$$

$$\tau_{ff} = \tau - \xi^2/[(\sigma_{ff} \pm \delta)d_m/r_0], \tag{4.46}$$

$$T_{ff} = (\sigma_{ff} \pm \delta)\overline{p}.$$

Here $d_m = (d_1 + d_2)/2$ is the mean of the focal distances, where d_1 is the focal distance for the primary wave with frequency f_1 and d_2 is the focal distance for the primary wave with frequency f_2. The minus sign is used for $\sigma_{ff} \leq 0$, and the plus sign is used for $\sigma_{ff} \geq 0$. Substitution of Eqs. 4.46 in Eq. 2.1 yields

$$\frac{\partial^2 T_{ff}}{\partial \sigma_{ff} \partial \tau_{ff}} = \alpha d_m \frac{\partial^3 T_{ff}}{\partial \tau_{ff}^3} + \frac{d_m}{4r_0(\sigma_{ff} \pm \delta)^2} \nabla^2_{\underline{u}_{ff}} T_{ff} + \frac{d_m}{2l_D(\sigma_{ff} \pm \delta)} \frac{\partial^2 (T_{ff})^2}{\partial \tau_{ff}^2}, \tag{4.47}$$

where $\nabla^2_{\underline{u}_{ff}} = \partial^2/\partial u_{ff}^2 + (1/u_{ff})\partial/\partial u_{ff}$ and $u_{ff} = |\underline{u}_{ff}|$. If we assume that the boundary condition is periodic with period $2\pi\omega^{-1}$, we can seek a solution of Eq. 4.47 in the form of a Fourier series

$$T_{ff} = \sum_{n=1}^{\infty} (c_{ff,n} \cos n\tau_{ff} + d_{ff,n} \sin n\tau_{ff}), \tag{4.48}$$

where $c_{ff,n}$ and $d_{ff,n}$ are functions of spatial variables. Substituting Eq. 4.48 in Eq. 4.47, we obtain

$$\begin{aligned}
&\frac{\partial c_{ff,n}}{\partial \sigma_{ff}} = -\alpha d_m n^2 c_{ff,n} - \frac{d_m}{4r_0 n(\sigma_{ff} \pm \delta)^2} \nabla^2_{\underline{u}_{ff}} d_{ff,n} + \\
&\frac{d_m n}{2l_D(\sigma_{ff} \pm \delta)} \left[\sum_{i=1}^{n-1} (c_{ff,n-i} d_{ff,i}) + \sum_{i=n+1}^{\infty} (d_{ff,i} c_{ff,i-n} - c_{ff,i} d_{ff,i-n}) \right], \\
&\frac{\partial d_{ff,n}}{\partial \sigma_{ff}} = -\alpha d_m n^2 d_{ff,n} + \frac{d_m}{4nr_0(\sigma_{ff} \pm \delta)^2} \nabla^2_{\underline{u}_{ff}} c_{ff,n} + \\
&\frac{d_m n}{2l_D(\sigma_{ff} \pm \delta)} \left[\frac{1}{2} \sum_{i=1}^{n-1} (d_{ff,n-i} d_{ff,i} - c_{ff,n-i} c_{ff,i}) - \sum_{i=n+1}^{\infty} (c_{ff,i} c_{ff,i-n} + d_{ff,i} d_{ff,i-n}) \right],
\end{aligned} \tag{4.49}$$

$n = 1, 2, \ldots.$

For an axisymmetric focused source that oscillates bisinusoidally with uniform amplitude distribution and focusing gain $G_1 = r_1/d_1$ for the highest primary frequency and focusing gain $G_2 = r_2/d_2$ for the lowest primary frequency, the boundary condition is

$$\overline{p}(\sigma = 0, \xi, \tau) = U(\xi)\sin(N_1\tau + G_1\xi^2) + U(\xi)\sin(N_2\tau + G_2\xi^2), \tag{4.50}$$

which gives the following boundary conditions for $c_{ff,n}$ and $d_{ff,n}$ when use is made of Eqs. 4.46 and Eq. 4.48:

$$c_{ff,N_1}(\sigma_{ff} = -1, u_{ff}) = -(1+\delta)U\left(u_{ff}(1+\delta)\right)\sin\left(G_1\delta(1+\delta)u_{ff}^2\right) \tag{4.51}$$

$$d_{ff,N_1}(\sigma_{ff} = -1, u_{ff}) = -(1+\delta)U\left(u_{ff}(1+\delta)\right)\cos\left(G_1\delta(1+\delta)u_{ff}^2\right) \tag{4.52}$$

$$c_{ff,N_2}(\sigma_{ff} = -1, u_{ff}) = -(1+\delta)U\left(u_{ff}(1+\delta)\right)\sin\left(G_2\delta(1+\delta)u_{ff}^2\right) \tag{4.53}$$

$$d_{ff,N_2}(\sigma_{ff} = -1, u_{ff}) = -(1+\delta)U\left(u_{ff}(1+\delta)\right)\cos\left(G_2\delta(1+\delta)u_{ff}^2\right) \tag{4.54}$$

with $c_{ff,n}(\sigma_{ff} = -1, u_{ff}) = 0$ and $d_{ff,n}(\sigma_{ff} = -1, u_{ff}) = 0$ for $n \neq N_1, N_2$. We have compared results from computations using Eq. 4.49 to the results reported by Naze Tjøtta and Tjøtta in Ref. 69. In Fig. 4.18 we have reproduced two curves from Ref. 69. The computations agree well. We note that there are no oscillations in the on-axis amplitude of the difference frequency component as is the case for the primary and second harmonic components.

One might think that the efficiency of parametric generation of sound can be increased by focusing the primary waves. Usually when we consider parametric arrays we want the amplitude and directivity to be as high as possible in the farfield. We have compared the difference frequency wave generated from interaction between two primary waves with various focal distances and the results are shown in Fig. 4.19. We have compared the difference frequency wave for the cases $G_m = 50, 10, 1, 0$, where $G_m = 0$ corresponds to the unfocused case. It is seen that the maximum on-axis

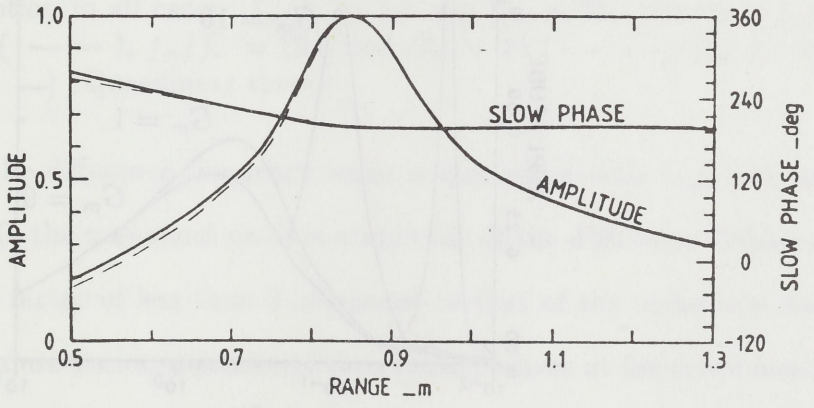

FIG. 4.18. On-axis amplitude and slow phase for the difference frequency wave. Reproduced from Ref. 69(———), and computed using Eqs. 4.49(— —).

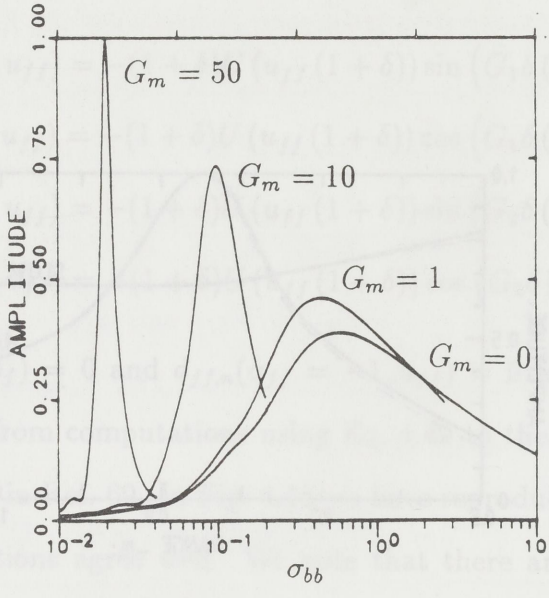

FIG. 4.19. On-axis normalized amplitude for the difference frequency wave for various values of focusing gain G_m, with no absorption and $f_m/f_- = 4.5$. Quasilinear theory.

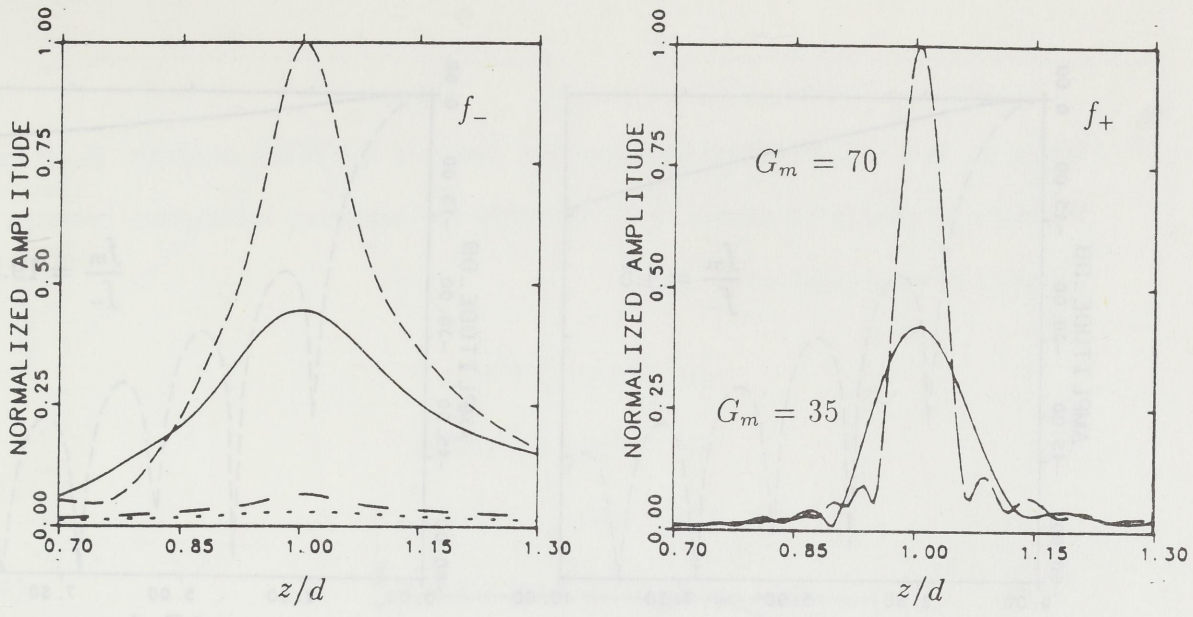

FIG. 4.20. On-axis normalized amplitude for the difference and sum frequency waves, with no absorption in all cases. $f_m/f_- = 4.5$ and $G_m = 35$ (———), $f_m/f_- = 4.5$ and $G_m = 70$ (— —), $f_m/f_- = 19.5$ and $G_m = 35$ (- - - -), $f_m/f_- = 19.5$ and $G_m = 70$ (— —) . Quasilinear theory.

amplitude of the difference frequency wave is increasing with G_m, but very slowly. When $G_m = 50$, the maximum on-axis amplitude of the difference frequency wave is increased by a factor of less than 3 compared to that of the unfocused source, even if the maximum on-axis amplitudes of the primary waves at focus are increased by a factor of 50. This is not unexpected since an increase in focusing gain for the primary waves is followed by a shortening of the interaction region.

In Figs. 4.20 and 4.21 the amplitude of the difference and the sum frequency waves are shown both along axis and in the focal plane. The effect of increasing f_m/f_- is, as expected, to lower the efficiency of the parametric generation of the difference frequency wave. The amplitude of the difference frequency wave varies more slowly both along the axis and across the axis, and the width of the beam increases, when f_m/f_- increases. For the sum frequency wave the change in f_m/f_- has nearly no effect at all.

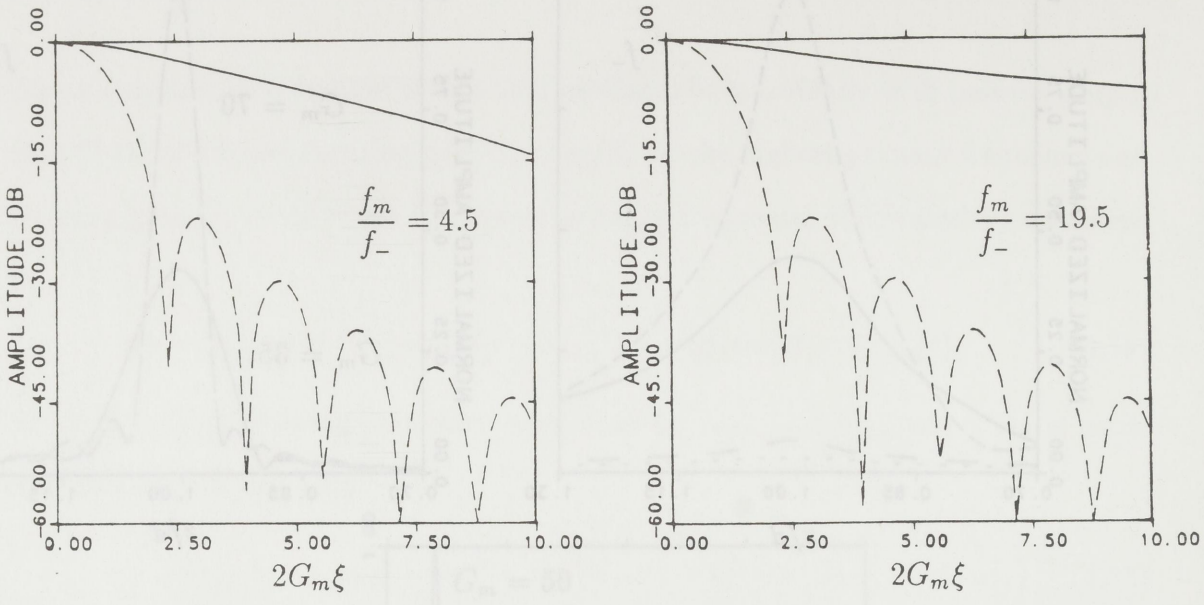

FIG. 4.21. Beam pattern for the difference frequency wave (———) and sum frequency wave (— — —), with no absorption and $G_m = 35$.

Comparing the amplitude of the sum and difference frequency waves along the axis, we see that the difference frequency wave does not have the oscillations in amplitude as does the sum frequency wave. In the focal plane the difference frequency wave is broader than the sum frequency wave and has no sidelobes. The sum frequency wave has a fine structure consisting of sidelobes and fingers.

We have calculated the power of the difference frequency wave $\overline{\mathcal{P}}_{av,N_-}(\sigma)$, given by Eq. 2.7, as a function of distance from the source in the case of no absorption, and with $G_m = 50$ and $f_m/f_- = 4.5$. The result is shown in Fig. 4.22. As for the second harmonic component we see that the maximum power occurs a little after the focus.

As in Sec. 4.2.2, we now seek a solution of the KZK equation in form of a complex Fourier series

$$\overline{p} = \sum_{n=1}^{\infty} (q_n e^{jn\tau} + q_n^* e^{-jn\tau}), \tag{4.55}$$

where q_n is a complex coefficient and q_n^* its complex conjugate, and, we obtain

$$L_n q_n = \epsilon \Big(\sum_{m=1}^{n-1} q_m q_{n-m} + 2 \sum_{m=n+1}^{N} q_m q_{m-n}^* \Big), \tag{4.56}$$

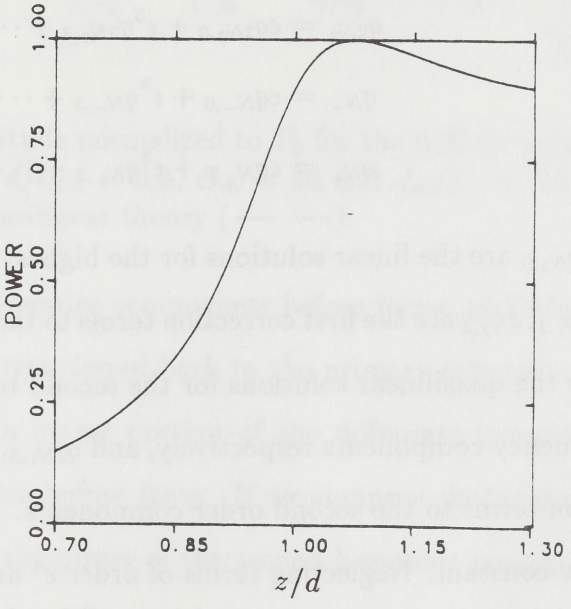

FIG. 4.22. Normalized power of the difference frequency wave, with no absorption, $f_m/f_- = 4.5$ and $G_m = 50$. Quasilinear theory.

where L_n is a linear differential operator, and ϵ is the Mach number. If we follow the same procedure as in Sec. 4.2.2 to study the nonlinear interaction between two primary waves we obtain

$$\begin{aligned} q_{N_1} &= q_{N_1,0} + \epsilon^2 q_{N_1,2} + \cdots, \\ q_{N_2} &= q_{N_2,0} + \epsilon^2 q_{N_2,2} + \cdots, \\ q_{2N_1} &= \epsilon q_{2N_1,0} + \epsilon^3 q_{2N_1,3} + \cdots, \\ q_{2N_2} &= \epsilon q_{2N_2,0} + \epsilon^3 q_{2N_2,3} + \cdots, \\ q_{N_-} &= \epsilon q_{N_-,0} + \epsilon^3 q_{N_-,3} + \cdots, \\ q_{N_+} &= \epsilon q_{N_+,0} + \epsilon^3 q_{N_+,3} + \cdots, \end{aligned} \tag{4.57}$$

where $q_{N_1,0}, q_{N_2,0}$ are the linear solutions for the highest and lowest primary waves respectively, $q_{N_1,2}, q_{N_2,2}$ are the first correction terms to the primary waves, $q_{2N_1,1}, q_{2N_2,1}, q_{N_-,1}$ and $q_{N_+,1}$ are the quasilinear solutions for the second harmonic, difference frequency and sum frequency components respectively, and $q_{2N_1,3}, q_{2N_2,3}, q_{N_-,3}$ and $q_{N_+,3}$ are the first correction terms to the second order components. In abscence of absorption the total power is constant. Neglecting terms of order ϵ^4 and higher we obtain

$$\int_0^\infty (|q_{N_1,0} + \epsilon^2 q_{N_1,2}|^2 + |q_{N_2,0} + \epsilon^2 q_{N_2,2}|^2 + |\epsilon q_{2N_1,1}|^2 + |\epsilon q_{2N_2,1}|^2 + \tag{4.58}$$

$$|\epsilon q_{N_-,1}|^2 + |\epsilon q_{N_+,1}|^2)\xi d\xi = const. + O(\epsilon^4). \tag{4.59}$$

To order ϵ^3 the sum of the powers of the primary, second harmonic, difference frequency, and sum frequency components is constant. Further, it is consistent within this approximation to calculate the soundfield in the quasilinear approximation. The power of the sum frequency wave increases up to a maximum a little after focus in the same way as the power of the difference frequency wave and the power of the second harmonic waves do. This means that energy is pumped from the primary

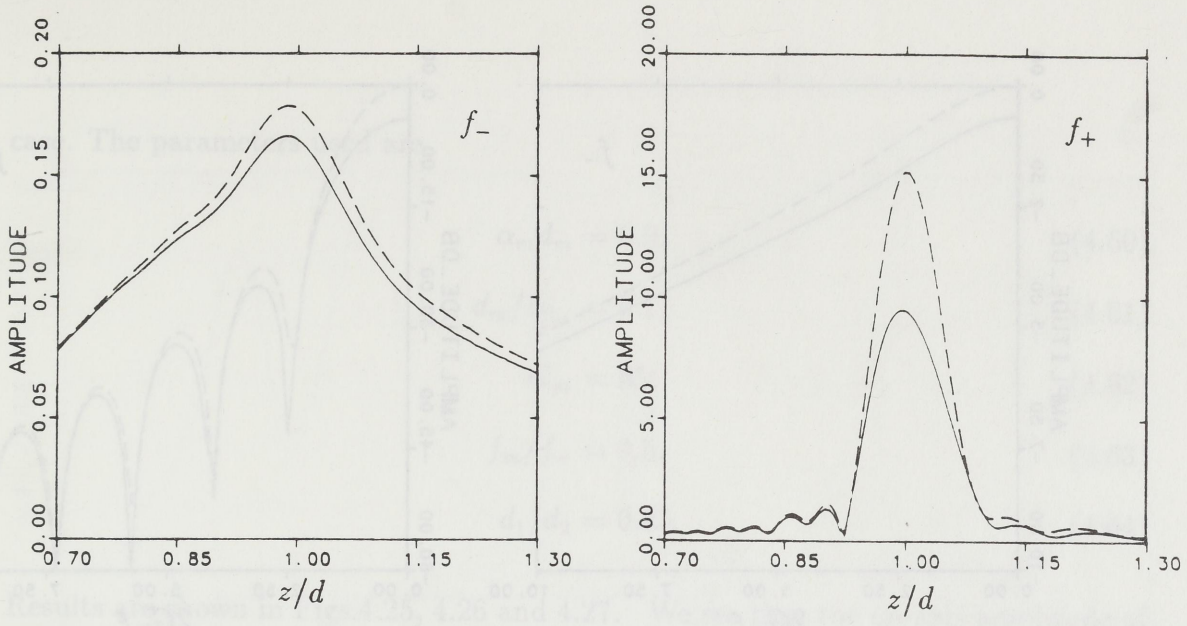

FIG. 4.23. On-axis amplitude normalized to P_0 for the difference and sum frequency waves, with $\alpha_m d = 1.0$, $d/l_{Dm} = 0.5$, $G_m = 50$ and $f_m/f_- = 9.5$. Fully nonlinear theory (———) and quasilinear theory (— —).

components to the second-order components before focus, and slightly after focus a portion of this energy is transferred back to the primary components.

We also notice that a major portion of the difference frequency component is generated in the focal area before focus. If we compare the power of the difference frequency component to the power of the second harmonic component, we find that the decreas in power of the difference frequency component after focus is less than for the second harmonic component. Since the power of the difference frequency component decreases only slightly after focus, it must be the geometrical spreading which causes the amplitude of the difference frequency component to decrease so quickly after focus when G_m is large.

In Figs. 4.23 and 4.24 we have considered the case $\alpha_m d = 1.0$, $d/l_{Dm} = 0.5$, $G_m = 50$ and $f_m/f_- = 9.5$, and have compared fully nonlinear theory to quasilinear theory. For both the difference frequency wave and the sum frequency wave see that the discrepancy between fully nonlinear theory and quasilinear theory is largest near

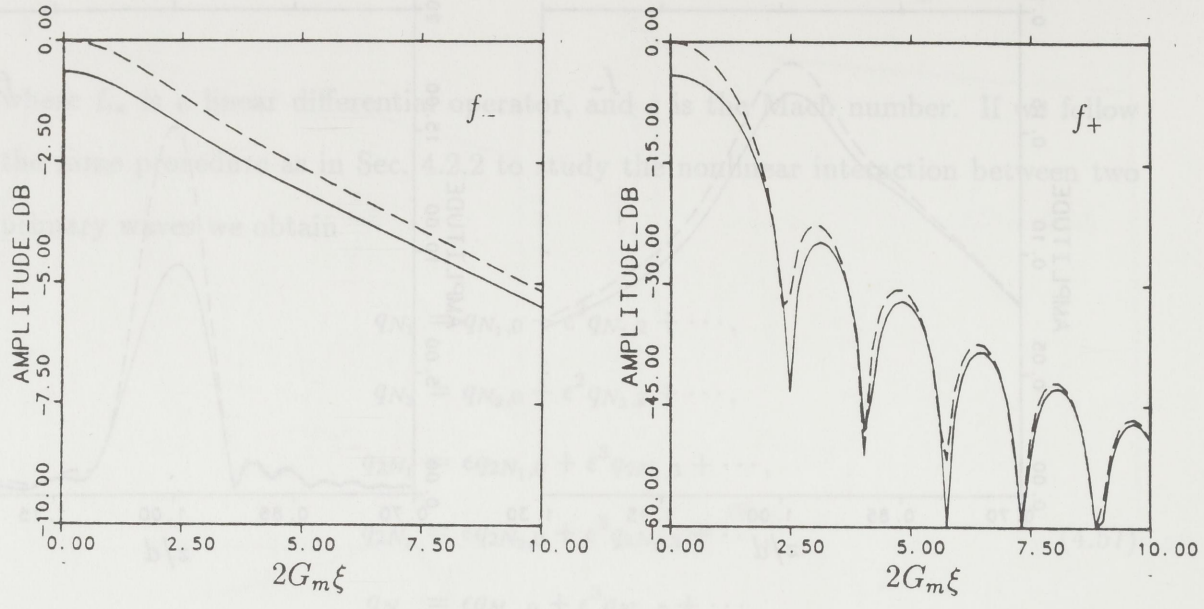

FIG. 4.24. Beampatterns for the difference and sum frequency waves, with $\alpha_m d = 1.0$, $d/l_{Dm} = 0.5$, $G_m = 50$ and $f_m/f_- = 9.5$. Fully nonlinear theory (———) and quasilinear theory (— — —).

focus. We find this to be reasonable, since the amplitudes are highest, and therefore the nonlinear effects strongest, near focus. The discrepancy between nonlinear theory and quasilinear theory is larger for the sum frequency wave than for the difference frequency wave.

The beam patterns show a nonlinear damping of the difference frequency wave which is very uniform. Note that the scales on the plots are different. Again we note the outward shift of the beam structure as a nonlinear effect in the sum frequency wave.

Interaction between two focused soundbeams with different focal distances

In Refs. 67,68 the focused sound fields were generated by using a biconcave lens in front of a plane source. If the sound speed in the lens depends upon frequency, the result will be that the primary waves will be focused at different ranges. In this case we have two focal distances, d_1 and d_2. We have considered a rather extreme

case. The parameters used are

$$\alpha_m d_m = 0.0, \tag{4.60}$$

$$d_m / l_{D_m} = 0.1, \tag{4.61}$$

$$G_m = 55, \tag{4.62}$$

$$f_m / f_- = 9.5, \tag{4.63}$$

$$d_1 / d_2 = 0.85. \tag{4.64}$$

Results are shown in Figs.4.25, 4.26 and 4.27. We see that the on-axis amplitude of the difference frequency wave experiences two maxima of nearly the same magnitude. The maximas are located at the focal distances of the primary waves ($z = d_1$ and $z = d_2$). There is a dip in the beam pattern for the difference frequency wave at $z = d_m$. The sum frequency wave has a maximum at $z = d_m$ and two other maximas of smaller amplitude at $z = d_1$ and $z = d_2$. Figure 4.28 compares the computations to the case when the focal distances are equal. For the difference frequency wave we see that the amplitude is much lower when the focal distances are different. The sum frequency wave has a lower maximum when the focal distances are different, but for $z > d_2$ or $z < d_1$ the amplitudes do not differ very much in magnitude.

4.2.4. Numerical investigation of the parametric receiving array

Nonlinear interaction between waves can also be used for detection of signals. The parametric receiving array (PARRAY) consists of a pump transducer and a receiving transducer, rigidly connected with one another. The high frequency pump transducer (frequency f_1) generates a high amplitude wave which interacts with the incoming signal (frequency f_2) and generates a difference frequency wave and a sum frequency wave. The direction of the signal is found by rotating the PARRAY. The direction

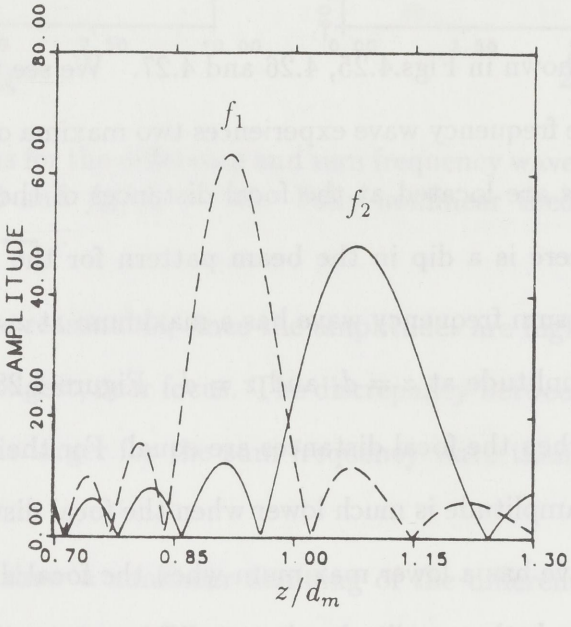

FIG. 4.25. On axis amplitude normalized by P_0 for the primary waves, with no absorption, $d_m/l_{Dm} = 0.1$, $f_m/f_- = 9.5$, $G_m = 55$ and $d_1/d_2 = 0.85$. Linear theory.

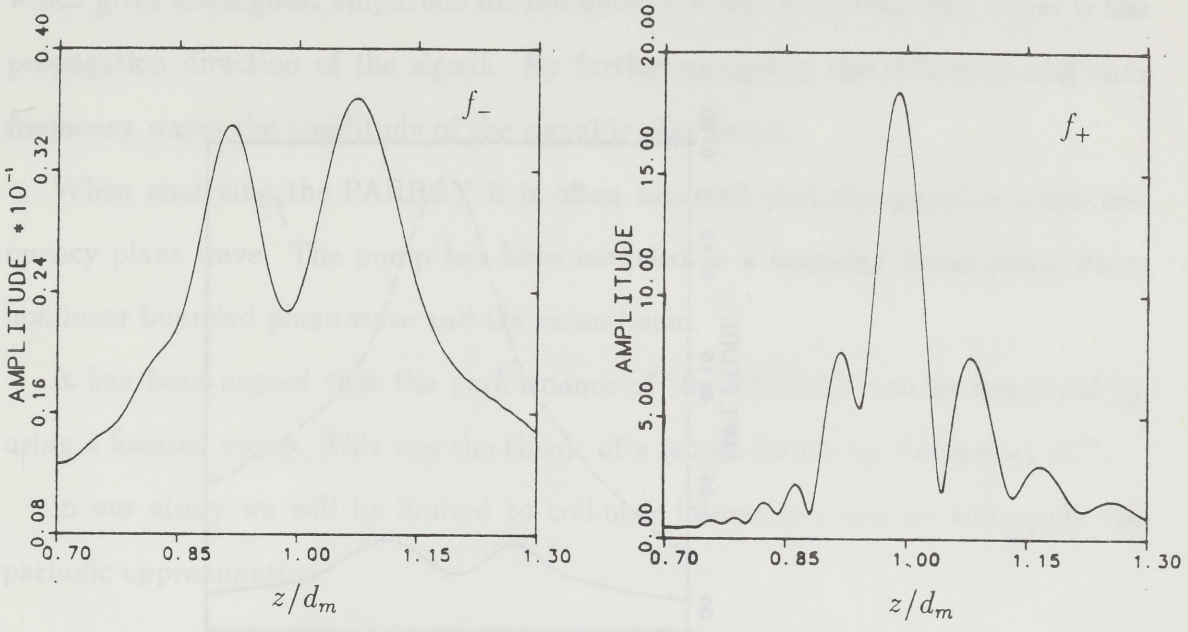

FIG. 4.26. On-axis amplitude normalized to P_0 for the difference frequency and sum frequency wave, with no absorption, $d_m/l_{Dm} = 0.1$, $f_m/f_- = 9.5$, $G_m = 55$ and $d_1/d_2 = 0.85$. Quasilinear theory.

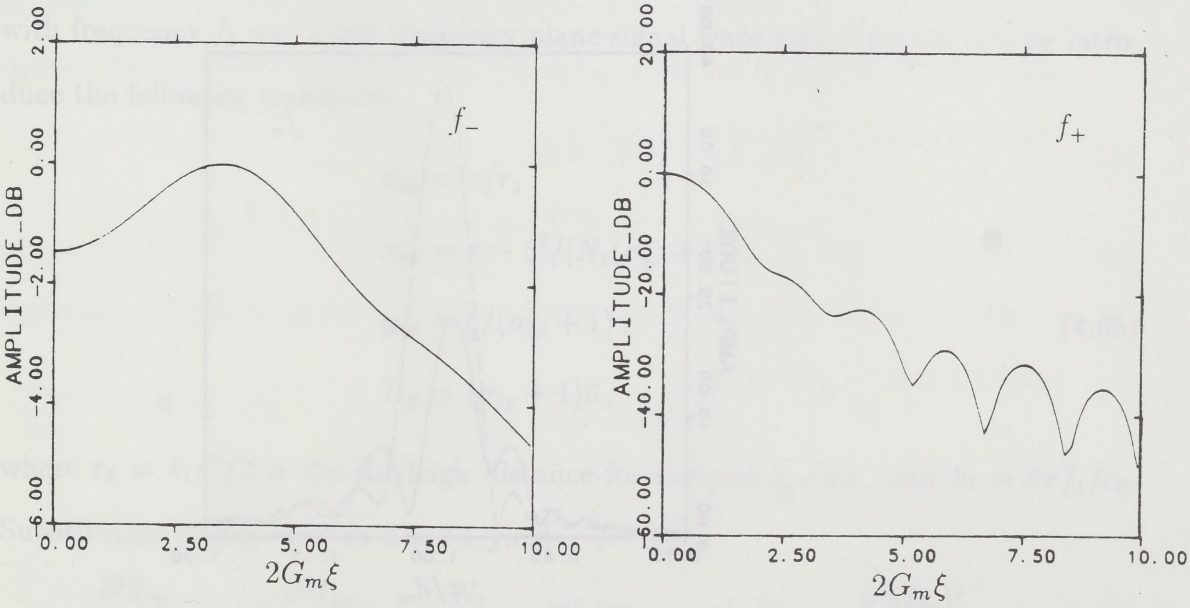

FIG. 4.27. Beam patterns in the focal plane $z = d_m$ for the difference frequency and sum frequency wave, with no absorption, $d_m/l_{Dm} = 0.1$, $f_m/f_- = 9.5$, $G_m = 55$ and $d_1/d_2 = 0.85$. Quasilinear theory.

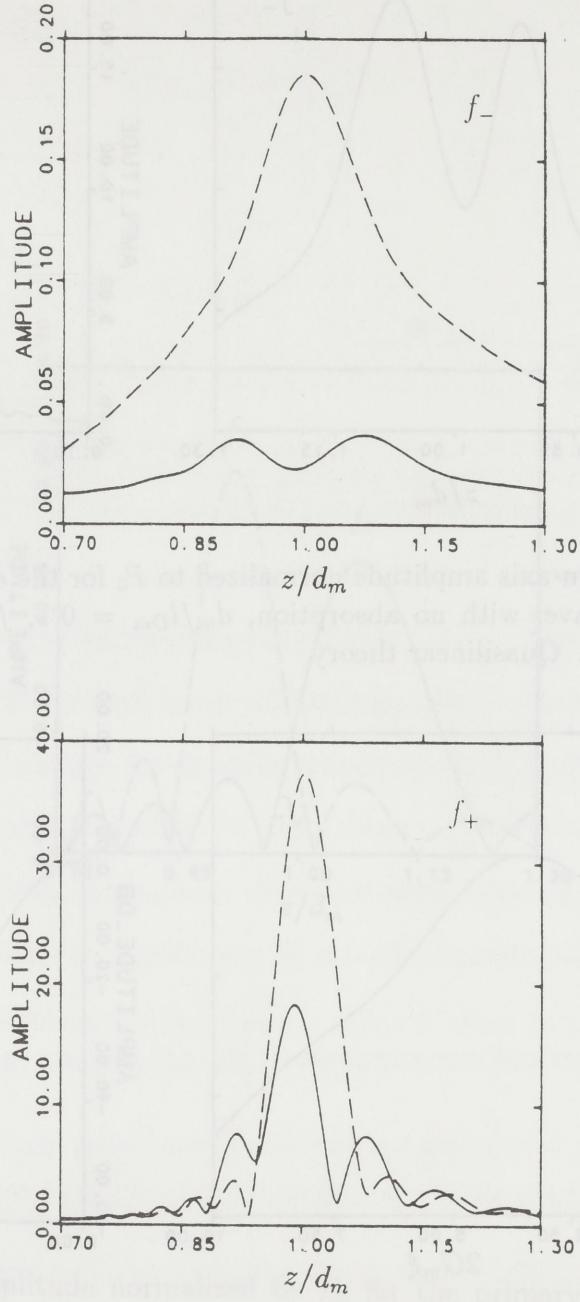

FIG. 4.28. On-axis amplitude for the difference and sum frequency wave, with no absorption, $d_m/l_{Dm} = 0.1$, $G_m = 55$ and $f_m/f_- = 9.5$. $d_1/d_2 = 0.85$ (——) and $d_1/d_2 = 1.0$(— —). Quasilinear theory.

which gives the highest amplitude for the difference and sum frequency waves is the propagation direction of the signal. By further analyzing the difference and sum frequency waves the amplitude of the signal is also found.

When analyzing the PARRAY it is often assumed that the signal is a low frequency plane wave. The pump has been modeled as a bounded linear plane wave, nonlinear bounded plane wave and Gaussian beam.

It has been argued that the performance of the PARRAY can be improved by using a focused pump. This was the theme of a recent article by Donskoi et al.[13].

In our study we will be limited to collinear interaction and we will apply the parbolic approximation.

The use of focused pump in PARRAY

In order to study the interaction between a high frequency unfocused pump wave with frequency f_1 and a low frequency plane signal wave with frequency f_2 we introduce the following transform:

$$\begin{aligned} \sigma_{bp} &= z/r_1\,, \\ \tau_{bp} &= \tau - \xi^2/[N_1(\sigma_{bp}+1)]\,, \\ \underline{u}_{bp} &= \underline{\xi}/(\sigma_{bp}+1)\,, \\ T_{bp} &= (\sigma_{bp}+1)\overline{p}\,, \end{aligned} \tag{4.65}$$

where $r_1 = k_1 a^2/2$ is the Rayleigh distance for the pump wave, and $k_1 = 2\pi f_1/c_0$. Substitution of Eqs. 4.65 in Eq. 2.1 yields

$$\frac{\partial^2 T_{bp}}{\partial\sigma_{bp}\partial\tau_{bp}} = \alpha r_1 \frac{\partial^3 T_{bp}}{\partial\tau_{bp}^3} + \frac{N_1}{4(\sigma_{bp}+1)^2}\nabla^2_{\underline{u}_{bp}} T_{bp} + \frac{r_1}{2l_D(\sigma_{bp}+1)}\frac{\partial^2 (T_{bp})^2}{\partial\tau_{bp}^2}, \tag{4.66}$$

where $\nabla^2_{\underline{u}_{bp}} = \partial^2/\partial u_{bp}^2 + (1/u_{bp})\partial/\partial u_{bp}$ and $u_{bp} = |\underline{u}_{bp}|$. If we assume that the boundary condition is periodic with period $2\pi\omega^{-1}$, we can seek a solution of Eq. 4.66

in the form of a Fourier series

$$T_{bp} = \sum_{n=1}^{\infty} (c_{bp,n} \cos n\tau_{bp} + d_{bp,n} \sin n\tau_{bp}), \tag{4.67}$$

where $c_{bp,n}$ and $d_{bp,n}$ are functions of spatial variables. Substituting Eq. 4.67 into Eq. 4.66 we obtain

$$\begin{aligned}
&\frac{\partial c_{bp,n}}{\partial \sigma_{bp}} = -\alpha r_1 n^2 c_{bp,n} - \frac{N_1}{4n(\sigma_{bp}+1)^2} \nabla^2_{\underline{u}_{bp}} d_{bp,n} + \\
&\frac{r_1 n}{2l_D(\sigma_{bp}+1)} \left[\sum_{i=1}^{n-1} (c_{bp,n-i} d_{bb,i}) + \sum_{i=n+1}^{\infty} (d_{bp,i} c_{bp,i-n} - c_{bp,i} d_{bp,i-n}) \right], \\
&\frac{\partial d_{bp,n}}{\partial \sigma_{bp}} = -\alpha r_1 n^2 d_{bp,n} + \frac{N_1}{4n(\sigma_{bp}+1)^2} \nabla^2_{\underline{u}_{bp}} c_{bp,n} + \\
&\frac{r_1 n}{2l_D(\sigma_{bp}+1)} \left[\frac{1}{2} \sum_{i=1}^{n-1} (d_{bp,n-i} d_{bp,i} - c_{bp,n-i} c_{bp,i}) - \sum_{i=n+1}^{\infty} (c_{bp,i} c_{bp,i-n} + d_{bp,i} d_{bp,i-n}) \right], \\
&n = 1, 2, ...
\end{aligned} \tag{4.68}$$

For an axisymmetric source that oscillates bisinusoidally with uniform amplitude distribution for the highest primary frequency and a plane wave for the lowest primary frequency, the boundary condition is

$$\overline{p}(\sigma = 0, \xi, \tau) = U(\xi) \sin N_1 \tau + (P_{02}/P_0) \sin N_2 \tau, \tag{4.69}$$

where P_{02} is the amplitude of the signal at $\sigma = 0$. This gives the following boundary conditions for $c_{bp,n}$ and $d_{bp,n}$:

$$c_{bp,N_1}(\sigma_{bp} = 0, u_{bp}) = U(u_{bp}) \sin u^2_{bp}, \tag{4.70}$$

$$d_{bp,N_1}(\sigma_{bp} = 0, u_{bp}) = U(u_{bp}) \cos u^2_{bp}, \tag{4.71}$$

$$c_{bp,N_2}(\sigma_{bp} = 0, u_{bp}) = (P_{02}/P_0) \sin \frac{N_2}{N_1} u^2_{bp}, \tag{4.72}$$

$$d_{bp,N_2}(\sigma_{bp} = 0, u_{bp}) = (P_{02}/P_0) \cos \frac{N_2}{N_1} u^2_{bp}, \tag{4.73}$$

with $c_{bp,n}(\sigma_{bp} = 0, u_{bp}) = 0$ and $d_{bp,n}(\sigma_{bp} = 0, u_{bp}) = 0$ for $n \neq N_1, N_2$.

In order to study the interaction between a high frequency focused pump wave with frequency f_1 and a low frequency plane signal wave with frequency f_2 we introduce the following transform:

$$\begin{aligned} \sigma_{fp} &= (z-d)/d, \\ \underline{u}_{fp} &= \underline{\xi}/(\sigma_{fp} \pm \delta), \\ \tau_{fp} &= \tau - \xi^2/[(\sigma_{fp} \pm \delta)d/r_0], \\ T_{fp} &= (\sigma_{fp} \pm \delta)\overline{p}. \end{aligned} \tag{4.74}$$

Substitution of Eqs. 4.74 in Eq. 2.1 yields

$$\frac{\partial^2 T_{fp}}{\partial \sigma_{fp} \partial \tau_{fp}} = \alpha d \frac{\partial^3 T_{fp}}{\partial \tau_{fp}^3} + \frac{d}{4r_0(\sigma_{fp} \pm \delta)^2} \nabla^2_{\underline{u}_{fp}} T_{fp} + \frac{d}{2l_D(\sigma_{fp} \pm \delta)} \frac{\partial^2 (T_{fp})^2}{\partial \tau_{fp}^2}, \tag{4.75}$$

where $\nabla^2_{\underline{u}_{fp}} = \partial^2/\partial u_{fp}^2 + (1/u_{fp})\partial/\partial u_{fp}$ and $u_{fp} = |\underline{u}_{fp}|$. If we assume that the boundary condition is periodic with period $2\pi\omega^{-1}$, we can seek a solution of Eq. 4.75 in the form of a Fourier series

$$T_{fp} = \sum_{n=1}^{\infty} (c_{fp,n} \cos n\tau_{fp} + d_{fp,n} \sin n\tau_{fp}), \tag{4.76}$$

where $c_{fp,n}$ and $d_{fp,n}$ are functions of spatial variables. Substituting Eq. 4.76 into Eq. 4.75 we obtain

$$\begin{aligned} &\frac{\partial c_{fp,n}}{\partial \sigma_{fp}} = -\alpha d n^2 c_{fp,n} - \frac{d}{4r_0 n(\sigma_{fp} \pm \delta)^2} \nabla^2_{\underline{u}_{fp}} d_{fp,n} + \\ &\frac{dn}{2l_D(\sigma_{fp} \pm \delta)} \left[\sum_{i=1}^{n-1} (c_{fp,n-i} d_{fp,i}) + \sum_{i=n+1}^{\infty} (d_{fp,i} c_{fp,i-n} - c_{fp,i} d_{fp,i-n}) \right], \\ &\frac{\partial d_{fp,n}}{\partial \sigma_{fp}} = -\alpha d n^2 d_{fp,n} + \frac{d}{4nr_0(\sigma_{fp} \pm \delta)^2} \nabla^2_{\underline{u}_{fp}} c_{fp,n} + \\ &\frac{dn}{2l_D(\sigma_{fp} \pm \delta)} \left[\frac{1}{2} \sum_{i=1}^{n-1} (d_{fp,n-i} d_{fp,i} - c_{fp,n-i} c_{fp,i}) - \sum_{i=n+1}^{\infty} (c_{fp,i} c_{fp,i-n} + d_{fp,i} d_{fp,i-n}) \right], \\ &n = 1, 2, ... \end{aligned} \tag{4.77}$$

For an axisymmetric source that oscillates bisinusoidally with uniform amplitude distribution and focusing gain $G_1 = r_1/d_1$ for the highest primary frequency, and with a uniform amplitude distribution and zero focusing gain a for the lowest primary frequency, the boundary condition is

$$\overline{p}(\sigma = 0, \xi, \tau) = U(\xi)\sin(N_1\tau + G_1\xi^2) + (P_{02}/P_0)\sin(N_2\tau), \tag{4.78}$$

where P_{02} is the amplitude of the plane wave at the source. This gives the following boundary conditions for $c_{fp,n}$ and $d_{fp,n}$ when use is made of Eqs. 4.74 and Eq. 4.76:

$$c_{fp,N_1}(\sigma_{fp} = -1, u_{fp}) = -(1+\delta)U\left(u_{fp}(1+\delta)\right)\sin\left(G_1\delta(1+\delta)u_{fp}^2\right) \tag{4.79}$$

$$d_{fp,N_1}(\sigma_{fp} = -1, u_{fp}) = -(1+\delta)U\left(u_{fp}(1+\delta)\right)\cos\left(G_1\delta(1+\delta)u_{fp}^2\right) \tag{4.80}$$

$$c_{fp,N_2}(\sigma_{fp} = -1, u_{fp}) = -(1+\delta)\sin\left(G_2\delta(1+\delta)u_{fp}^2\right) \tag{4.81}$$

$$d_{fp,N_2}(\sigma_{fp} = -1, u_{fp}) = -(1+\delta)\cos\left(G_2\delta(1+\delta)u_{fp}^2\right) \tag{4.82}$$

with $c_{fp,n}(\sigma_{fp} = -1, u_{fp}) = 0$ and $d_{fp,n}(\sigma_{fp} = -1, u_{fp}) = 0$ for $n \neq N_1, N_2$. To see the effect of focusing we have in Fig. 4.29 compared the difference frequency wave generated using unfocused pump wave with the difference frequency wave generated using three different focused pumps. The gain of these focused pumps are 50, 10 and 1. We keep the source amplitude, frequency and radius of the of the pump fixed, and vary the focal distance. The amplitude of the signal P_{02} is set to $10^{-6}P_0$. For simplicity we have neglected absorption and applied the quasilinear approximation. The amplitudes are scaled to 6 x $10^{-7}P_0$. We find only small variations in the maximum on-axis amplitude of the difference frequency waves generated using the various pump waves. When $G_1 = 50$ the amplitude of the pump wave at focus is 50 times as high as in the case of $G_1 = 1$, but when $G_1 = 50$ the focal distance is only 1/50 times the focal distance in the case of $G_1 = 1$. Focusing closer to the

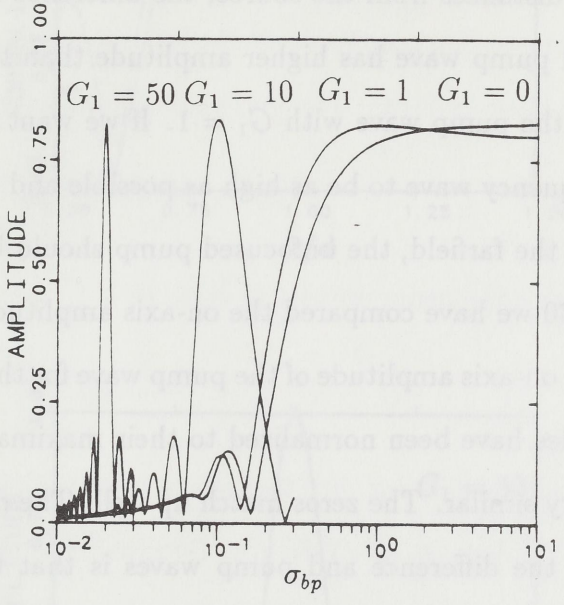

FIG. 4.29. On-axis amplitude normalized to 6 x $10^{-7}P_0$ for the difference frequency wave for various focusing gains, with no absorption and $f_1/f_2 = 150$. Quasilinear theory.

source increases the amplitude of the pump, but the distance the nonlinear effects can accumulate decreases. These effects balance each other for the values of focusing gain considered here. For $G_1 = 10, 50$ the amplitude of the difference frequency wave falls off very quickly after focus. Comparing the cases $G_1 = 1$ and $G_1 = 0$ we see that the on-axis amplitude of the difference frequency wave does not change very much, except for the fact that the maxima are closer to the source in the case of $G_1 = 1$. Beyond two Rayleigh distances from the source, the difference frequency wave generated by the unfocused pump wave has higher amplitude than the difference frequency wave generated by the pump wave with $G_1 = 1$. If we want the on-axis amplitude of the difference frequency wave to be as high as possible and the directivity to be as sharp as possible in the farfield, the unfocused pump should be used.

In Fig. 4.30 we have compared the on-axis amplitude of the difference frequency wave with the on-axis amplitude of the pump wave for the cases $G_1 = 50$ and $G_1 = 10$. The amplitudes have been normalized to their maxima. In the case of $G_1 = 50$ the curves are very similar. The zeros match up well. The difference between the on-axis amplitude of the difference and pump waves is that the on-axis amplitude of the difference frequency wave is lower in the prefocal region and higher in the postfocal region. This is probably because the difference frequency wave is generated by an accumulative effect. For $G_1 = 10$ the curves are quite similar. The zeros before focus match up well and the amplitude of the difference frequency wave is lower before focus and higher after focus. We also notice that the on-axis amplitude of the difference frequency wave has a maximum very close to the focus, even if the pump has a maximum more than $1/10$ of the focal distance away from the focus. We have seen this effect even more clearly for lower values of G_1.

The beam patterns at focus are nearly identical for the difference frequency wave

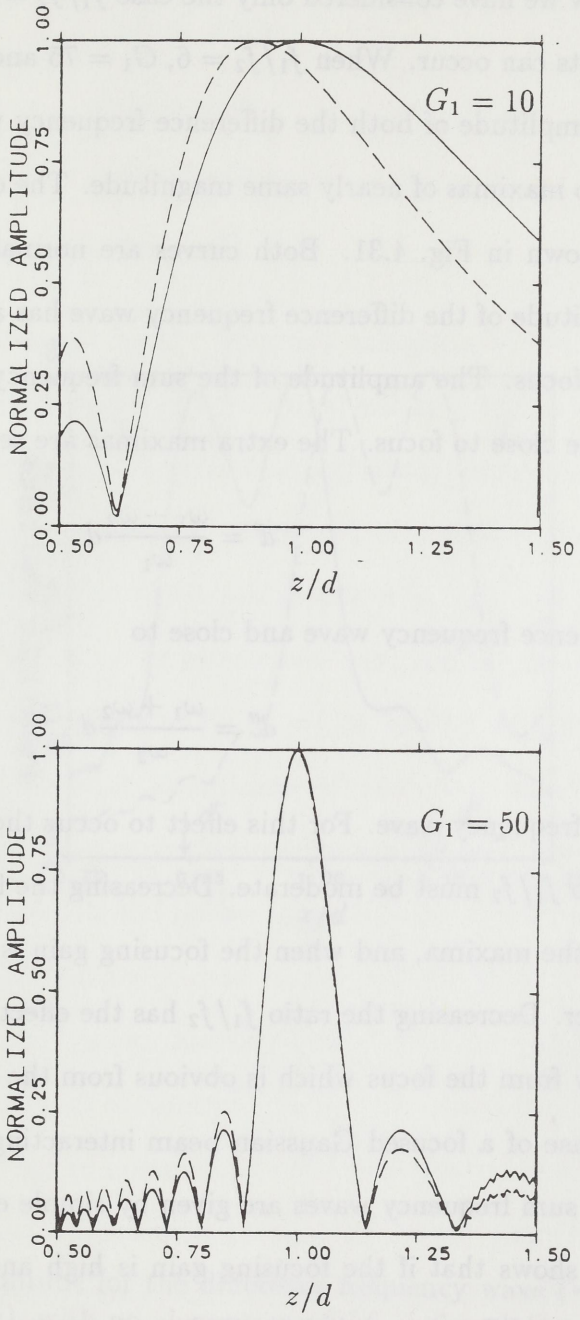

FIG. 4.30. On-axis amplitude for the difference frequency wave (———) and the pump wave (— —), with no absorption and $f_1/f_2 = 150$. Linear/quasilinear theory.

and the pump wave when $G_1 = 50$ and $G_1 = 10$.

Up to now we have considered only the case $f_1/f_2 = 150$. For low values of f_1/f_2 peculiar effects can occur. When $f_1/f_2 = 6$, $G_1 = 75$ and $\alpha = 0$ it was observed that the on-axis amplitude of both the difference frequency wave and the sum frequency wave had two maximas of nearly same magnitude. The difference and sum frequency waves are shown in Fig. 4.31. Both curves are normalized to their maxima. The on-axis amplitude of the difference frequency wave has a maximum before focus and one close to focus. The amplitude of the sum frequency wave has a maximum after focus and one close to focus. The extra maximas are seen to be close to

$$d' = \frac{\omega_1 - \omega_2}{\omega_1} d \tag{4.83}$$

for the difference frequency wave and close to

$$d'' = \frac{\omega_1 + \omega_2}{\omega_2} d \tag{4.84}$$

for the sum frequency wave. For this effect to occur the focusing gain must be high, and the ratio f_1/f_2 must be moderate. Decreasing the focusing gain has the effect of broadening the maxima, and when the focusing gain is low enough the maxima will melt together. Decreasing the ratio f_1/f_2 has the effect of moving the extra maxima further away from the focus which is obvious from the expressions 4.83 and 4.84.

In the case of a focused Gaussian beam interacting with a plane wave, the difference and sum frequency waves are given by simple expressions. Analysis of these expressions shows that if the focusing gain is high and the ratio f_m/f_- is not too large, then the difference and the sum frequency waves will have extra maxima located at the positions given by 4.83 and 4.84. When studying the PARRAY for collinear interaction, we can in addition to diffraction also include absorption and

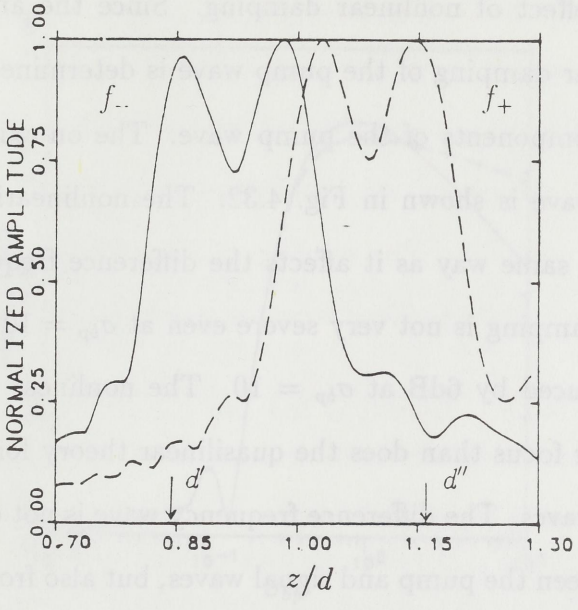

FIG. 4.31. On-axis amplitude for the difference frequency wave (———) and sum frequency wave (— —), with no absorption, $f_1/f_2 = 6$ and $G_1 = 75$. Quasilinear theory.

nonlinear effects. We have studied the case

$$f_1/f_2 = 150, \tag{4.85}$$

$$\alpha r_1 = 0.01, \tag{4.86}$$

$$r_1/l_{D1} = 1.0, \tag{4.87}$$

$$G_1 = 1.0, \tag{4.88}$$

to see the effect of nonlinear damping. Since the amplitude of the signal is low the nonlinear damping of the pump wave is determined by the generation of higher harmonic components of the pump wave. The on-axis amplitude of the difference frequency wave is shown in Fig. 4.32. The nonlinearity affects the sum frequency wave in the same way as it affects the difference frequency wave. We see that the nonlinear damping is not very severe even at $\sigma_{bp} = 10$. The amplitude of the pump wave is reduced by 6dB at $\sigma_{bp} = 10$. The nonlinear theory predicts a higher amplitude near focus than does the quasilinear theory for both the difference and sum frequency waves. The difference frequency wave is not only generated from the interaction between the pump and signal waves, but also from the interaction between the sum frequency wave and the second harmonic component of the pump wave. When nonlinear effects start to become important, energy is transfered from the pump wave to the second harmonic component. Because of the nonlinear damping of the pump wave, less difference frequency wave is generated by the interaction between the pump wave and the signal wave. This loss of generation is compensated by the interaction between the second harmonic and sum frequency components. In the same way the sum frequency wave is generated both by the interaction between the pump wave and the signal wave, and the interaction between the second harmonic wave and the difference frequency wave.

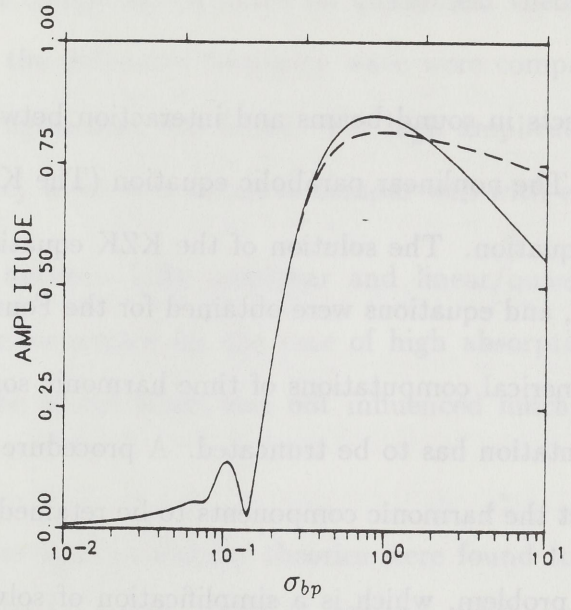

FIG. 4.32. On-axis amplitude for the difference frequency wave. Fully nonlinear theory (———) and quasilinear theory (— —), with $\alpha_1 d_1 = 0.01, r_1/l_{D1} = 1.0$, $f_1/f_2 = 150$ and $G_1 = 1.0$.

Chapter 5

Summary and conclusions

Nonlinear effects in sound beams and interaction between sound beams have been investigated. The nonlinear parabolic equation (The KZK equation) has been used as a model equation. The solution of the KZK equation was written in form of a Fourier series, and equations were obtained for the Fourier coefficients.

1. For numerical computations of time harmonic sound fields, the Fourier series representation has to be truncated. A procedure has been developed for how to select the harmonic components to be retained in the Fourier series.

2. A test problem, which is a simplification of solving the KZK equation, was introduced. Two finite difference methods were applied to this test problem and analyzed. The analysis gave a good understanding of the qualitative and quantitative behaviour of the two methods.

3. The analysis of the test problem gave rise to an efficient algorithm for solving the KZK equation.

4. A computer code was implemented. Different integration regions were used for different harmonic components. When a high number of harmonic components are retained in the computations, this technique reduces the computation time

by about a factor of four. A stabilization procedure was given which facilitates the computation of sound beams well beyond the shock formation distance.

Applications were made to the parametric array:

5. In order to test the computer code, numerical results were compared to experiments and earlier computations based on quasilinear theory. For low amplitudes, results for the difference frequency wave were compared to quasilinear theory and good agreement was found. For high amplitudes, results for the difference frequency wave were found to compar well with experiments.

6. The comparison between fully nonlinear and linear/quasilinear theory was found to be more favourable for the case of high absorption. The high frequency part of the sound beam was not influenced much by the downshift ratio.

7. The fully nonlinear and quasilinear theories were found to predict the same numerical results up to ranges, which for the case of the difference frequency wave was 10 times that of the sum frequency wave. This can be explained by the fact that the difference frequency wave to some extent also is generated from the interaction between higher harmonic and combination frequency components of the primary waves.

8. Studying beampatterns for the primary, sum frequency and the difference frequency waves it was found that the effect of nonlinearity not only caused an erosion of the mainlobes, but also lead to an outward shift of the beam structure.

9. Higher harmonic components of the difference frequency wave were computed, and it was found that they were built up around the shock formation distance. A general trend was that the successive higher harmonic components had higher directivity, and that dips occured in the beampatterns near the symmetry axis.

10. Monofrequency wave excitation was compared to bifrequency wave excitation. We found that the primary wave was more influenced by nonlinear damping in the bifrequency case.

11. Waveforms were computed. The process from initial waveforms, through the developement of shocks, via strong shocks to stable waveforms, and finally to a pure difference frequency wave was shown.

12. The possibility of matching the solution of the KZK equation with the solution of the spherical Burgers' equation was studied in the case of low amplitudes. It was found that the primary and sum frequency waves, but not the difference frequency wave could be matched well at about a Rayleigh distance from the source.

Focused sound beams, nonlinear effects in focused sound beams and interaction between focused sound beams have also been investigated:

13. The power of the second harmonic component in the vicinity of focus was computed, and it was found that the power had a maximum right after focus. An analysis of the power of the different harmonic components shows that energy is transferred from the second harmonic to the primary component in the post focal region.

14. Beam patterns for the fundamental and second harmonic components were studied in the vicinity of focus. As in the unfocused case it was found that the effect of nonlinearity was an erosion of the mainlobes and an outward shift of the beam structure.

15. Applications were made to interaction between focused sound beams. In order to check the computer code, comparison was made for the difference frequency wave with quasilinear results for reported in the literature.

16. For given primary frequencies, source radius and source amplitude we found that the maximum amplitude of the difference frequency wave increased only slightly by increasing the focusing gain of the primaries. When going from $G_m = 1$ to $G_m = 50$ the amplitude of the difference frequency wave only increased by a factor of less than 3.

17. The power of the difference frequency component generated by two focused sound beams was computed, and we found that the difference frequency component attained a maximum a little after focus. The power of the second harmonic and sum frequency components has the same qualitative behaviour as the difference frequency wave. An analysis of the power of the harmonic components gives that energy is transferred from the second-order components to the primary components in the post focal region

18. Interaction between two focused beams with different focal distances has also been studied. When the focal distances are not too close to each other, and for high focusing gains, the on-axis amplitude of the difference frequency wave attains two maxima of nearly the same magnitude, one close to each focal

point. The on-axis amplitude of the sum frequency wave has a maximum near the midpoint between the two focal points.

19. The maximum amplitudes of the difference and sum frequency waves are substantially higher when the focal distances of the primaries are equal than when they are different.

We have also studied the interaction between a plane wave and a focused or unfocused beam:

20. For given primary frequency, signal frequency, source radius and source amplitude the maximum amplitudes of the difference frequency and sum frequency waves are nearly invariant with respect to focusing gain of the pump.

21. For low values of focusing gain the on-axis amplitude of the difference and sum frequency waves have maxima very close to focus even though the on-axis amplitude of the focused pump has a maximum significantly before focus.

22. For high focusing gains and pump frequencies much larger than the signal frequency, the pressure amplitude distribution both along axis and in the focal plane is similar for the difference frequency, sum frequency and pump waves.

23. When the pump frequency is only moderately larger than the signal frequency and the pump is strongly focused, peculiar effects can occur. The on-axis amplitude of the difference frequency wave attains one maximum before focus and one at focus. The on-axis amplitude of the sum frequency wave also attains two maxima with one maximum at focus and one after focus. These effects are

also found analytically, when investigating the interaction between a Gaussian beam and a plane wave.

REFERENCES

[1]P. J. Westervelt, "Parametric Acoustic Array," J. Acoust. Soc. Am. **35**, 535-537 (1963)

[2]D. Rugar, "Resolution beyond the diffraction limit in the acoustic microscope: A nonlinear effect," J. Appl. Phys. **56**, 1338-1346 (1984)

[3]*Extracorporeal Shock Wave Lithotripsy*, edited by Ch. Chaussy (Krager, Munich, 1986)

[4]E. A. Zabolotskaya and R. V. Khokhlov, "Quasi-plane waves in the nonlinear acoustics of confined beams," Sov. Phys. Acoust. **15**, 35-40 (1969)

[5]V. P. Kutznetsov, "Equations of nonlinear acoustics," Sov. Phys. Acoust. **16**, 467-470 (1971)

[6]S. I. Aanonsen, T. Barkve, J. Naze Tjøtta, and S. Tjøtta, "Distortion and harmonic generation in the nearfield of a finite amplitude sound beam," J. Acoust. Soc. Am. **75**, 749-768 (1984)

[7]J. Berntsen and E. Vefring, "Numerical computation of a finite amplitude sound beam," Dep. of Appl. Math., Univ. of Bergen, Norway, Report no. 81, (1986)

[8]S. I. Aanonsen, "Numerical computation of the nearfield of a finite amplitude sound beam," Rep No. 73, Department of Mathematics, University of Bergen, Bergen Norway (1983).

[9]S. I. Aanonsen, M. F. Hamilton, J. Naze Tjøtta, and S. Tjøtta, "Nonlinear effects in sound beams," in *Proceedings of the 10th International Congress of Nonlinear*

Acoustics, edited by Akira Nakamura (Teikohsha Press, Kodoma, Japan, 1984), 45-48

[10]M. F. Hamilton, J. Naze Tjøtta, and S. Tjøtta, "Nonlinear effects in the farfield of a directive sound source," J. Acoust. Soc. Am. **78**, 202-216 (1985)

[11]T. S. Hart and M. F. Hamilton, "Nonlinear effects in focused sound beams," J. Acoust. Soc. Am. **84**, 1488-1496 (1988)

[12]T. S. Hart, "Numerical investigation of nonlinear effects in focused sound beams," M. S. thesis, The University of Texas at Austin, (1987)

[13]D. M. Donskoi, A. M. Pavlenko and A. M. Sution, "Parametric reception of acoustic signals with the application of a focused pump," Sov. Phys. Acoust. **32** 243-245 (1986)

[14]J. Naze Tjøtta and S. Tjøtta, "Nonlinear equations of acoustics, with applications to parametric acoustic arrays," J. Acoust. Soc. Am. **69**, 1644-1652 (1981)

[15]A. Korpel, "Frequency approach to nonlinear dispersive waves," J. Acoust. Soc. Am. **67**, 1954-1958 (1980)

[16]Ya. M. Zhileikin, "Numerical solution of the equation for non-linear acoustics of confined beams," U.S.S.R. Comput. Maths. Math. Phys., **22** (5), 140-156, (1982)

[17]J. Berntsen and E. Vefring, User documentation, Programs SOLTRI, SOLFIV and SOLSEV, Dep. of Appl. Math., Univ. of Bergen, Norway, (1986)

[18]M. K. Jain, *Numerical solution of differential equations,* (John Wiley, 1984)

[19]R. D. Richtmeyer, "Difference methods for initial value problems," Interscience Tracts in Pure and Appl. Math., Tract 4, Interscience, New York (1957)

[20]G. Fairweather and A. R. Gourlay, "Some stable difference approximations to a fourth-order parabolic partial differential equation," Math. Comp. **21**,1 (1967)

[21]G. D. Smith, "Numerical solution of partial differential equations," Oxford University Press (1966)

[22]J. Berntsen, "On the use of the Richtmyer procedure to compute a finite amplitude sound beam from a piston source," Dep. of Appl. Math., University of Bergen, Norway, Report no. 82, (1987)

[23]J. Berntsen. Private communication.

[24]D. H. Trivett and A. L. Van Buren, "Propagation of plane, cylindrical, and spherical finite amplitude waves," J. Acoust. Soc. Am. **69**, 943-949 (1981)

[25]J. Naze Tjøtta and S. Tjøtta, "Nonlinear interaction of two sound beams," J. Acoust. Soc. Am. **68**, 174-175 (1965)

[26]J. L. S. Bellin and R. T. Beyer, "Experimental investigation of an endfire array," J. Acoust. Soc. Am. **34**, 1051-1054 (1962)

[27]V. Lauvstad, J. Naze Tjøtta and S. Tjøtta, "Nonlinear interaction of two sound waves," Acta Universitatis Bergensis series Mathematica Rerumque Naturalium, No. 12, 1964

[28]H. O. Berktay, "Possible exploitation of nonlinear acoustics in underwater transmitting applications," J. Sound Vib. **2**, 435-461 (1965)

[29]H. O. Berktay, "Some proposals for underwater transmitting applications of nonlinear acoustics," J. Sound Vib. **6**, 244- 254 (1967)

[30]T. G. Muir and J. G. Willette, "Parametric acoustic transmitting arrays," J. Acoust. Soc. Am. **52**, 1481-1486 (1972)

[31]H. Hobæk, " Experimental investigation of an acoustic end-fire array," J. Sound. Vib. **6**, 460-463 (1967)

[32]H. Hobæk and M. Vestrheim, "Axial distribution of difference frequency sound in a collimated beam of circular cross section," *Proceedings of Symposium on Nonlinear Acoustics*, University of Birmingham 1.-2. April 1971 (British Acoustical Society, London, 1972)

[33]M. Vestrheim and H. Hobæk, "Angular distribution of nonlinearly generated difference frequency sound, *Proceedings of Symposium on Nonlinear Acoustics*, University of Birmingham 1.-2. April 1971 (British Acoustical Society, London, 1972)

[34]J. F. Bartram, "A Useful Model for the Parametric Acoustic Array," J. Acoust. Soc. Am. **52**, 1042-1044 (1972)

[35]H. M. Merklinger, "Fundamental frequency component of a finite amplitude plane wave," J. Acoust. Soc. Am. **54**, 1760-1761 (1973)

[36]H. M. Merklinger, R. H. Mellen and M. B. Moffet, "Finite amplitude losses in spherical waves," J. Acoust. Soc. Am. **59**, 755-759 (1976)

[37]M. B. Moffett and R. H. Mellen, "Model for parametric acoustic sources," J. Acoust. Soc. Am. **61**, 325-337 (1977)

[38]M. B. Moffet and R. H. Mellen, "Nearfield characteristics of parametric acoustic sources," J. Acoust. Soc. Am. **69**, 404-409 (1981)

[39]B. K. Novikov, O. V. Rudenko, V. I. Timoshenko, *Nonlinear Underwater Acoustics*," (Am. Ins. Phys., New York 1987)

[40]B. K. Novikov, O. V. Rudenko and S. I. Soluyan, "Parametric ultrasonic radiators," Sov. Phys. Acoust. **21**, 365-368 (1975)

[41]B. K. Novikov, M. S. Rybachek and V. I. Timoshenko, "Interaction of diffracting sound beams and the theory of highly directional ultrasonic radiators," Sov. Phys. Acoust. **23**, 354-357 (1977)

[42]N. S. Bakhvalov, Ya. M. Zhileikin, E. A. Zabolotskaya, *Nonlinear Theory of Sound beams*," (Am. Ins. Phys., New York 1987)

[43]N. S. Bakhvalov, Ya. M. Zhileikin, E. A. Zabolotskaya and R. V. Khoklov, "Nonlinear propagation of a sound beam in a nondissipative medium," Sov. Phys. Acoust. **22**, 272-274 (1976)

[44]N. S. Bakhvalov, Ya. M. Zhileikin, E. A. Zabolotskaya and R. V. Khoklov, "Propagation of finite amplitude sound beams in a dissipative medium," Sov. Phys. Acoust. **24**, 271-275 (1978)

[45]N. S. Bakhvalov, Ya. M. Zhileikin, E. A. Zabolotskaya and R. V. Khoklov, "Harmonic generation in sound beams," Sov. Phys. Acoust. **25**, 101-106 (1979)

[46]N. S. Bakhvalov, Ya. M. Zhileikin, E. A. Zabolotskaya, "Nonlinear propagation of Gaussian beams," Sov. Phys. Acoust. **25**, 458-460 (1979)

[47]N. S. Bakhvalov, Ya. M. Zhileikin, E. A. Zabolotskaya, "Nonlinear propagation of sound beams with a uniform amplitude distribution," Sov. Phys. Acoust. **26**, 95-100 (1980)

[48]N. S. Bakhvalov, Ya. M. Zhileikin, O. V. Rudenko, "Operating characteristics of high-power parametric acoustic radiators," Sov. Phys. Acoust. **24**, 68-70 (1978)

[49]N. S. Bakhvalov, Ya. M. Zhileikin, E. A. Zabolotskaya, "Parametric interaction of sound beams," Sov. Phys. Acoust. **25**, 280-283 (1979)

[50]J. Naze Tjøtta and S. Tjøtta, "An analytical model for the nearfield of a baffled piston transducer," J. Acoust. Soc. Am. **68**, 334-339 (1980)

[51]G. S. Garrett, J. Naze Tjøtta and S. Tjøtta, "Nearfield of a large transducer, Part I: Linear radiation", J. Acoust. Soc. Am. **72**, 1056-1061 (1982)

[52]G. S. Garrett, J. Naze Tjøtta, and S. Tjøtta, "Nearfield of a large acoustic transducer. Part II: Parametric radiation," J. Acoust. Soc. Am. **74**, 1013-1020 (1984)

[53]G. S. Garrett, J. Naze Tjøtta, and S. Tjøtta, "Nearfield of a large acoustic transducer. Part III: General results," J. Acoust. Soc. Am. **75**, 769-778 (1984)

[54]J. Berntsen, J. Naze Tjøtta, and S. Tjøtta, "Nearfield of a large acoustic transducer. Part IV: Second harmonic and sum frequency radiation," J. Acoust. Soc. Am. **75**, 1383-1391 (1984)

[55]A. C. Baker, K. Anastasiadis, and V. F. Humphrey, "The nonlinear pressure field of a plane circular piston: Theory and experiment," J. Acoust. Soc. Am. **84**,1483-1487 (1988)

[56]T. Kamakura, N. Hamada, K. Aoki, and Y. Kumamoto, "Nonlinearly generated spectral components in the nearfield of a directive sound source," J. Acoust. Soc. Am. **85**,2331-2337 (1989)

[57]H. O. Berktay, "Possible exploitation of nonlinear acoustics in underwater transmitting applications," J. Sound. Vib. **2**, 435-461 (1965)

[58]L. Germain and J. D. N. Cheeke, "Generation and detection of high-order harmonics in liquids using a scanning acoustic micrscope," J. Acoust. Soc. Am. **83**, 942-949 (1988)

[59]P. Y. Hennion, "Étude de l'émission paramétrique en champ proche par analyse de Fourier: Application à un émetteur focalisant," J. Phys. (Paris) **40**, C8-126 (1979)

[60]B. G. Lucas and T. G. Muir, "Field of a finite amplitude focusing source," J. Acoust. Soc. Am. **74**, 1522-1528 (1983)

[61]H. T. O'Neil, "Theory of focusing radiators," J. Acoust. Soc. Am. **21**, 516-526 (1949)

[62]V. M. Levin, O. I. Lobkis and R. G. Maev, "Field of a spherical focusing transducer with arbitrary aperture angle," Sov. Phys. Acoust. , **33**, 87-89 (1987)

[63]K. A. Naugol'nykh, S. I. Soluyan and R. V. Khoklov, "Spherical waves of finite amplitude in a viscous thermally conducting medium," Sov. Phys. Acoust. **9**, 42-46 (1963)

[64]C. W. Smith and R. Beyer, "Ultrasonic radiation field of a focusing Spherical Source at finite amplitudes," J. Acoust. Soc. Am. **46**, 806-813, (1969)

[65]L. A. Ostrovskii and A. M. Sutin, "Focusing of finite amplitude acoustic waves," Sov. Phys. Dokl. **24**, 275-277 (1975)

[66]A. M. Sutin, "Influence of nonlinear effects on the properties of acoustic focusing systems," Sov. Phys. Acoust. **24**, 334-339 (1978)

[67]B. G. Lucas and T. G. Muir, "The field of a focusing source," J. Acoust. Soc. Am. **72**, 1289-1296 (1982)

[68]B. G. Lucas, J. Naze Tjøtta and T. G. Muir, "Field of a parametric focusing source," J. Acoust. Soc. Am. **73**, 1966-1971 (1983)

[69]J. Naze Tjøtta and S. Tjøtta, "Sound field of a parametric focusing source," J. Acoust. Soc. Am. **75**, 1392-1394 (1984)

[70]S. Saito, B. C. Kim and T. G. Muir, "Second harmonic component of a nonlinearly distorted wave in a focused sound field," J. Acoust. Soc. Am. **82**, 621-628 (1987)

[71]E. A. Barannik, O. G. Kadnikov, and V. V. Papakitsa," Scattering of sound by sound in the superposition of focused wave beams," Sov. Phys. Acoust. , **32**, 319-322 (1986)

[72]E. A. Barannik and O. G. Kadnikov,"Nonlinear sources in a region of superposition of convergent spherical waves," Sov. Phys. Acoust. , **33**, 206-207 (1987)

[73]N. S. Bakhvalov, Ya. M. Zhileikin, E. A. Zabolotskaya and R. V. Khoklov, "Focused high amplitude sound beams," Sov. Phys. Acoust. **24**, 10-15 (1978)